UNIVERSITÀ DEGLI STUDI DI NAPOLI

FEDERICO II

PhD THESIS IN CHEMICAL SCIENCES

XXXVI COURSE

Investigation of new antimicrobial compounds: identification of bacterial protein targets

Tutor:

Prof. Angela Duilio

Author:

Carolina Cané

Coordinator:

Prof. Angelina Lombardi

Table of contents

List of abbreviations

Abbreviations	Meaning
A. baumannii	*Acinetobacter baumannii*
ACC	Acetyl-CoA Carboxylase
ACN	Acetonitrile
AMBIC	Ammonium bicarbonate
AMPs	AntiMicrobial Peptides
B. vulgaris	*Berberis vulgaris*
Bam	β-Barrel assembly machinery
BCA	Bicinchoninic acid
CD	Circular Dichroism
CF	Cystic Fibrosis
CFU	Colony-Forming Units
CHAPS	3-((3-cholamidopropyl)dimethylammonium)-1-propanesulfonate
CID	Collision-Induced Dissociation
DDA	Data Dependent Acquisition
DLS	Dynamic Light Scattering
DMEM	Dulbecco's Modified Eagle Medium
DTT	Dithiothreitol
ΔG	Gibbs free energy
E. coli	*Escherichia coli*
ECL	Enhanced chemiluminescence
ED	Effector domain

EDTA	Ethylenediamine tetraacetic acid
EI	Electron Impact
EPIs	Efflux pump inhibitors
Esc(1-21)	Esculentin(1-21)
Esc(1-21)-1c	Esculentin(1-21)-1c
Esc-1a	Esculentin-1a
FAS II	Fatty Acid Synthetase
FBS	Fetal Bovine Serum
FCs	Fold changes
FIC	Fractional Inhibitory Concentration
FtsZ	Filamentous temperature sensitive Z
GC-MS	Gas chromatography-mass spectrometry
GTPase	Guanosine Triphosphatase
GuHCl	Guanidinium Chloride
HEPES	4-(2-hydroxyethyl)-1-piperazineethanesulfonic acid
HK	Histidine kinase
HPLC	High Performance Liquid Chromatography
HRP	Horseradish peroxidase
IAM	Iodoacetamide
IMAC	Immobilized Metal Ion Affinity Chromatography
IPTG	Isopropyl β-D-1-thiogalactopyranoside
ITC	Isothermal titration calorimetry
K_d	Dissociation constant
K_i	Inhibition constant

K_M	Michaelis-Menten constant
LB	Luria Bertani
LC-MS/MS	Liquid Chromatography Tandem Mass Spectrometry
LFQ	Label-free quantification
LPS	Lipopolysaccharides
Lpt	LPS transport
M. tuberculosis	*Mycobacterium tuberculosis*
Mag-2	Magainin-2
MALDI-TOF	Matrix-Assisted Laser Desorption/Ionization-Time of Flight
MDR	Multidrug-Resistance
MH	Mueller Hinton
MIC	Minimum Inhibitory Concentration
MOI	Multiplicity of Infection
MRM	Multiple Reaction Monitoring
MRSA	Methicillin-resistant *Staphylococcus aureus*
MS	Mass spectrometry
MSCRAMMs	Microbial Surface Components Recognizing Adhesive Matrix Molecules
N. meningitis	*Neisseria meningitidis*
Ni-NTA	Nickel- Nitrilotriacetic acid
NMR	Nuclear magnetic resonance
NPs	Natural Products
OM	Outer Membrane
OMPs	Outer Membrane Proteins

P. aeruginosa	*Pseudomonas aeruginosa*
PBS	Phosphate-Buffered Saline
PIPES	1,4-Piperazin-bis-(ethansulfonsaure)
PLIP	Protein-Ligand Interaction Profiler
PMSF	Phenylmethylsulfonyl fluoride
POTRA	Periplasmic polypeptide transport-associated
PPIs	Protein-Protein Interactions
PTA	Phosphotungstic acid
PVDF	Polyvinylidene fluoride
qRT-PCR	Quantitative Reverse Transcription-Polymerase Chain Reaction
RD	Receiver Domain
RP	Reversed-Phase
RP2	2-(2-Aminophenyl) indole
RR	Response Regulator
S. aureus	*Staphylococcus aureus*
SD	Standard Deviation
SDS-PAGE	Sodium Dodecyl Sulphate - PolyAcrylamide Gel Electrophoresis
TCS	Two-Component Systems
TEM	Transmission Electron Microscopy
Temp-L	Temporin-L
TFA	Trifluoroacetic acid
TQ-S	Tandem Quadrupole mass spectrometer
TRAP	Target of RNAIII Activating Protein

UPLC	Ultra Performance Liquid Chromatography
UTIs	Urinary Tract Infections
WHO	World Health Organization

Summary

The rapid emergence of resistant bacteria is occurring worldwide, compromising the efficacy of antibiotic-based therapies. In this context, the interest is focused on the development of new alternative therapeutic strategies effective against both Gram-positive and Gram-negative bacteria. The phenomenon of resistance is closely related to the mechanism of action of antimicrobial agents, and the identification of new protein targets involved in vital bacterial functions is central to the search for new pharmacological agents to fight resistant bacteria. Proteomics is a powerful tool to understand which biological functions are altered by an antimicrobial agent, with the goal of identifying key target proteins that might be addressed by new and more effective drugs to overcome the dramatic increase in MDR bacterial strains.

In these perspectives, the present Ph.D. project has been focused to the investigation of the molecular mechanisms of AMPs and NPs using targeted and untargeted proteomics approaches to identify novel protein targets in the prokaryotic system.

In chapter two, *in vitro* and *ex-vivo* strategies were employed to characterize the binding of Mag-2 to its target protein BamA in *E. coli*. BamA belongs to the Bam complex, previously identified as putative interactor of Mag-2 by functional proteomics. The recombinant form of BamA was expressed in *E. coli*, purified, and characterized; physico-chemical methodologies were then applied to demonstrate the peptide/protein interaction *in vitro*. Subsequently, the effective impairment of OMPs folding in the presence of Mag-2 was investigated using biochemical techniques and a targeted proteomic approach.

Chapter three focused on evaluating the effect of Temp-L on *S. aureus*, a Gram-positive bacterium, one of the world's leading human pathogens. Previous

morphological studies and differential proteomic approaches had suggested that Temp-L induces bacterial vesicle formation as a possible protective mechanism and impairs the expression of virulence factors. These hypotheses were confirmed by biological assays and spectroscopic analyses, suggesting that targeting virulence factors might be considered a novel strategy to replace conventional antimicrobial agents that can be used to treat the infections caused by the resistant pathogen *S. aureus*.

In Chapter four, a comparative analysis of the inhibitory action of berberine derivatives on the recombinant FtsZ protein of *E. coli* has been performed. Medicinal plants belonging to the genus Berberis are considered an interesting source of drugs to counteract the MDR. Their important properties are due to the antimicrobial properties of berberine, which interacts with FtsZ protein of *E. coli*. It is a tubulin-like protein belonging to the cell division machinery that represents the most widely studied bacterial target for novel drug development. This knowledge led to the synthesis of new simplified analogues of berberine in an attempt to maximize their interaction with FtsZ. The recombinant form of FtsZ was expressed in *E. coli*, purified and characterized to study the inhibitory capabilities, both *in silico* and *in vitro*, of berberine derivatives on FtsZ.

Lastly, in the Chapter five, the mechanism of action of Esc(1-21) diastereoisomer, named Esc(1-21)-1c, on *P. aeruginosa PAO1* has been investigated. Differential proteomic and transcriptional analyses were performed to elucidate the impact of Esc(1-21)-1c on the expression profile of *P. aeruginosa*, revealing a reduction in the production of the MexAB-OprM efflux pump. Furthermore, LC-MS/MS in MRM scan mode validated the proteomic findings. The precise mechanism of action of Esc(1-21)-1c on *P. aeruginosa* was explored by functional proteomics, leading to the identification of a transcriptional regulator responsible for activating the mexAB-oprM operon.

Chapter 1- Introduction

1.1 Antibiotic Resistance: The challenge posed by bacteria

1.1.1 How bacteria develop resistance?

Throughout human history, pathogenic bacteria have been a major cause of disease and mortality until the introduction of antibiotics. In recent decades, bacteria have steadily developed resistance to antibiotics due to their innate genetics and physiology, leading to an accumulation of MDR phenotypes in many bacterial species[1] (Figure 1). According to the United Kingdom government, 10 million deaths due to antimicrobial resistance could occur annually by 2050, becoming one of the leading causes of death in the world[2]. Antibiotic resistance in bacteria refers to the ability of these microorganisms to withstand the effects of antibiotics, rendering the drugs less effective or completely ineffective in treating bacterial infection[3]. The overuse and misuse of antibiotics in medical, agricultural, and veterinary settings contribute to the selection and proliferation of antibiotic-resistant strains. As a result, bacterial infections are becoming more challenging to treat, leading to prolonged illnesses, increased healthcare costs, and a higher risk of mortality[4].

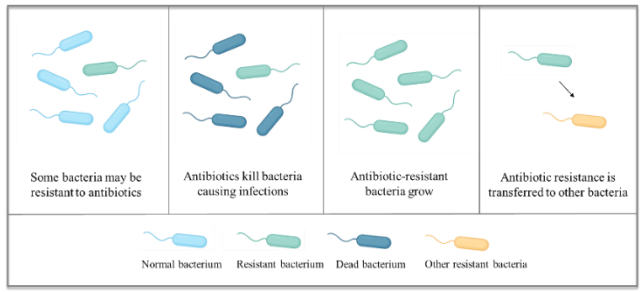

Figure 1. Stages in the development of antibacterial resistance.

The massive emergence of MDR pathogens and the rapid spread of new applications is pushing healthcare organizations and the pharmaceutical industry around the world to change their strategy and to stop the slow-growing production of synthetic antibiotics against the rapid growth of antibiotic-resistant microorganisms[5]. The 2012 Chennai Declaration in India served as evidence, where global experts formulated action plans in response to the unstoppable progression of superbugs[6]. Antimicrobial resistance poses one of the most significant challenges in the global health landscape, with intrinsic (or natural) and acquired resistance playing distinct roles against pathogens[7]. The distinction between these two types of resistance is crucial in addressing the complexity of antimicrobial resistance:

- ***Intrinsic resistance*** refers to the inherent ability of certain bacterial species to withstand the effects of antimicrobial agents due to specific structural or functional characteristics, including reduced permeability of the OM and efflux pumps activity of Gram-negative bacteria, which restricts the access of many antibiotics to their cells[8]. This intrinsic resistance is often encoded in the bacterial genome and is a result of millions of years of evolutionary adaptation. Therefore, it is a type of resistance inherent in the biology of certain microorganisms, making them naturally less susceptible to antimicrobial agents;

- ***Acquired resistance*** concerns the development of resistance in response to repeated exposure of antibiotics. Bacteria can acquire resistance through genetic mutations or the acquisition of resistance genes from other bacteria via horizontal gene transfer mechanisms. This enables bacteria to rapidly acquire new genetic elements containing information on how to evade the effects of antibiotics. A well-known example is the spread of plasmids containing antibiotic resistance genes among bacteria[9].

Intrinsic resistance necessitates personalized approaches, while acquired resistance calls for judicious management of antimicrobial use to slow the spread of resistant strains. Understanding these differences is crucial for developing targeted therapeutic approaches that take into account both forms of resistance in the design of treatment and prevention strategies. Addressing antibiotic resistance requires a multifaceted approach, including responsible antibiotic use, the development of new antimicrobial agents more effective for therapies used to counteract microbial diseases, and global efforts to enhance surveillance and stewardship practice[10].

1.1.2 Mechanisms of resistance

Antimicrobial resistance encompasses a variety of mechanisms employed by microorganisms to withstand the effects of drugs. These mechanisms include limiting uptake of drugs, modification of drug targets, inactivation of drugs, and activation of drug efflux systems. Intrinsic resistance may make use of different mechanisms such as limiting uptake, drug inactivation, and drug efflux, while acquired resistence provides drug target modification, drug inactivation and drug efflux mechanisms[11] (Figure 2):

- ***Limiting uptake of drugs***. Bacteria can restrict the entry of drugs into their cells. This mechanism involves the modification or reduction of pathways responsible for drug uptake. Bacteria can create a barrier to the effectiveness entry of antibiotics through the LPS layer. Microorganisms can also evolve structural alterations in their cell membranes or walls, creating barriers that limit the efficient absorption of drugs. Additionally, they may regulate the expression of transport proteins or channels involved in drug uptake, thereby controlling the income of antimicrobial agents[12];

- ***Modification of drug targets***. The molecular structure of the specific targets undergoes to adaptive changes, leading to modifications in the targeted sites. These modifications can reduce the binding affinity of drugs, rendering them less effective in disrupting essential microbial processes[13]. Over the years, various strains of the opportunistic *P. aeruginosa* have developed this resistance mechanism, causing modifications in the target sites of β-lactam antibiotics[14];

- ***Inactivation of drug***. Bacteria produce enzymes capable of neutralizing the activity of drugs, reducing their potency. The enzymatic inactivation occurs through various biochemical processes such as acetylation, phosphorylation, or hydrolysis, which result in chemical alterations of the drug molecules, rendering them inactive or significantly less effective;

- ***Activation of drug efflux systems***: Pumping out of drugs from the microbial cell. This process is facilitated by specialized efflux pumps that actively transport antimicrobial agents out of the cell, preventing them from reaching the necessary concentrations for therapeutic efficacy. By actively expelling drugs, microbial cells can maintain homeostasis and evade the lethal effects of therapeutic agents[15].

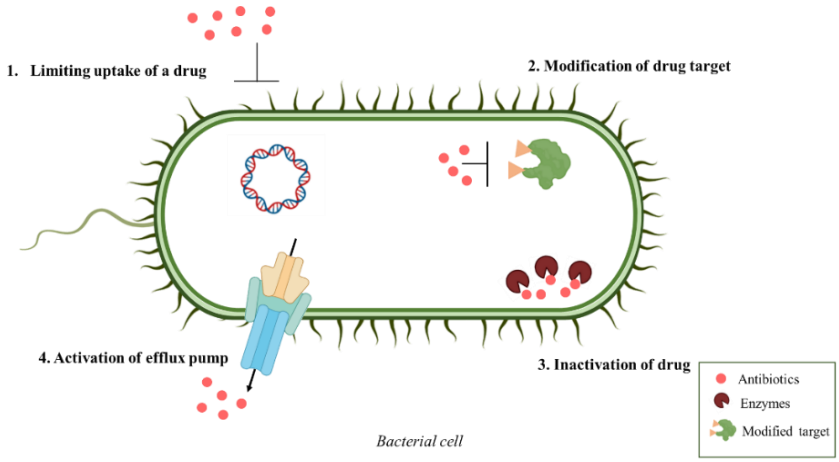

Figure 2. Schematic representation of resistance mechanisms.

Understanding the complexities of these resistance mechanisms is pivotal in formulating strategies capable of mitigating their impact, thereby preserving the effectiveness of antimicrobial treatments.

1.2 Investigating Novel Antimicrobial Agents to counteract antibiotic resistance

In the ongoing fight against antibiotic resistance, researchers are intensively focused on investigating novel antimicrobial agents to counteract the growing challenges posed by drug-resistant bacteria. This research involves new innovative strategies able to effectively target and eliminate resilient bacterial strains. The exploration of novel antimicrobial agents is crucial in the pursuit of alternative solutions, ensuring the sustenance of antimicrobial treatment efficacy in the face of emerging resistance threats. Among the novel classes able to slowing down the development of drug resistance, the use of AMPs[16] and NPs[17] is gaining the upper hand.

1.2.1 Beyond Antibiotics: The Promise of Antimicrobial Peptides in bacterial infections

AMPs have emerged as a class of antibiotics currently undergoing trials. They are considered promising candidates as new alternative therapeutic agents because of their wide range of bactericidal and antimicrobial activity, less toxicity and reduced development of resistance by target cells[18]. AMPs are also known as host defence peptides and are integral components of the innate immune system, ubiquitously distributed across the animal and plant kingdoms[19]. They comprise ~10–50 amino acids and exhibit protective capabilities against diverse kinds of infectious agents, including bacteria, yeast, fungi, viruses, and protozoa[20].

Among the natural AMPs of interest in scientific research, the majority are isolated from the amphibian skin, offering new perspectives in the development of innovative antibacterial therapies[21]. The skin of amphibians produce a diverse arrays of AMPs serving as a innate immune defense against microbial threats,

showing antimicrobial activity against both Gram-positive and Gram-negative bacteria[22].

To date, it is well-established that AMPs, owing to their net positive charge, show a high selectivity in targeting the negatively charged bacterial membranes. These membranes typically feature a high concentration of acidic phospholipids and a low amount of cholesterol[23-24]. The interaction between AMPs and bacterial membranes involves the exploitation of three different models: the barrel-stave model, the carpet-like model, and the toroidal model[25] (Figure 3).

- ***Barrel-stave model***: AMPs are perpendicularly inserted into the plane of the bacterial phospholipid bilayer, forming a transmembrane tunnel. The amphipathic AMPs align their hydrophobic regions with the lipid core of the membrane, while their hydrophilic regions are positioned inside the tunnel, creating a pore. These pores are proposed to allow the leakage of cytoplasmic components and disrupt the membrane potential. The barrel-stave model is favored by tyrosine and tryptophan residues, mainly located either at the C-terminus or N-terminus, which tend to share the interface in α-helix sections. This results in pore formation and in helix bundles that disrupt the membrane continuum;

- ***Carpet model***: AMPs accumulate and align parallel to the double layer, resembling a carpet covering the membrane. Throughout the permeation and membrane destruction process, peptides remain in contact with phospholipid head groups through electrostatic interactions. At high concentrations, peptides induce bilayer destruction through a detergent-like action, potentially leading to micelle formation. This interaction results in thinning of the OM layer relative to the inner layer, causing

large cracks, release of cytoplasmic components, interruption of membrane potential, and membrane disintegration;

- ***Toroidal model***: AMPs are perpendicularly inserted into the bilayer, inducing phospholipids to curve towards the inside of pore, forming a toroidal opening. The inner part of the pore consists of the hydrophilic regions of peptides associated with polar phospholipid groups. Unlike the barrel-stave model, the pore in this model is delimited by both peptides and hydrophilic lipid heads of phospholipids.

These models are not separate mechanisms, as the peptide-phospholipid interaction is dynamic and continuously transitioning.

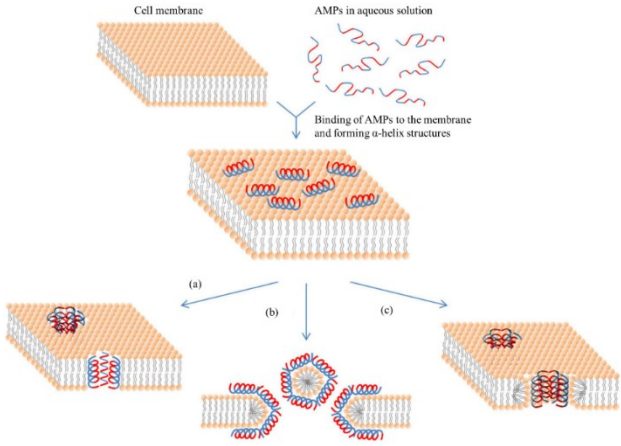

Figure 3. Mechanisms of action of AMPs. **(a)** Barrel-Stave model, **(b)** Carpet model, **(c)** Toroidal Pore model. Hydrophobic portions of AMPs are depicted in blue, while hydrophilic portions are represented in red[26].

However, recent insights suggest that AMP-induced microbial death may occur through mechanisms different from membrane disruption. Substantial evidence indicates that certain AMPs can interact with intracellular protein

targets, inducing cellular damage[27]. As research in this field progresses, a deeper understanding of the precise mechanisms of action will likely contribute to the development of effective therapeutic interventions against bacterial infections.

1.2.2 Natural Products from Plant Origins: An Innovative Approach to Antibacterial Intervention

NPs have garnered increasing attention in the scientific community for their potential as antibacterial agents. Due to their diverse chemical compositions and inherent bioactivity, they can be a valid alternative to antibiotics either as monotherapy or as adjuvant in order to improve the effectiveness of the failing drugs, making them an important source of antibacterial potential[28] (Figure 4).

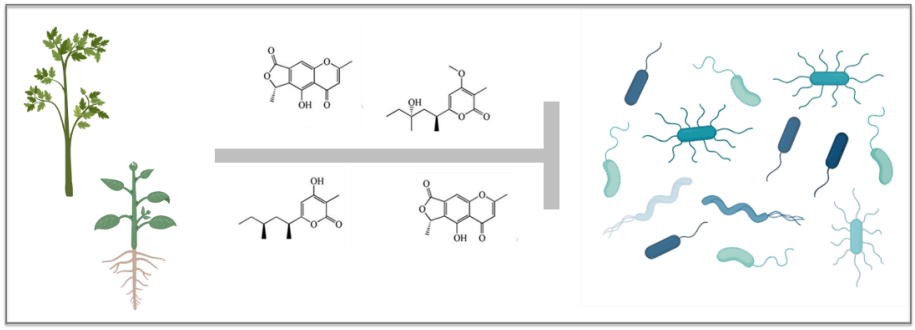

Figure 4. Schematization of plant-derived NPs inhibiting the activity of a broad spectrum of bacteria.

Plants constitute a primary reservoir of NPs due to their ability to develop adaptive responses across various ecosystems and adverse conditions, thereby establishing a resilient defense system against external challenges, including bacterial infections. The adaptive responses of plants involve the synthesis of secondary metabolites, which are chemical compounds not directly involved in the growth of the plant but play significant roles in interactions with the

environment, defense mechanisms, and communication with other organisms[29]. The robust defense system developed by plants encompasses a wide array of natural compounds, including alkaloids, flavonoids, terpenes, and phenolic compounds, which have been shown to possess antimicrobial properties. These compounds act as chemical defenses, deterring herbivores, pathogens, and competing plant species.

Since ancient times, plants have been extensively employed in the form of powders, tinctures, poultices, and herbal teas, serving as antibiotics to ward off infections, antineoplastics, analgesics, and cardioprotective agents. Even today, approximately 70-90% of the population in developing countries continues to rely on ancient remedies based on plant extracts, while in developed countries, the isolation and identification of biologically active compounds derived from NPs have led to the discovery of new therapies. NPs, in fact, account for about 50% of modern drugs, and plants have contributed to more than 60% of drugs either directly or indirectly in the treatment of major tumor forms. Medicinal plant drug discovery continues to provide new and important tools against various pharmacological targets, and their antibacterial potential has been reported in many studies[30].

In the context of bacterial infections, plants and their derivatives have been employed as antibiotics to combat microbial pathogens. The antimicrobial properties of certain plant compounds can inhibit the growth and reproduction of bacteria, providing a natural defense mechanism against infections. In a recent study, Manandhar et al. assessed the antimicrobial potential of four different plant extracts against twelve pathogenic microorganisms and two reference bacterial strains. The results confirmed the efficacy of certain selected plant extracts as natural antimicrobials, suggesting the possibility of employing them in pharmaceuticals for the treatment of infectious diseases[31].

Unfortunately, NPs pose inherent challenges, both in terms of their demanding and time-consuming isolation processes and the impracticality of large-scale total synthesis, primarily due to their elevated structural complexity and molecular weight[32]. The current strategic approach involves simplifying their structure through the removal of redundant atoms that do not actively participate in binding with the target. This structural simplification strategy aims to facilitate the chemical synthesis of smaller fragments, which retain or even enhance crucial biological parameters such as potency and/or selectivity. By eliminating non-essential components, the synthesis process becomes more streamlined, allowing for increased efficiency in the production of these bioactive compounds. In light of these challenges, the pursuit of developing new compounds derived from existing NPs becomes imperative. While the isolation and synthesis of these molecules present obstacles, their unique and diverse chemical structures often provide a rich source of inspiration for drug discovery. Additionally, the strategic simplification of these structures can lead to the creation of analogs or derivatives with improved pharmacological properties, enhancing their potential as therapeutic agents[33]. In conclusion, despite the challenges associated with NPs, the strategic simplification approach not only addresses synthesis difficulties but also opens avenues for creating bioactive compounds with enhanced attributes. The importance of this pursuit lies in the continued exploration of nature's chemical diversity for the development of novel pharmaceuticals, underscoring the significance of harnessing the untapped potential of existing NPs for the advancement of medical science.

1.3 The Promising Frontier of Antibacterial Therapies Development

Exploration of the mechanism of action of molecules exhibiting promising antimicrobial activity, as previously mentioned, can lead to the discovery of novel therapeutic agents. Advancements in antibacterial research are imperative to develop innovative treatments that effectively address bacterial infections and mitigate the emergence of resistant strains, thereby safeguarding public health against evolving microbial threats[34].

1.3.1 Advancements in Countering Multidrug-Resistant Bacterial Challenges

The discovery of antimicrobial strategies is intricately linked to the precise targets within bacterial systems, encompassing both Gram-positive and Gram-negative organisms. Bacteria are equipped with highly evolved defense systems, and various vital targets crucial for bacterial processes.

The OM, typical of Gram-negative bacteria, represents a potential target for antimicrobial strategies[35]. The lipid bilayer, composed of phospholipids and lipopolysaccharides, acts as a formidable barrier that protects the bacterium from environmental threats and hinders the penetration of antibiotics. Targeting the OM is a promising avenue for drug development., as it provides access to essential processes such as nutrient uptake, cell division, and virulence factors[36]. Recent studies have elucidated the mechanisms by which certain AMPs disrupt OM integrity, increasing the susceptibility of the MDR pathogen *A. baumannii* to conventional antibiotics[37]. Vetterli et al. have shown that the peptide thanatin is able to inhibit the formation of the Lpt complex in *E. coli*, compromising LPS assembly at the OM and affecting the permeability barrier properties[38]. In

addition, diterpenes such as totarol have been shown to inhibit multidrug efflux pump activity in MRSA[39]. Bacterial efflux pumps represent a integral component of microbial defense mechanisms against antimicrobial agents. These membrane-spanning proteins are involved in the active extrusion of a diverse array of substrates, including antibiotics, toxins, and other xenobiotics, thereby conferring a multi-drug resistance phenotype to bacteria[40] (Figure 5).

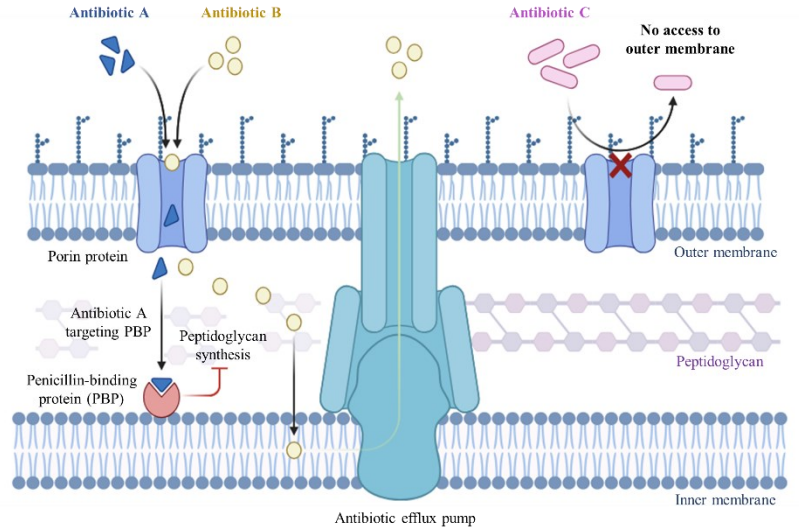

Figure 5. Bacterial efflux pumps in Gram-negative bacteria.

The defense mechanisms developed by bacteria over the years could be altered by designing inhibitors to block pump activity or by identifying alternative drug targets to bypass these defense mechanisms. Consequently, EPIs have emerged as therapeutic agents against antibiotic resistance[41], able to impair the active extrusion of antimicrobial agents from bacterial cells. In this way, EPIs can also act synergistically with antibiotics to enhance their intracellular concentrations[42]. A plethora of research studies have explored the synthesis and evaluation of novel EPIs, aiming to mitigate the challenges posed by efflux pumps in various bacterial pathogens. For instance, Tambat et al. elucidated the potential of RP2 as a potent

EPI, demonstrating its ability to synergistically potentiate the antibacterial activity of conventional antibiotics against different *S. aureus* strains[43]. Additionally, recent investigations have highlighted some natural and synthetic compounds acting as EPIs against *M. tuberculosis*[44].

Another approach gaining prominence in the perspective of attenuating the pathogenic potential of bacteria without exerting a strong selective pressure leading to resistance development is the targeting of virulence[45]. By elucidating the molecular mechanisms underlying virulence, researchers can identify key components critical for the progression of infections. Attenuating virulence may render bacteria less harmful, thereby mitigating the need for the rapid evolution of resistance mechanisms.

Recent studies have demonstrated the efficacy of inhibiting key virulence determinants to attenuate pathogenicity for a number of important pathogens. For instance, in a study published by Quinn et al. in 2021, the inhibition of quorum sensing systems in *P. aeruginosa* resulted in a significant reduction in biofilm formation and virulence[46]. Additionally, literature data also highlighted the potential of disrupting bacterial Type II secretion systems as a means to attenuate the pathogenicity of various Gram-negative bacteria[47].

Cusumano *et al.* have developed a series of mannoside compounds as alternative to conventional antimicrobial drugs. They revealed the remarkable capability of these agents to disrupt the binding interaction between uropathogenic *E. coli* and bladder epithelial cells, specifically targeting the FimH receptor. This interference effectively interrupts the life cycle of *E. coli*, resulting in the resolution of the infection[48].

Finally, one of the most studied vital targets in bacteria is the machinery governing cell division, which plays a pivotal role in their survival and

proliferation (Figure 6). The process of bacterial cell division, characterized by binary fission, is regulated by a highly coordinated interplay of proteins and regulatory mechanisms[49].

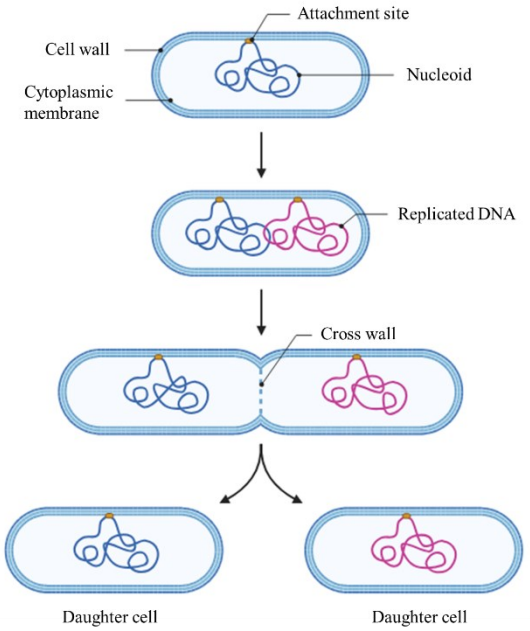

Figure 6. Binary fission steps. Initiation of DNA replication in a prokaryotic parent cell triggers the synthesis of a duplicate DNA strand. Cell elongation ensues, accompanied by the formation of a cross wall, ultimately leading to the separation of daughter cells.

Targeting essential proteins responsible for bacterial cell division can lead to cell death and hinder the ability of bacteria to propagate. Proteins involved in bacterial cell division often do not have a counterpart in eukaryotic cells, rendering them promising candidates for antimicrobial intervention[50].

1.3.2 Bacterial Proteins as Therapeutic Targets: A Comprehensive Proteomic Approach

The growing threat of bacterial strains resistant to multiple drugs requires continued innovation in the approaches used to effectively combat these pathogens. This era encompasses a spectrum of strategies, ranging from the development of new antibiotics to the repurposing of existing drugs. However, the development of new antimicrobial substances requires a comprehensive understanding of the bacterial targets to be addressed. This knowledge is crucial for the design of new molecules capable of addressing emerging challenges in the antimicrobial field. In this context, proteins identification stands out, and significant progress has been made in the field of proteomics, a recent and innovative 'omics' technology assisting progress made in biochemical sciences. Proteomics addresses the challenge of identifying novel protein targets among the numerous protein products encoded by prokaryotic genomes[51]. The information stored in protein databases (UniProt) enables an understanding of the functions performed by proteins in different species. The synergy of utilizing sophisticated bioinformatics tools, such as STRING or Cytoscape, further enhances our ability to decipher the complex interplay of proteins within cellular systems. This allows the clustering of identified proteins, highlighting their interactions, and the discovery of altered pathways or the identification of proteins targeted by specific antimicrobial agents.

Proteomic applications can be systematically grouped into two primary categories: differential and functional proteomics (Figure 7).

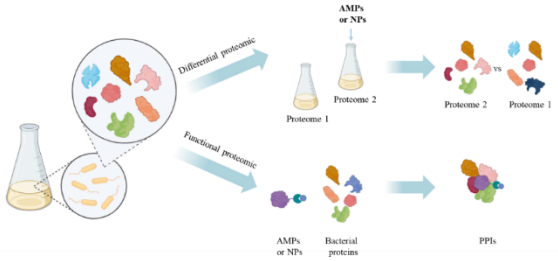

Figure 7. General representation of differential and functional proteomic approaches on bacterial cells.

Differential proteomics focuses on qualitative and quantitative variations in protein expression levels, a critical aspect of understanding the dynamic cellular responses to various stimuli, including antimicrobial treatments[52]. This methodological framework holds promise in the context of antimicrobial treatments and in a broader spectrum of research areas, contributing to our comprehension of cellular dynamics and signaling pathways.

Functional Proteomics allows to identify PPIs in order to comprehensively assemble protein complexes, thereby elucidating the intricate cellular pathways involved in specific biological processes[53]. This ability can also be addressed to identify the specific protein(s) targeted by individual antibiotics.

The integration of these approaches with MS has propelled significant advancements in the investigation of PPIs within the realm of proteomics. The discovering of novel putative targets, coupled with the identification of protein-ligand interacting regions, provides a foundation for the future design of highly specific and effective drugs, especially crucial in addressing the challenge of MDR bacteria[54].

1.4 Aims of the project

Antibiotic resistance poses a significant challenge in modern healthcare, leading to the urgent need for alternative therapeutic strategies. One promising approach is the identification of protein targets within bacterial systems to develop innovative therapeutic interventions[55]. This pursuit originates from the comprehension of the mechanism of action of antimicrobial molecules capable of overcoming antibiotic resistance, such as AMPs and NPs. By elucidating how these molecules interact with specific bacterial targets and disrupt essential cellular processes, new weaknesses in bacterial pathogens can be discovered.

This serves as the background for the present thesis project. Primarily, the project aims to identify protein targets by elucidating the mechanism of action of AMPs derived from frog skin, specifically Mag-2 and Temp-L, on Gram-negative and Gram-positive bacteria, respectively. To date, the membrane-disrupting mechanism of these peptides has been predominantly described, with limited attention given to potential intracellular targets. Accordingly, the identification of protein targets for the mentioned AMPs represents a starting point for the development of targeted antimicrobial strategies. However, these well-known AMPs exhibit several limitations, including hemolytic and toxic activies, as well as susceptibility to degradation by bacterial proteases, rendering them unsuitable for prospective therapeutic applications[56].

Therefore, in the same perspective as the identification of protein targets, the secondary aim of the project is to develop new antimicrobial compounds that have not been previously explored, and to examine their mechanisms of action against Gram-negative bacteria. In particular, the mode of action of novel berberine derivatives and a diastereoisomeric form of the Esc(1-21) peptide, known as Esc(1-21)-1c, was investigated on *E. coli* and *P. aeruginosa*, respectively. This investigation aims to elucidate the molecular-level mechanisms underlying the

modulation of biological processes following treatment with these antimicrobial agents.

Various methodologies have been employed to achieve these aims, encompassing biochemical assays, in silico modeling, and *in vitro* and *in vivo* validation studies. This approach provides a robust framework for investigating the efficacy and mechanisms of action of both established and novel antimicrobial compounds, thereby advancing our comprehension of antimicrobial resistance and facilitating the development of innovative strategies through the identification of protein targets.

Chapter 2- Characterization of Magainin-2 binding to the target protein BamA in *E. coli*

2.1 Introduction

Mag-2 belongs to the magainins, a family of linear, amphipathic and cationic AMPs. It was isolated by Zasloff in 1987 from the skin of the clawed African frog *Xenopus laevis*[57] and was one of the first evidences demonstrating the potential of frog skin secretions as a source of new antibacterial agents. Mag-2 is an α-helical peptide (Figure 8), composed of 23 amino acid residues (GIGKFLHSAKKFGKAFVGEIMNS-NH_2), with a net positive charge of +3.

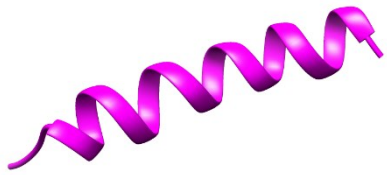

Figure 8. 3D structure of Mag-2. The image has been generated with UCSF CHIMERA software[58].

The peptide exerts its antimicrobial activity on bacterial membranes according to a toroidal mechanism, leading to the formation of a transient pentameric pore, followed by the peptide translocation through the bilayer and a disruption of the membrane[59] (Figure 9).

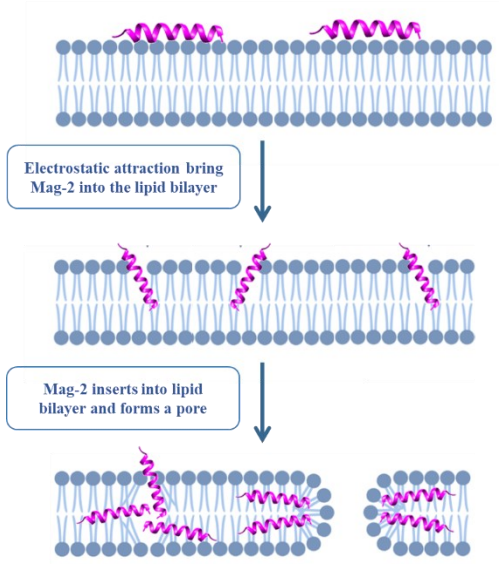

Figure 9. Mag-2 toroidal pore. The peptide structures perpendicular to the bilayer within the pore. The hydrophobic residues of the peptide face away from the inner surface of the pore which contains hydrophilic components.

The interactions between Mag-2 and the membrane have been investigated extensively through various biophysical techniques such as fluorescence spectroscopy, CD spectroscopy, NMR spectroscopy, and ITC[60-61-62-63].

However, despite most studies performed on Mag-2 membranolytic effect, the molecular events underlying its mechanism of action remains not yet completely understood. Recent functional proteomics experiments in *E. coli* identified Mag-2 protein targets, including OMPs like Omp N/C/A and the Bam complex (ABCD), as reported by A. Di Somma, PhD thesis "Regulation of biofilm development in Gram-negative bacteria: new antimicrobial strategies", 2020.

OMPs are involved in multiple critical cellular functions in Gram-negative bacteria, including nutrient uptake, proteins secretion, and virulence-related adhesion. In *E. coli*, OMP β-barrels assume a configuration characterized by

closed antiparallel β-sheets, which are stabilized by hydrogen bonds formed between the initial β-strand and a conserved C-terminal β-strand. This arrangement results in the formation of a structural feature termed the 'β-seam'[64]. Following synthesis in the cytoplasm, OMPs undergo translocation across the inner membrane via the SecYEG translocon in a SecA dependent manner within the periplasm. The Skp protein and the SurA chaperon drive nascent OMPs into the BAM complex, to complete folding preventing their aggregation[65].

The BAM complex, initially identified in *N. meningitidis* and then in *E. coli*, is a heterooligomer with a mass of ~ 200 kDa, composed of 5 proteins designated as BamA-BamE[66]. While BamA is an integral protein of the OM, BamB-E are lipoproteins. BamA, a conserved component across all Gram-negative bacteria, serves as the central element of the BAM complex. This complex is a crucial target because of its involvement in the folding of OMPs within the OM, providing partial protection to bacterial cells against harmful chemicals[67]. Despite a well-established understanding of the general function of the Bam complex, the mechanistic contributions of its individual constituents (BamA to -E) remain incompletely understood. BamA and BamD are considered core components due to their high degree of conservation. BamD functions in recruiting incoming OMP substrates, while BamA is central to OMP folding owing to its transmembrane nature. The functions of BamB, -E, and -C have yet to be fully elucidated[68]. Since BamA plays a crucial role in the folding and insertion of nascent β-barrel OMPs in the OM, it might represent a significant antibiotic target in Gram-negative bacteria. Structurally, BamA has a β-barrel structure composed of 16 β-strands and five N-terminal POTRA domains. These domains, located in the periplasm, are involved in the interactions with the four lipoprotein components. Together, they assemble into a ring-like structure beneath the β-barrel. Each POTRA domain, comprising approximately 75 residues and organized into two antiparallel

α-helices folded on a three-layered β-sheet, serves as an autonomously folding unit[69] (Figure 10).

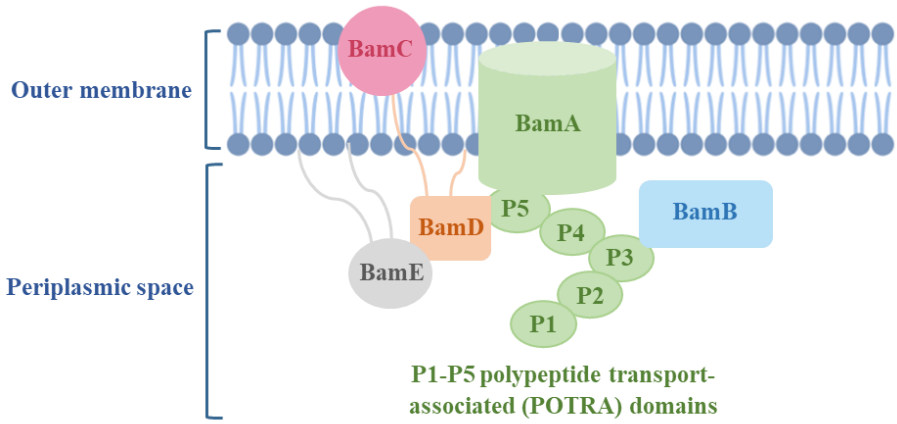

Figure 10. Polypeptide transport-associated (POTRA) domains.

In the periplasm, OMPs bind the POTRA domains adopting a closed β-hairpin conformation that bridges the two terminals, leading to protein folding[70]. This results in the destabilization of the junction between the β1 and β16 strands of the BamA β-barrel, allowing OMPs to leave BamA through the lateral opening of the β-barrel domain and to be incorporated into the bilayer of the OM[71] (Figure 11).

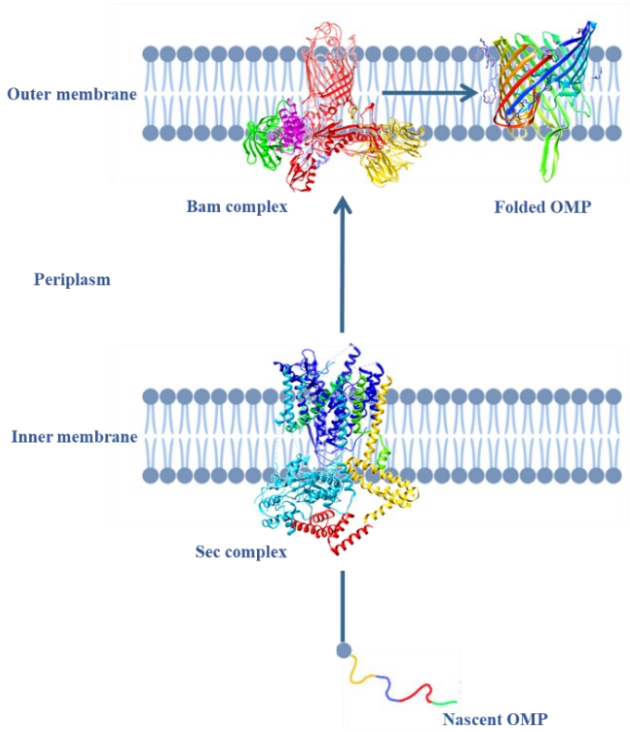

Figure 11. Representation of OMPs folding.

Recently, molecular docking analysis highlighted a strong interaction between Mag-2 and BamA, with the peptide predicted to bind the transmembrane β-barrel domain of BamA, crucial for OMPs binding and folding (Figure 12).

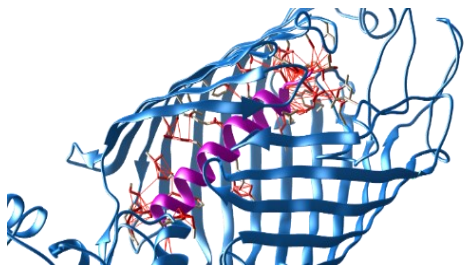

Figure 12. Docking between BamA (in blue) and Mag-2 (in purple). Adapted with the permission from Di Somma et al. 2022 Frontiers in Chemistry.

In this Chapter the *in vitro* and *in vivo* interaction between Mag-2 and BamA was verified by biochemical and spectroscopic methodologies. A recombinant form of BamA was expressed, purified and characterized in *E. coli*. Fluorescence spectroscopy and DLS investigations confirmed the interaction of Mag-2 with the recombinant protein BamA, suggesting that Mag-2 might inhibit BamA activity and impair the folding of OMPs. The effect of the Mag-2/BamA complex formation on the correct folding of OMPs in *E. coli* was clarified by a targeted proteomic approach.

2.2 Experimental methods

2.2.1 Recombinant production and purification of the protein target $BamA_{p5}$

The 6XHis-tagged *E. coli* $BamA_{p5}$, consisting of the β-barrel domain and the fifth POTRA domain (residues 344-810), was cloned into the pET30b_BamA_PD5 plasmid and expressed in *E. coli* K12. The induction of protein expression occurred in LB (Oxoid) medium with 50 $\mu g \cdot \mu L^{-1}$ kanamycin by adding 1 mM IPTG at 0.5 $OD_{600nm} \cdot mL^{-1}$. After the incubation for 3 h at 180 rpm at 37°C, bacterial cells were harvested by centrifugation for 15 min at 5000 rpm at 4°C, and the resulting pellets were resuspended in lysis buffer (150 mM NaCl, 20 mM Tris-HCl pH 8.0, 1 $mg \cdot mL^{-1}$ lysozyme). The purification of $BamA_{p5}$ was performed from inclusion bodies. Bacterial cells were sonicated, the pellet was washed with lysis buffer, and resuspended in lysis buffer containing 5 $mg \cdot mL^{-1}$ lysozyme and 1 % Triton. The solution was stirred for 3 h and centrifugated for 20 min at 15000 rpm at 4°C. The process was repeated without lysozyme, followed by centrifugation. The pellet was washed with lysis buffer to remove the detergent and centrifuged for 20 min at 15000 rpm at 4°C.

The obtained pellet was resuspended in denaturing buffer (6 M Gu-HCl, 20 mM Tris-HCl pH 8.5) and homogeneized using ultraturax. After centrifugation, the solution was loaded onto a 20 mL Ni-NTA column with denaturing buffer containing 20 mM imidazole. Elution of $BamA_{p5}$ was achieved with denaturing buffer containing 300 mM imidazole. Subsequent protein refolding was carried out by adding the eluate dropwise to a tenfold volume of 20 mM Tris-HCl and 0.5% Triton for 12 h at 8°C under stirring. The solution was diluted with 20 mM Tris-HCl pH 8.4 until 0.2 % Triton was reached. Protein concentration was quantified using the Bradford assay (Bio-Rad protein assay) according to the

manufacturer's instructions. Protein purity was assessed by 10% SDS-PAGE and visualized using Coomassie Brilliant Blue staining solution (Bio-Rad, USA).

2.2.2 Structural characterization of $BamA_{p5}$ by MALDI-TOF and Circular Dichroism

The primary structure of $BamA_{p5}$ was validated by mass mapping using MALDI-TOF on a MALDI Voyager-DET STR spectrometer. Following electrophoresis and staining, the gel band corresponding to the molecular weight of $BamA_{p5}$ was excised and subjected to in-situ hydrolysis. Reduction was achieved using 10 mM DTT in 50 mM AMBIC (Sigma-Aldrich) for 45 min at 56°C to reduce cysteine residues involved in disulfide bridges. The gel band was dehydrated with 100 % ACN and then rehydrated with 50 mM AMBIC, containing 55 mM IAM for the alkylation reaction of cysteine residues in a dark environment at room temperature for 30 min. The dehydrated gel band was treated with 10 $ng \cdot \mu L^{-1}$ trypsin (Sigma-Aldrich) solution in 50 mM AMBIC pH 8.0 for 1 h at 4°C. The sample was then incubated for 16 h at 37°C in 50 mM AMBIC. Following hydrolysis, the supernatant was collected, acidified with 20 % TFA, (Sigma-Aldrich), and any remaining peptides in the gel were extracted with 50 µL of ACN. A second extraction was performed using 20 µL of 0.2 % formic acid (HCOOH, Chem-Lab, Eernegem, BE) followed by ACN. The obtained peptide mixture was dried by a Speed-Vac system and resuspended in 0.2 % HCOOH.

The sample was co-crystallized on a MALDI plate together with 10 mg/mL of α-cyano-4-hydroxycinnamic acid dissolved in 70 % ACN and ionized by laser pulse. The analysis was performed positively, using the instrument in reflectron mode (range of 400-500 m/z). The correct folding of the protein was subsequently analyzed by CD using a JASCO J-715 spectropolarimeter equipped with a Peltier thermostatic cell holde (Model PTC-348WT) in 1 cm optical path-lenght quartz cell. CD spectra were acquired in the range 190-250 nm, performing three

accumulations for each measure, a scanning speed of 100 nm·min^{-1} and data pitch of 0.2 nm.

2.2.3 Fluorescence Spectroscopy

Fluorescence titration experiments were performed using a Fluoromax-4 spectrofluorometer from Horiba Scientific, employing a 1 cm optical path-lenght quartz cell under controlled temperature conditions with a Peltier control system at 20°C. Titrations were conducted in 20 mM Tris-HCl pH 8.4 and 0.2 % Triton. The intrinsic fluorescence intensity of $3.7 \cdot 10^{-6}$ M $BamA_{p5}$ was monitored at 280 nm (slit 4 nm), while the emission was recorded at 308 nm (slit 4 nm), both in the absence and the presence of increasing concentrations of Mag-2 peptide (ranging from 2 to 18.64 µM). All experiments were carried out in duplicate. The changes in fluorescence intensity were analyzed by fitting the data to the "one site-specific binding" equation of GraphPad Prism 9 (GraphPad Software, San Diego, CA, USA).

2.2.4 Dynamic Light Scattering (DLS)

A homemade instrument composed by a Photocor compact goniometer, an SMD 6000 Laser Quantum 50 mW light source operating at 532.5 nm, a photomultiplier (PMT-120-OP/B), a correlator (Flex 02-01 D), and a thermostat bath for the temperature control was used to carry out DLS measurements. Ten independent measurements were performed for $BamA_{p5}$ without and in presence of Mag-2. The analysis was performed with the Precision Deconvolve program[72], and the regularization procedure returned an average diffusion coefficient, used to calculate the hydrodynamic radius by Stokes-Einstein relation:

$$D = \frac{TK_b}{6\pi\eta R_h}$$

where D is the diffusion coefficient, K_b is the Boltzmann constant, T is the temperature, η is the viscosity of the solvent[73].

2.2.5 Extraction of membrane proteins and Western Blot analysis

The *E. coli* K12 cells were grown in the presence and absence of 50 µM Mag-2 for 1h, 2h and 3h, using biological duplicates. Subsequent to cell lysis, supernatants were obtained and subjected to ultracentrifugation for 2h at 54000 rpm at 4°C to separate cytosolic proteins (supernatant) from membrane proteins (pellet). The membrane proteins were resolubilized in 50 mM di Tris-HCl, 500 mM di NaCl, 10 % glycerol, 4 mM DTT, 1 mM PMSF and 6 mM CHAPS at a ratio of 1mL per gram of pellets for 16 h at 4°C. This was followed by another round of ultracentrifugation for 2h at 54000 rpm at 4°C[74].

20 µg of OMPs were loaded and separated on a 10% SDS-PAGE gel. The samples were prepared with Laemli Buffer (100 mM Tris HCl pH 6.8, 4 % SDS, 20 % glycerol, bromophenol blue, 100 mM DTT) and boiled at 99°C for 10 minutes. The electrophoretic run started at 100 V. Separated proteins were transferred onto a PVDF membrane (Millipore, Darmstadt, Germany) by electroblotting. Membrane was blocked with 5% nonfat milk in PBS for 1 hour and were incubated overnight at 4°C with rabbit polyclonal anti-OmpA antibody (Antibody Research Corporation, USA) at a dilution 1:10000 in PBS, 0.2% Tween 20. Membranes were incubated with an anti-rabbit HRP secondary antibody (Sigma Aldrich, Milan, Italy) at a dilution 1:10000 in PBS, 0.2% Tween 20 for 1 h at room temperature. Immunoreactive bands were developed by Pierce™ ECL Western Blotting Substrate (ThermoFisher Scientific, Waltham, MA), and the proteins were visualized by exposing the membrane to autoradiography films. The amount of OmpA was evaluated by densitometric analysis of the corresponding western blot band using ImageLab software and the obtained data were

statistically analyzed by t-test, using GraphPad Prism 9 (GraphPad Software, San Diego, CA, USA).

2.2.6 *In solution* digestion and LC-MS/MS analysis in MRM scan mode

A total of 100 µg of *E. coli* OMPs, both treated and untreated with 50 µM Mag-2, were subjected to MS analysis. Protein hydrolysis involved an in-solution digestion approach, followed by desalination on a Pierce C18 spin column (Thermo Scientific, Rockford, USA)[75]. The resulting peptide mixtures were analyzed through LC-MS/MS in MRM ion mode, using a Xevo TQ-S (Waters, Milford, MA, United States) equipped with an IonKey UPLC Microflow Source coupled to an UPLC Acquity System (Waters, Milford, MA, United States). For each run, 1µL of peptide mixture was injected and separated on a TS3 1.0 mm x 150 mm analytical RP column (Waters, Milford, MA, United States) at 45°C with a flow rate of 3 $\mu L \cdot min^{-1}$. Elution of peptides occurred through a 55-min linear gradient of 0.1 % HCOOH in ACN (eluent B) against 0.1 % HCOOH in water (eluent A) from 7 % to 95 %.

The MRM analyses were performed in positive ion mode, monitoring the best peptides of OmpA and OmpF. The selection of the best precursor ion-product ion transitions and the instrumental parameters, including CE, dwell time with a minimal of 5 ms, and cone voltage (35 V), were employed by Skyline software (3.7, 64-bit version MacCoss Lab Software, University of Washington, United States)[76]. The selection of prototypic peptides for each protein target was calculated by matching data from the Skyline software and those collected in online repositories, e.g., SRM Atlas. Peptides with no missed cleavages were considered, and two to five best transitions per peptide were chosen from the top-ranked y- and b- fragments. A total of 18 peptides for OmpA and OmpF proteins were selected, and 140 transition were monitored during a single analysis. Each

experiment was performed in duplicate and the obtained data were statistically analyzed by t-test, using GraphPad Prism 9 (GraphPad Software, San Diego, CA, USA).

2.3 Results and Discussion

2.3.1 *In vitro* study of the Mag-2/BamA complex formation

Prior functional proteomics and molecular docking analyses have elucidated the interaction between Mag-2 and the BamA protein, which has recently emerged as a target for antimicrobial development[77]. Due to its pivotal role in bacterial viability, inhibition of BamA function could potentially compromise OM integrity, heightening susceptibility to antibiotics. Motivated by these findings, the investigation of the potential binding mechanism was performed. A fragment of BamA, named $BamA_{p5}$, encompassing the β-barrel domain and the fifth POTRA domain (residues 344-810), was expressed in recombinant form in *E. coli*. Specifically, the protein was produced in inclusion bodies, purified through IMAC affinity chromatography under denaturing conditions, and underwent a refolding process. SDS-PAGE confirmed protein purity (Figure 13), while validation of its primary structure was achieved through peptide mapping using MALDI-TOF, resulting in a sequence coverage of 90% (Figure 14).

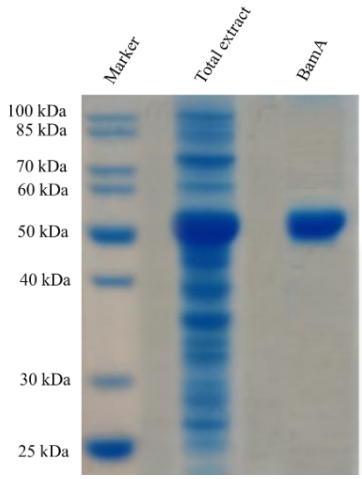

Figure 13. 10% SDS-PAGE gel showing the fractions from the refolding process.

(a)

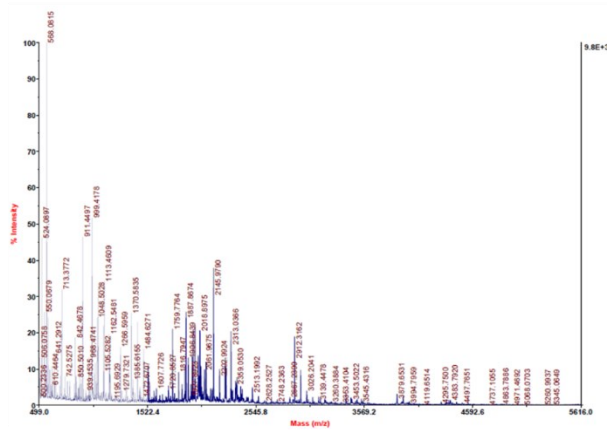

(b)

MGNRFYVRKI	RFEGNDTSKD	AVLRREMRQM	EGAWLGSDLV
DQGKERLNRL	GFFETVDTDT	QRVPGSPDQV	DVVYKVKERN
TGSFNFGIGY	GTESGVSFQA	GVQQDNWLGT	GYAVGINGTK
NDYQTYAELS	VTNPYFTVDG	VSLGGRLFYN	DFQADDADLS
DYTNKSYGTD	VTLGFPINEY	NSLRAGLGYV	HNSLSNMQPQ
VAMWRYLYSM	GEHPSTSDQD	NSFKTDDFTF	NYGWTYNKLD
RGYFPTDGSR	VNLTGKVTIP	GSDNEYYKVT	LDTATYVPID
DDHKWVVLGR	TRWGYGDGLG	GKEMPFYENF	YAGGSSTVRG
FQSNTIGPKA	VYFPHQASNY	DPDYDYECAT	QDGAKDLCKS
DDAVGGNAMA	VASLEFITPT	PFISDKYANS	VRTSFFWDMG
TVWDTNWDSS	QYSGYPDYSD	PSNIRMSAGI	ALQWMSPLGP
LVFSYAQPFK	KYDGDKAEQF	QFNIGKTWLE	HHHHHH

Figure 14. (a) Mass spectrum of $BamA_{P5}$ illustrating the relative abundance of ions plotted against the mass/charge (m/z) ratio. **(b)** The highlighted amino acids depict the peptide map of the $BamA_{P5}$ protein sequence. Sequence coverage was determined by comparing experimental molecular weights with theoretical values obtained through in silico tryptic hydrolysis on the known protein sequence.

The correct folding of the protein was assessed using CD (Figure 15). The CD spectrum exhibited a distinct minimum at approximately 217 nm and a maximum at 195 nm. Deconvolution of the CD spectrum revealed the presence of 44.6% β sheet structure, 1.3% α-helix and 15.5% turn, confirming the anticipated folding.

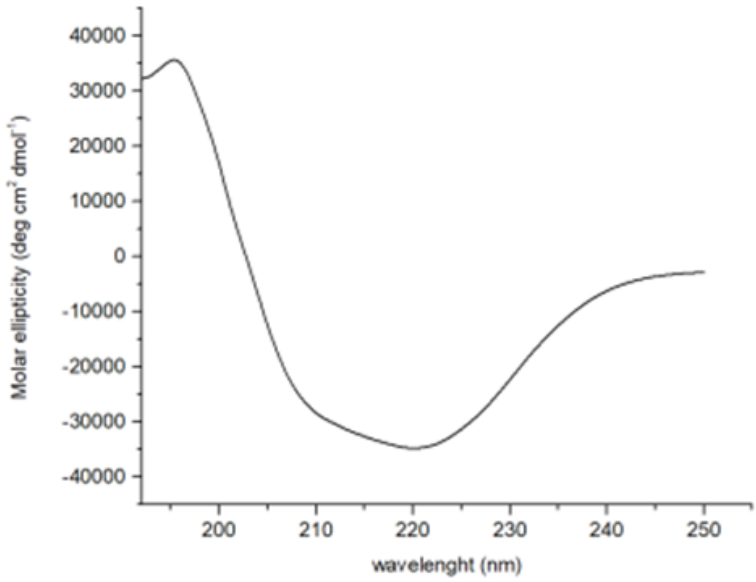

Figure 15. The CD spectrum depicts the structural characteristics of the $BamA_{p5}$ protein at a concentration of $3.7 \cdot 10^{-6}$ M in 20 mM Tris-HCl pH 8.4 buffer.

The *in vitro* interaction between Mag-2 and $BamA_{p5}$ was investigated using fluorescence binding assays. These experiments were specifically designed to monitor changes in the tertiary structure of the protein following its binding with Mag-2. This objective was accomplished by measuring the intrinsic fluorescence emitted by $BamA_{p5}$ as it was incubated with increasing concentrations of Mag-2. The collection of emission spectra of $BamA_{p5}$ at different Mag-2 concentrations is depicted in Figure 16.

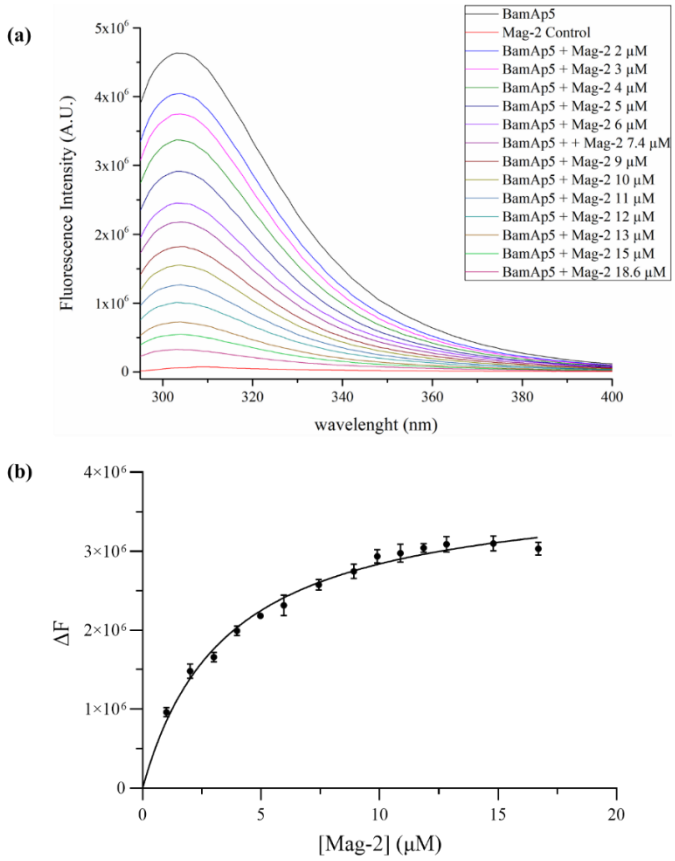

Figure 16. Fluorescence binding assay of Mag-2 and $BamA_{p5}$ **(a)** Intrinsic fluorescence spectra (λex = 280 nm) of $3.7 \cdot 10^{-6}$ M $BamA_{p5}$ by adding different concentration of Mag-2 every 5 min at 20°C. **(b)** Experimental data were adjusted to a non-linear regression and the Kd binding constant was estimated using GraphPad Prism 9. The experiments were performed in duplicate, and the SD is reported as error bars. The figure was adapted with the permission from Di Somma et al. 2022 Frontiers in Chemistry.

The fluorescence of $BamA_{p5}$ is decreased with increasing concentrations of the peptide, demonstrating the interaction between the peptide and protein. Mag-2 alone does not significantly absorb radiation, thereby not influencing the fluorescence of the protein-peptide complex. Data analysis revealed a high

affinity of Mag-2 for $BamA_{p5}$, with a Kd value of $3.5 \cdot 10^{-6}$ M ± 0.1. The low nanomolar value of Kd strongly confirmed the high affinity of the peptide for BamA.

Complementary to the fluorescence binding, DLS measurements were performed on the protein (2 $mg \cdot ml^{-1}$) both in the absence and the presence of the peptide at a concentration ten times higher than the protein one. The experiments were carried out in collaboration with the research group of Prof. Luigi Paduano (Department of Chemical Sciences – University Federico II – Naples). The analyses demonstrated the exclusive existence of the protein in its monomeric form in both samples. Furthermore, a clear reduction in the hydrodynamic radius of the protein from 4.7 ± 0.1 to 4.3 ±0.1 nm was observed in the presence of Mag-2 (Figure 17). These findings are in agreement with the hypsochromic shift recorded by fluorescence spectroscopy, providing robust support for the *in vitro* interaction between the protein and the peptide.

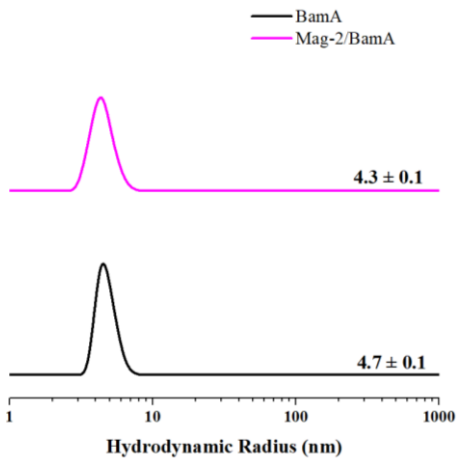

Figure 17. Distribution curves of the hydrodynamic radius of the aggregates in solution.

2.3.2 Functional characterization of Mag-2/BamA complex

All Gram-negative bacteria OMPs perform many biological processes. These proteins are inserted and folded into the OM by the BAM complex[78]. The interaction between Mag-2 and BamA is expected to hinder the binding of OMPs within the BamA β-barrel, thus compromising their proper folding. Based on this premise, the impact of sub-MIC concentrations of Mag-2 (50 μM and 75 μM) on the production of OMP proteins in *E. coli* was investigated, using appropriate controls. At first, the amount of the OmpA protein was analyzed by Western Blot with a specific antiOmpA antibody. OMPs were purified from the *E. coli* extract and results clearly shows a gradual decrease in OmpA levels ranging from 20 to 90% compared to untreated cells, over various time intervals (Figure 18a). The same experiment was repeated using a higher Mag-2 concentration (75 μM) for a fixed time equal to 1 h (Figure 18b). The results demonstrated a decrease in the abundance of OmpA within the *E. coli* membrane following treatment with Mag-2. The reduction in OmpA levels exhibits a dual dependency. In details, Figure 18a a shows the temporal dynamics of OmpA reduction, revealing a time-dependent modulation in response to Mag-2 treatment. The varying intervals of exposure highlight the evolving impact of the peptide on OmpA levels over time. Figure 18b delineates the dose-response relationship, underscoring the influence of Mag-2 quantity on the observed reduction in OmpA.

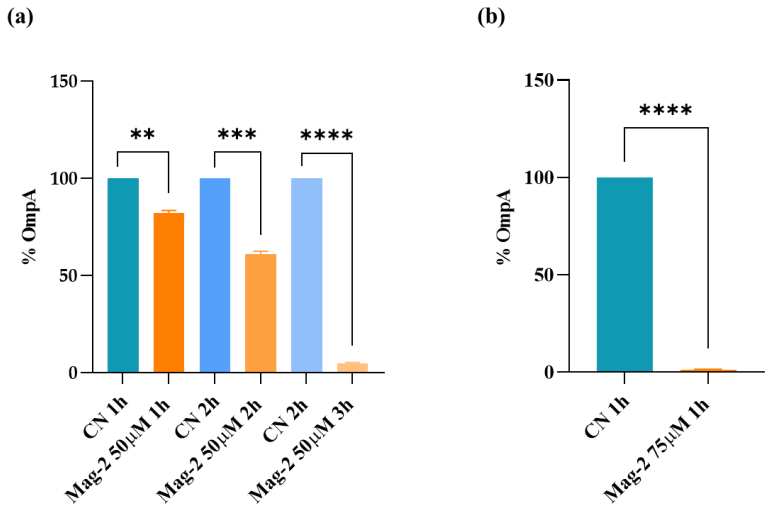

Figure 18. Densitometric analysis of OmpA content derived from Western Blot experimentation using Image Lab software. The y-axis represents the percentage of OmpA, while the x-axis delineates the experimental conditions. Results are presented as the mean ± SD from two independent experiments. Statistical significance was determined through t-test analysis using GraphPad Prism 9 and p-value < 0.0001 was indicated as **** in the graph.

The abundance of *E. coli* membrane proteins, OmpA and OmpF, was also evaluated by LC-MS/MS in MRM mode, employing identical experimental conditions as those used in the Western Blot analysis. The experiments were carried out in collaboration with the research group of Prof. Angela Amoresano (Department of Chemical Sciences – University Federico II – Naples). *E. coli* OMPs were digested with trypsin, and the resulting peptide mixtures were analysed in biological triplicate. A panel of 18 peptides derived from OmpA and OmpF was selected, encompassing the monitoring of 140 transitions in a single analytical run. Figure 19 illustrates the co-elution of all monitored precursor ion-product ion transitions for the 252-263 OmpA peptide, and the corresponding quantitative analysis.

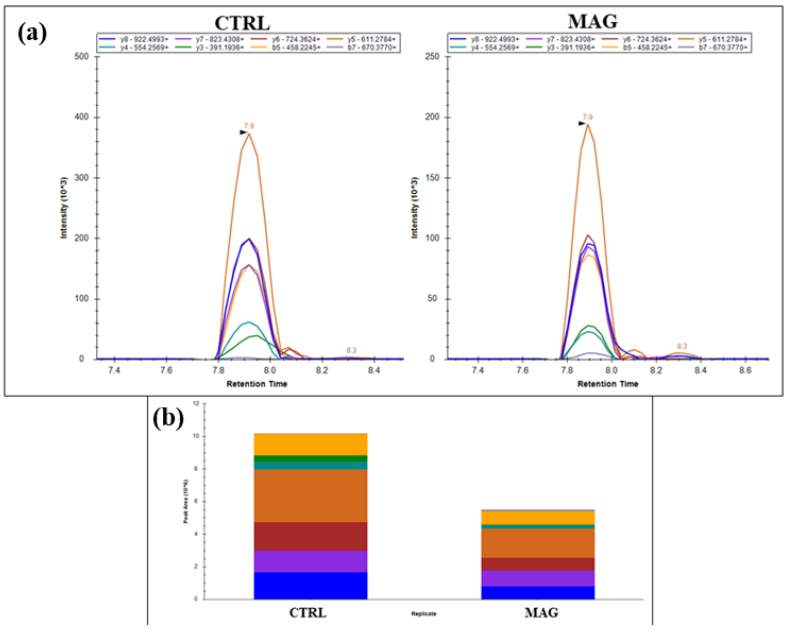

Figure 19. (a) co-elution of all monitored precursor ion-product ion transitions for the 252-263 OmpA peptide. **(b)** quantitative analysis of peak areas, providing an assessment of the abundance of the peptide. The figure was adapted with the permission from Di Somma et al. 2022 Frontiers in Chemistry.

Quantitative assessments of peak areas were performed from different replicates for each OmpA and OmpF peptide, and their statistical significance was validated through *t*-test analysis ($P<0.05$). The quantitative representation of MRM/MS data are shown in Figure 20.

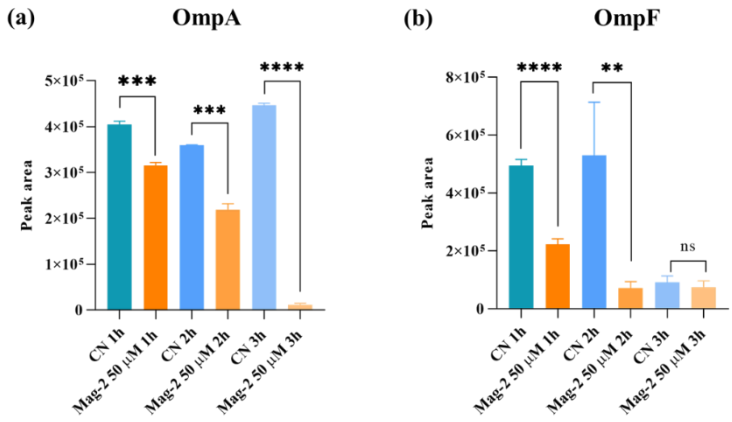

Figure 20. MRM/MS data of OmpA protein at different times of incubation of *E. coli* cells with Mag-2. Results are presented as the mean ± SD from two independent experiments. Statistical significance was determined through t-test analysis using GraphPad Prism 9 and p-value < 0.0001 was indicated as **** in the graph.

The decrease in the levels of both OmpA and OmpF was observed following prolonged Mag-2 incubation, suggesting significant alterations in bacterial membrane composition and function. The decrease in OmpA levels is particularly noteworthy due to its multifaceted roles in bacterial physiology. Similarly, the decline in OmpF levels has significant implications for bacterial physiology, especially regarding nutrient uptake and antibiotic susceptibility[79].

The consistency between the observed trends in Western Blot experiments and the decrease in OmpA and OmpF levels underscores the reliability of the findings, corroborating the interaction between the Mag-2 peptide and BamA, and unveiling a consequential disruption in the proper folding of OMPs within the OM of *E. coli*.

These results highlighted the specificity of the peptide for its protein target and revealed functional consequences that hold significance for the overall functionality of the bacterial OM.

2.4 Conclusions

The study of the Mag-2/BamA complex formation allowed us to gather informations on the molecular mechanism of Mag-2, once the peptide enters within *E. coli* cells. Mag-2 can specifically bind BamA within the large cavity of the β–barrel structure contacting several key residues of the protein and impairing the proper folding and allocation of OMPs. The interaction could physically hinder the entry of unfolded OMPs into the β–barrel cavity, thereby obstructing the proper completion of the folding process. Otherwise, peptide binding may disrupt the opening of the lateral gate, a mechanism through which folded OMPs are typically released from the BAM complex into the OM bilayer. The results demonstrated the robustness of previous functional proteomic investigation and molecular docking calculations, suggesting BamA as a possible target for the rational design of new antibiotics, since the protein is responsible for a crucial biological event in *E. coli* and is absent in humans.

The results discussed in this chapter were included in the following publication: Di Somma, A.*, **Cané, C.***, Moretta, A., Illiano, A., Pinto, G., Cavasso, D., ... & Duilio, A. (2022). The antimicrobial peptide Magainin-2 interacts with BamA impairing folding of *E. coli* membrane proteins. *Frontiers in Chemistry*, *10*. doi: 10.3389/fchem.2022.1013788

* The authors equally contributed to the work.

Chapter 3 – Investigation of Temporin-L effect on *S. aureus* cells

3.1 Introduction

MRSA is a Gram-positive bacterium, first described in England in 1961 by Jevons et al. and is recognized as one of the microbial agents capable of causing bacterial infections in both healthcare and community settings, such as bacteremia, pneumonia and toxic shock syndrome[80-81]. The incidence of MRSA infections is rising at alarming levels worldwide due to antimicrobial resistance. To date, more than 95% of *S. aureus* strains are resistant to penicillin, 60% to methicillin and several cases of *S. aureus* resistance to the glycopeptide vancomycin, used for a long time in the treatment of MRSA infections[82]. MRSA stands out among other pathogens due to its capability to produce numerous virulence factors[83] (Figure 21).

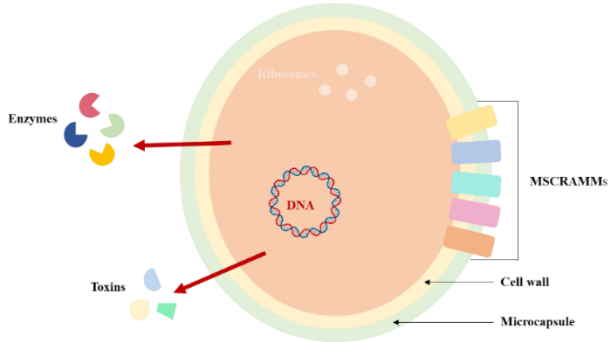

Figure 21. Cellular architecture and pathogenic determinants of *S. aureus*.

The MRSA infection process involves numerous surface proteins, called MSCRAMMs, that act as key mediators in the adhesion of the pathogen to host tissues and bind molecules such as collagen, fibronectin, and fibrinogen[84-85].

The adherence mediated by MSCRAMMs is a finely tuned process, with MSCRAMMs comprising adhesive proteins with specialized binding domains that facilitate targeted interactions with specific extracellular matrix proteins and host cell receptors[86]. This specificity enables pathogens to selectively engage with host surfaces, evade immune surveillance, and establish resilient infections. The molecular interplay between MSCRAMMs and host components is dynamic, with implications for both pathogen and host responses[87].

In this scenario, the limited number of effective antibiotics has led to the search for alternative antimicrobial solutions, including the use of AMPs. Most studies performed on the antimicrobial temporins demonstrated that they are mainly active against Gram-positive bacteria, including clinically isolated MRSA, with minimal inhibitory concentrations[88-89].

The isoform L, named Temp-L (FVQWFSKFLGRIL-NH_2), is a highly potent and α-elical AMP (Figure 22) with a net positive charge (+3) firstly identified in 1996 in the skin of the European red frog *Rana Temporaria*, and later also in North American and Eurasian frogs[90].

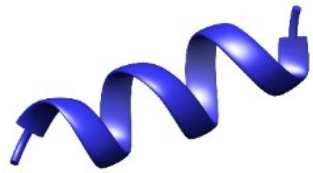

Figure 22. 3D structure of Temp-L. The image has been generated with UCSF CHIMERA software[58].

The proposed model for Temp-L interaction with bacterial membranes is the carpet model[91]. However, in the Gram-negative bacterial membranes, the mechanism of permeabilization could also involve a non-membranolytic

process[92], indicating Temp-L as a promising agent for targeting specific intracellular therapeutic proteins[93-94]. Nevertheless, a comprehensive understanding of the effect of Temp-L on Gram-positive *S. aureus* requires further elucidation.

Preliminary investigations employing TEM and differential proteomics showed a surprisingly effects of Temp-L on *S. aureus.* Notably, Temp-L induces the formation of vesicle-like structures on the bacterial membrane, without causing the leakage of cytosolic material, as illustrated in the Figure 23. This process is concomitant with the up-regulation of proteins involved into cell wall organization and fatty acid biosynthesis and the down-regulation of virulence-associated proteins.

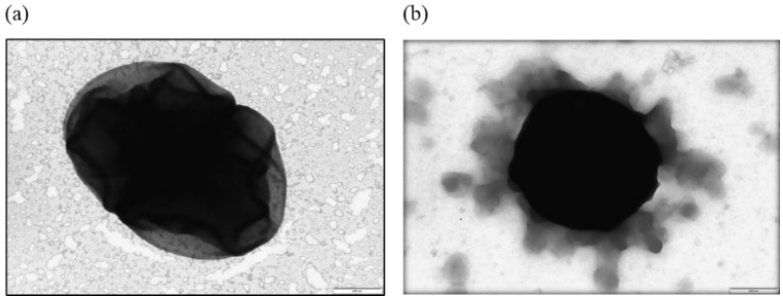

Figure 23. TEM analysis comparing **(a)** *S. aureus* cultures and **(b)** *S. aureus* cells treated with 4 μM Temp-L. Adapted with the permission from A. Di Somma, PhD thesis "Regulation of biofilm development in Gram-negative bacteria: new antimicrobial strategies", 2020.

The changes in morphologic and proteomic profilings in Temp-L-treated *S. aureus* may suggest its antimicrobial mechanisms, which could lead to the development of a new innovative strategies in treating *S. aureus* infections. However, the need for additional validation studies remains imperative.

Consequently, this chapter provides experimental groundwork to corroborate pevious investigations into ultrastructural changes and differential proteomics in Temp-L-treated *S. aureus*. Spectroscopic and GC-MS analyses elucidated the nature of distinct protrusions regularly distributed on the cell surface. These analyses also shed light on the correlation between the formation of vesicle-like structures and the up-regulated proteins identified by differential proteomics. Furthermore, investigations into the impact of Temp-L on *S. aureus* virulence were confirmed through biological assays on eukaryotic cells. The down-regulation of proteins involved in virulence and cell adhesion underscores the multifaceted effects of Temp-L on bacterial physiology. This comprehensive approach provided valuable insights into the potential therapeutic applications of Temp-L.

3.2 Experimental methods

3.2.1 Dynamic Light Scattering (DLS)

S. aureus cells NCTC 12493 were treated with 4 µM of Temp-L for 1h, 2h, 3h, 4h and 5h at 0.5 OD_{600nm}/mL. Untreated cells at the same times were used as control. Following incubation, bacterial cells with a growth corresponding to 1 OD_{600nm} were centrifuged for 15 minutes at 5000 rpm at 4°C, subjected to triple washes with PBS, and the resulting samples were resuspended in PBS. DLS measurements were performed as described in the paragraph 2.2.4.

3.2.2 Gas Chromatography-Mass Spectrometry (GC-MS) analysis

Fatty acids were extracted from *S. aureus* cells NCTC 12493, treated and not treated with 4 µM of Temp-L for 1h, and converted in methyl esters by adding methanol (MeOH), sulfuric acid (H_2SO_4) and chloroform ($CHCl_3$), using biological duplicate. The reaction was performed for 16 h at 90°C under stirring to ensure comprehensive conversion. The GC-MS analysis involved the use of a high-quality a HB-5 ms capillary column (30 m × 0.25 mm × 0.25 µm film thickness). Helium was employed as the carrier gas, flowing at a rate of 1 mL/min to facilitate the separation of methyl esters. 1 µl of sample was injected into the GC-MS system, with a 3 min of solvent delay time and split ratio of 10:1. The ionization occurred in the EI mode at 70 eV. MS data were acquired in full scan mode across the mass-to-charge ratio (m/z) range of 40–400, with an acquisition frequency of 12.8 scans per second. The external standard method was used to quantify the content of fatty acids.

The experiment was performed in duplicate and the obtained data were statistically analyzed by t-test, using GraphPad Prism 9 (GraphPad Software, San Diego, CA, USA).

3.2.3 Adhesion and invasion assays on A549 eukaryotic cells

S. aureus NCTC 12493 cultures were treated with or without 4 µM of Temp-L for 1h under stirring at 0.5 OD_{600}/mL. Following treatment, cells were pelleted, subjected to two washes with DMEM without FBS and 1% penicillin/streptomycin, and re-suspended in the same medium to attain a density of approximately $1 \cdot 10^7$ CFU/mL, defined as the original bacterial CFU.

Simultaneously, A549 human lung epithelial cells (ATCC CCL 185) were cultured in complete DMEM medium and $2 \cdot 10^5$ cells/ml were seeded into 12-well plates in DMEM medium, without FBS and 1% penicillin/streptomycin. The cells were cultivated to attain 90% confluence under standard conditions at 37°C with 5% CO_2. Upon reaching the desired confluence, on the day of infection, A549 cells underwent a two-fold wash with PBS and were subsequently exposed to 1 ml of the prepared bacterial inoculum to achieve a targeted MOI of 50:1 ($1 \cdot 10^7$ bacteria :$2 \cdot 10^5$ cells). Following inoculation, plates were centrifuged for 1 min at 500 g to enhance bacterial adhesion and incubated for 60 min at 37°C in 5% CO_2 (v/v) atmosphere. Post-incubation, A549 cells underwent a triple wash with PBS to remove non-adherent bacteria, followed by lysis through the addition of 1 ml of distilled water. To estimate the total number of cell-associated bacteria, encompassing both adherent and intracellular populations, serial 10-fold dilutions of the resultant cellular suspension were performed in PBS, plated on LB (Oxoid) agar plates, and incubated at 37°C for 18 hours. Quantification of bacterial adhesion in each well was achieved by determining the CFU, representing both adherent and intracellular bacteria. To establish a baseline, control wells treated with medium alone (without Temp-L) were considered to exhibit 100% adhesion. Adhesion values were subsequently normalized against the control conditions[95].

Each experiment was performed in triplicate and the obtained data were statistically analyzed by t-test, using GraphPad Prism 9 (GraphPad Software, San Diego, CA, USA).

3.3 Results and Discussion

3.3.1 Insights into vesicle formation induced by Temp-L in *S. aureus*

Previous data obtained through both TEM analyses and differential proteomic served as the foundation for the current investigation. These data revealed the formation of vesicle-like structures in *S. aureus* cells treated with 4 μM Temp-L. Concurrently, a coordinated increase in enzymatic machinery involved in the biosynthesis of fatty acid was observed, with a focus on several proteins belonging to ACC and FAS II complexes. These observations are indicative of a bacterium response to the antimicrobial peptide addressed to fortify its membrane structures[96]. ACC is a multi-subunit enzyme that catalyzes the first reaction in the fatty acid biosynthetic pathway, whereas the FAS II complex catalyze the elongation step to produce both straight and branched chain fatty acids. The activity of these machinery constitute the first step in bacterial membrane lipid synthesis[97]. These data were confirmed by DLS analysis, performed in collaboration with the research group of Prof. Luigi Paduano (Department of Chemical Sciences – University Federico II – Naples). The results highlighted an increase in size of *S. aureus* after one hour of Temp-L treatment, suggesting that bacteria are actively modifying their membrane composition. Following two hours of Temp-L treatment, the presence of a distinct population with reduced sizes indicated a dynamic process focused to vesicle formation, confirming the effect observed by TEM analysis and proposing the development of a defence mechanism in Gram-positive bacteria (Figure 24).

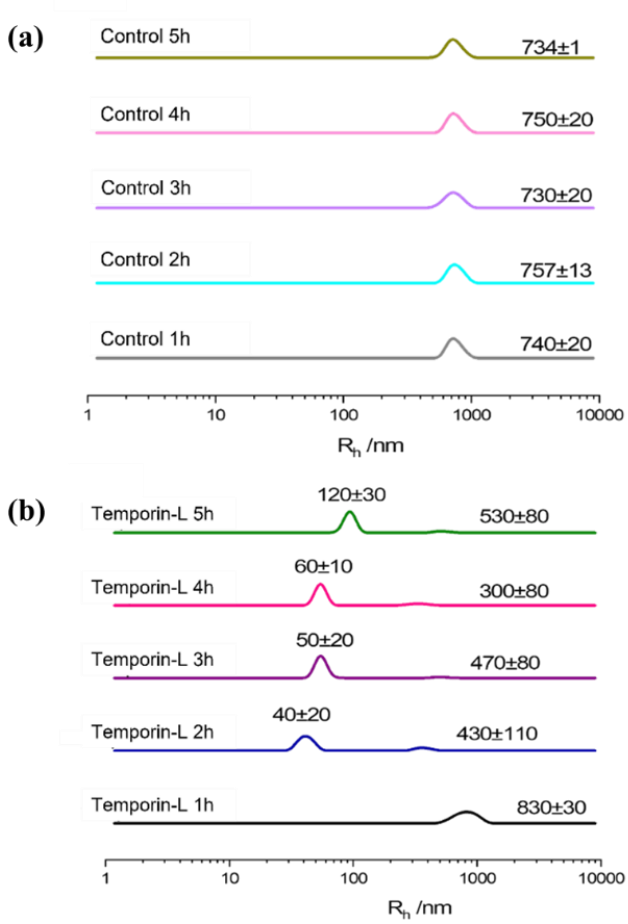

Figure 24. DLS analysis, illustrating (a) the size of untreated *S. aureus* and (b) *S. aureus* cells treated with 4 μM Temp-L.

Further informations on the Temp-L effect were gained by investigating the fatty acid content in *S. aureus* following Temp-L incubation. Total fatty acids, extracted and converted into methyl ester derivatives, were analyzed by GC-MS analysis. The observed increase in total fatty acids in the treated sample compared to the negative control (Figure 25) indicated a substantial alteration in the lipid composition of *S. aureus* membranes, consistent with the observed vesicle

formation. This effect is further supported by the observation that clinical isolates of MRSA increased their membrane fluidity[98].

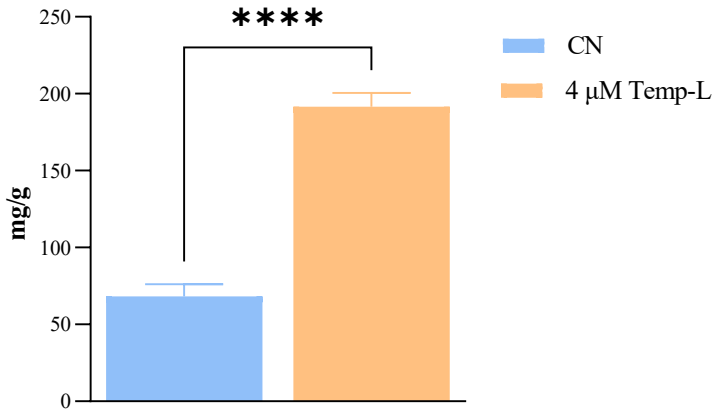

Figure 25. The graph illustrates the concentration of total fatty acids in milligrams per gram of bacterial extract in the absence and the presence of Temp-L. Results are presented as the mean ± SD from two independent experiments. Statistical significance was determined through t-test analysis using GraphPad Prism 9 and p-value < 0.0001 was indicated as **** in the graph.

These findings support the hypothesis that Temp-L treatment induced a mechanism of increased membrane production in *S. aureus* possibly leading to vesicles formation[99]. This behaviour had already been observed in other antibiotic-resistant strains, suggesting a common adaptive mechanism among bacteria in response to antimicrobial agents[100]. The efficacy of vancomycin against *S. aureus* was compromised by the formation of vesicles, leading to a substantial increase in MIC values and enhanced viability of bacterial cells pre-exposed to the antibiotic[101]. This phenomenon of lipid-coated vesicle formation is regarded as a pivotal determinant influencing antibiotic resistance mechanisms

and bolstering bacterial persistence in the presence of antibiotics, thus exacerbating the pathogenesis of *S. aureus*[102].

3.3.2 Temp-L action on the adhesive and invasive ability of *S. aureus*

Previous differential proteomic experiments has provided insights into the putative impact of Temp-L on diminishing the virulence of *S. aureus*. A considerable number of proteins associated with virulence and pathogenesis were affected by Temp-L. Notably, TRAP and SarA, integral components of *S. aureus* virulence regulatory systems, were particularly decreased by the presence of the peptide. Specifically, the inhibition of TRAP expression has been linked to the abrogation of toxin production and the inability of bacteria to induce disease, underscoring its critical role in the virulence modulation of *S. aureus*[103]. Additionally, SarA is implicated in the regulation of MSCRAMMs, which are also found to be down-regulated by proteomic data (i.e. Ebh, ClfB, fibrinogen, IsdA, SdrC and Sdrd), highlighting its significance in mediating adhesion-related processes[104].

This observation propelled an exploration into the hypothesis that Temp-L possesses the capability to attenuate the infectious properties of *S. aureus*. Adhesion/invasion assays were performed on eukaryotic cells, and the investigation focused on A549 cells, representative of human type 2 pneumocytes. The experiments were carried out in collaboration with the research group of Prof. Eliana De Gregorio (Department of Molecular Medicine and Medical Biotechnology – University Federico II – Naples). A sub-inhibitory concentration of Temp-L significantly decreased the relative adherence (%) of *S. aureus* NCTC 12493 to A549 epithelial cells (Figure 26), providing experimental validation of the potential of Temp-L as a modulator of *S. aureus* virulence.

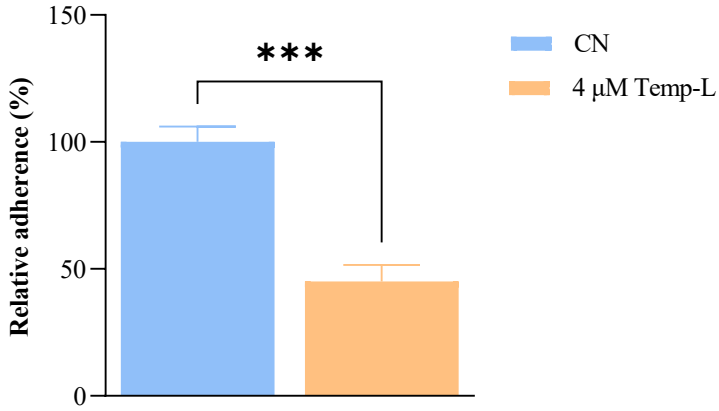

Figure 26. Adhesion assays show the relative adherence of *S. aureus* to A549 epithelial cells in the absence and the presence of Temp-L. Results are presented as the mean ± SD from two independent experiments. Statistical significance was determined through t-test analysis using GraphPad Prism 9 and p-value < 0.0004 was indicated as *** in the graph.

The findings presented herein provide compelling evidence of Temp-L's efficacy in diminishing the virulence and pathogenicity of *S. aureus*. This assertion aligns with existing literature demonstrating similar outcomes with other AMPs. For instance, previous studies have highlighted the capacity of defence peptides such as human defensins to attenuate virulence of *Streptococcus agalactiae* deficient in D-alanyl-lipoteichoic acid in mouse and neonatal rat models[105].

These collective findings underscore the promising therapeutic potential of Temp-L and related peptide compounds in combating *S. aureus* infections and addressing the growing challenge of antibiotic resistance.

3.4 Conclusions

Investigation into the impact of Temp-L on the Gram-positive bacterium *S. aureus* unveiled a novel aspect of the Temp-L mechanism, particularly in its ability to exert influence over MRSA cells. The data highlighted the possible involvement of Temp-L in the regulation of fatty acid biosynthesis and virulence factors within *S. aureus*. This study represents an example where empirical evidence elucidated the strategies employed by *S. aureus* to activate defense mechanisms in response to an antimicrobial peptide, such as the vesicle production on the bacterial membrane. Despite employing multiple defense mechanisms, the observed decrease in virulence-related proteins in *S. aureus* reveals the inherent limitations of these counteractive measures. These effects have been delineated through scientific methodologies, including spectroscopic assessments and cellular assays. Such elucidations not only significantly contributes to our understanding of *S. aureus* responses to Temp-L treatment but also suggest the targeting of virulence-related proteins as a possible antimicrobial strategy against MRSA infections.

The results discussed in this chapter were included in the following publication under revision: **Canè, C.**, Gallucci, N., Amoresano, A., Fontanarosa, C., Paduano, L., De Gregorio, E., Duilio, A. and Di Somma, A. The antimicrobial peptide Temporin-L induces vesicle formation and reduces the virulence in *S. aureus*. *Biochem. Biophys. Rep.*

Chapter 4 – Inhibitory action of berberine derivatives on the protein target FtsZ of *E. coli*

4.1 Introduction

Among the family of *Berberidaceae,* the largest and most important genus is *Berberis* well known for its antibacterial, anticancer, antidiabetic, anti-inflammatory, antihypertensive and hypolipidemic properties[106]. This genus consists of about 500 species including *B. vulgaris*, a thorny red shrub that grows in Asia, North Africa and Europe. *B. vulgaris* shows a high content of phytochemicals and bioactive components[107], including alkaloids such as berbamine, berberine and berberrubine. The most important properties associated with this genus are due to the presence of berberine, which can be extracted from the roots, rhizomes and stem of the plant[108]. Structurally, berberine is an isoquinoline alkaloid with planar polyoxygenated cycles and a net positive charge (Figure 27).

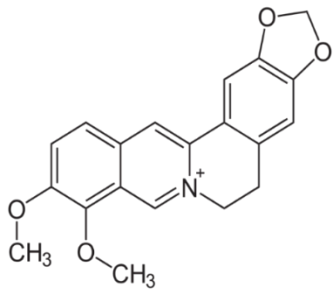

Figure 27. Chemical structure of berberine.

Berberine displays a wide range of pharmacological effects, including antimicrobial activity[109]. It is used in traditional Chinese, Native American and also in Western medicine, where it is recognised for its antimicrobial properties against both Gram-positive and Gram-negative bacteria[110].

To date, different antimicrobial mechanisms of action have been proposed for berberine[111] (Figure 28):

- ***Membranolytic mechanism***. Berberine induces damages on bacterial surface: The electrostatic interaction between berberine and bacterial membranes, especially Gram-negative microorganisms, alters the membrane potential causing leakage of cytoplasmic material and bacterial death;

- ***Berberine inhibition of DNA duplication, RNA transcription and protein biosynthesis***. Berberine structure is able to intercalate itself within both DNA and RNA molecules establishing electrostatic interactions. The consequence of this interaction is the damage or the structural variation of the nucleic acid filaments which prevents the correct DNA duplication, RNA transcription and proteins biosynthesis;

- ***Berberine inhibition of enzymatic activity***. Berberine can interfere with enzymatic activity either by inhibiting mRNA transcription, blocking enzyme biosynthesis or directly binding to specific enzymes, immediately affecting their enzymatic activity. If these enzymes are involved in vital processes for the bacterial cell, berberine exerts its antimicrobial activity;

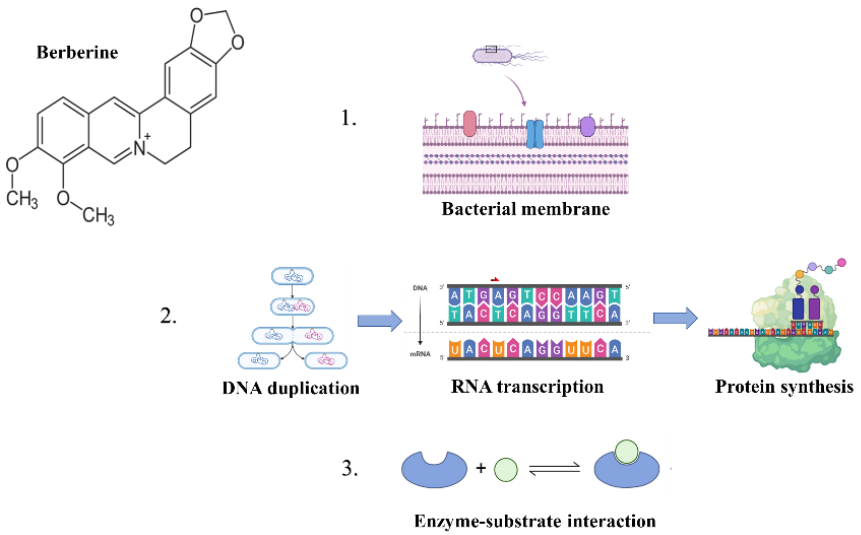

Figure 28. Proposed Mechanisms of Action of Berberine.

In recent years, a novel antibacterial mechanism of berberine in *E. coli* highlighted the inhibition of cell division through interaction with FtsZ protein[112]. It is highly conserved in bacteria and shares less than 20% sequence identity with the eukaryotic cytoskeleton protein tubulin, suggesting that antibacterial agents targeting FtsZ may exhibit low cytotoxicity toward eukaryotes[113].

FtsZ is a tubulin-like GTPase belonging to the divisome complex, that assembles into polar protofilaments, similar to tubulin ones, in which the GTP binding site of one monomer is at the binding interface with the next monomer. The assembly process is regulated by several accessory proteins[114], and FtsZ polymers form a dynamic ring-like structure, known as the Z-ring, at the future site of cell division. The Z-ring formation represents the earliest known step in bacterial cytokinesis and recruits a set of other cell division proteins essential for the function of dividing the cell[115-116]. A critical player is the FtsA protein, which interacts with FtsZ and anchors the Z-ring to the cell membrane[117]. The ZipA protein stabilizes the association between FtsZ and the membrane, contributing to

the integrity of the divisome[118]. FtsI is another crucial protein participating in the synthesis of septal peptidoglycan during cell division, ensuring proper cell wall formation[119] (Figure 29).

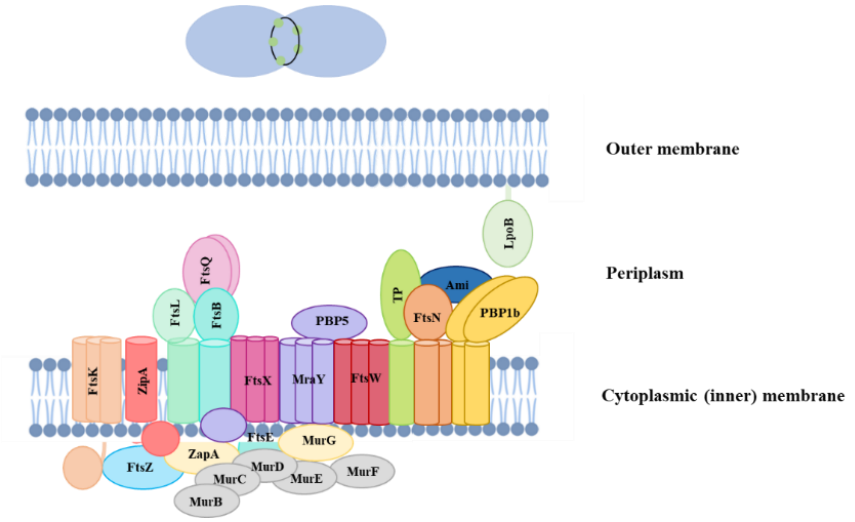

Figure 29. Schematic representation of the proteins involved in the process of cell division, constituting the divisome complex.

Among the myriad proteins orchestrating cell division, FtsZ assumes a pivotal role as the primary cytomotor organizer of the divisome in the majority of bacteria[120]. Given its central function in divisome assembly, FtsZ becomes a crucial target for interventions aimed at modulating or disrupting the cell division process. Strategies directed towards FtsZ may hold significant promise in developing approaches to control bacterial growth and proliferation

In this context, the advancement of inhibitors directed against FtsZ in *E. coli* constitutes a critical domain of investigation within antimicrobial drug discovery, as elucidated by Milani et al. Recent *in silico* predictions have shown that structurally simplified berberine derivatives display enhanced FtsZ inhibitory efficacy compared to their parent compound[121].

The current study focused on assessing the *in-silico* interaction of novel berberine derivatives (Figure 30) and elucidating inhibitory enzymatic mechanisms of both novel and previous derivatives[121], using in *vitro* biochemical assays, fluorescence measurements and microscopic investigations on recombinant FtsZ from *E. coli*.

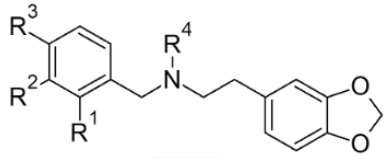

1c $R^1 = R^2 = OMe$, $R^3 = H$, $R^4 = Me$

1d $R^1 = R^2 = OMe$, $R^3 = H$, $R^4 = Et$

1f $R^1 = R^2 = OMe$, $R^3 = H$, $R^4 = n\text{-hexyl}$

1g $R^1 = R^2 = R^4 = H$, $R^3 = Cl$

1h $R^1 = R^2 =$ -CH=CH-CH=CH-, $R^3 = R^4 = H$

1i $R^1 = NO_2$, $R^2 = R^3 = R^4 = H$

2g $R^1 = R^2 = H$, $R^3 = Cl$, $R^4 = Me$

2h $R^1 = R^2 =$ -CH=CH-CH=CH-, $R^3 = H$, $R^4 = Me$

Figure 30. Berberine derivatives.

4.2 Experimental methods

4.2.1 Molecular Docking Analysis

The potential binding sites of berberine derivatives on the FtsZ protein were identified through molecular docking analysis. The three-dimensional structure of the FtsZ protein was modeled using the I-TASSER Server[122], while the structures of berberine derivatives were generated using the LigParGen Server[123] based on Isomeric SMILES Code to ensure accurate representation. The construction of the protein-ligand model utilized the PatchDock Server[124] and subsequent refinement of the model was carried out with the FireDock Server[125]. Protein-ligand interactions were analyzed using the PLIP Server, which provides a comprehensive examination of non-covalent interactions, such as hydrogen bonding and hydrophobic interactions[126]. Molecular visualizations and figures were generated using UCSF CHIMERA software[58] and the prediction of ΔG values for the interactions was carried out using the PRODIGY web server, aiding in the assessment of the dynamic stability of the formed complexes[127].

4.2.2 Recombinant production, purification and characterization of the protein target FtsZ

Untagged *E. coli* FtsZ was expressed in *E. coli* K12 cells using the pET28a plasmid. Cells were grown at 37°C in LB (Oxoid) medium supplemented with 50 µg/mL kanamycin. Protein expression was induced by the addition of 0.4 mM IPTG at 0.5 OD_{600nm}/mL. The culture was grown for 90 min at 37°C, followed by cell harvest through centrifugation for 15 min at 5000 rpm at 4°C. Cell pellets were resuspended in Tris-glycerol buffer (50 mM Tris-HCl, 50 mM KCl, 1 mM EDTA, 10% glycerol, pH 8.0) and lysed on ice using a sonicator. The resultant soluble fraction, containing the FtsZ protein, was separated from the cellular debris by centrifugation for 30 min at 13000 rpm at 4°C. The protein was

precipitated with 30% ammonium sulfate for 16 h at 4°C. The sample was centrifuged for 30 min at 10000 rpm at 4°C, and the pellet was resuspended in 5 mL Tris-glycerol buffer pH 8.0. Dialysis was employed to remove the ammonium sulfate. Protein purification involved anion exchange chromatography using a Mono-Q HR 5/5 column equilibrated with Tris-glycerol buffer at pH 8.0. FtsZ was retained on the column and eluted with a 0–100% gradient of 1 M NaCl in the same buffer[128].

Protein concentration was determined using the Bradford reagent (Bio-Rad protein assay) following the manufacturer's instructions. Purity assessment was analyzed via 12.5% SDS-PAGE, and the primary structure was characterized by mass mapping MALDI-TOF using a MALDI Voyager-DET STR spectrometer, as described in the section 2.2.2.

4.2.3 GTPase activity assays

6 μM of FtsZ was incubated in a reaction buffer consisting of 25 mM PIPES/NaOH, pH 6.8 for 30 min at 30°C. Subsequently, varying concentrations of GTP, ranging from 0 μM to 500 μM, were added into the FtsZ-containing mixture, performing the reaction for 10 min. The experiments were carried out both in the absence and the presence of 40 μM **1c, 1d, 1f, 1g, 1h, 1i, 2g** and **2h** derivatives. 100 μL of BIOMOL Green phosphate reagent (Biomol, Milan, Italy) were added to stop the reactions. The quantification of released Pi was determined after further incubation at 25°C for 25 minutes, measured by absorbance at 620 nm. Negative control readings were subtracted from all measurements. Experimental procedures were conducted in duplicate[93].

Data were processed to depict U/mg against substrate concentration, and kinetic parameters were determined via nonlinear regression using GraphPad Prism 9 (GraphPad Software, San Diego, CA, USA). The K_i for all competitive

inhibitors was calculated through kinetic analyses conducted in the presence of 20, 40, and 60 µM of compounds, utilizing the provided equation:

$$\text{Ki} = \frac{[I]}{\alpha - 1} \text{ where } \alpha = \frac{K_M^{app}}{K_M}$$

4.2.4 FtsZ Polymerization assays

Polymerization reactions were performed as described by Zheng et al. with some modifications[129]. A solution of FtsZ in 25 mM PIPES/NaOH at pH 6.8 was incubated at a final concentration of 6 µM with 150 µM GTP, varying concentrations of berberine derivatives (20 µM, 40 µM and 60 µM) at 25°C for 1h. The reactions were carried out in triplicate, using the protein incubated solely with GTP as control, and stopped by centrifugation for 60 min at 14000 rpm at 4°C. The resulting pellets were resuspended in 25 mM PIPES/NaOH, pH 6.8 and analyzed via 12.5% SDS- PAGE. Gels were stained with Comassie Brilliant Blue, and the images were acquired using the ChemiDocTM. Densitometric quantification of protein bands was conducted using Quantity One software to determine protein content.

4.2.5 Transmission Electron Microscopy (TEM)

The samples treated with 60 µM **1i** in the previous paragraph were also used for TEM analysis, using appropriate controls. The experiment was carried out by placing 5 µL drops of FtsZ on a carbon-coated copper TEM grid for 20 min. Excess solution was carefully removed using filter paper. Negative staining was performed using a 1% PTA solution adjusted to pH 7.0. A drop of the PTA solution was applied to the grid for 1 minute, followed by blotting to remove excess stain using filter paper[130]. Subsequently, the grid was left to air-dry. Imaging was conducted using a FEI TECNAI G2 S-twin apparatus operating at 120 kV with a LaB6 source.

4.2.6 Fluorescence Spectroscopy

Fluorescence titration experiments were performed using a Fluoromax-4 spectrofluorometer from Horiba Scientific, as described in the paragraph 2.3.3. Titrations were conducted in 50 mM Tris-HCl, 50 mM KCl, 1 mM EDTA pH 8.0. The intrinsic fluorescence intensity of 1 µM **1c** compound was monitored at 295 nm (slit 4 nm), while the emission was recorded at 327 nm (slit 4 nm), both in the absence and the presence of increasing concentrations of FtsZ protein (ranging from 0.010 to 0.120 µM). All experiments were carried out in duplicate. The changes in fluorescence intensity were analyzed by fitting the data to the "one site-specific binding" equation of GraphPad Prism 9 (GraphPad Software, San Diego, CA, USA).

4.3 Results and Discussion

4.3.1 *In silico* interaction of novel berberine derivatives with FtsZ

In silico methodologies were employed to explore the binding affinities of berberine-derived compounds **1g–i**, **2g,h** with the bacterial protein FtsZ. The main aim was to determine whether the modified analogs exhibit enhanced binding interactions with FtsZ compared to the parent compound, berberine. Molecular docking analyses were performed using PatchDock Server and FireDock Server. The structural representation of *E. coli* FtsZ was modeled using the I-TASSER Webserver, and the structural conformations for compounds **1g–i**, **2g,h** were generated using the LigParGen Server. Figure 31 shows that derivatives **1g**,**h** and **2h** exhibited a marked affinity for the active site pocket of FtsZ, interacting through hydrogen bonds, non-covalent interactions, and hydrophobic contacts, as detailed in Table 1.

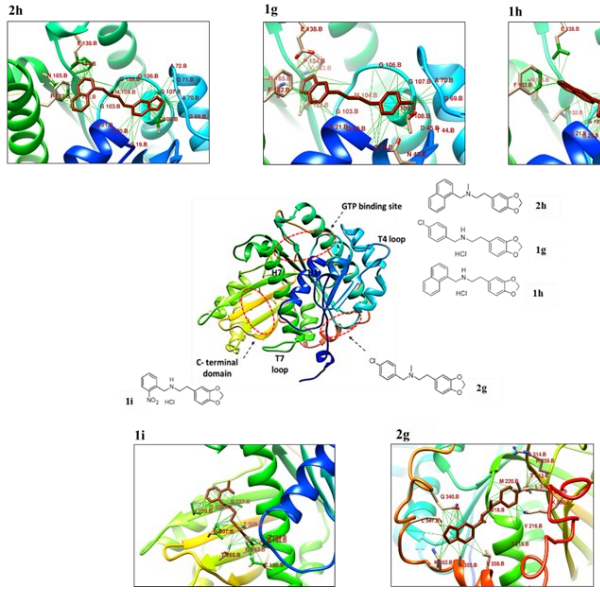

Figure 31. Binding sites of berberine derivatives with FtsZ protein. Adapted with permission from Di Somma et al. 2023 International Journal of Molecular Sciences.

Protein-Ligand	**Interaction**				
	Hydrophobic interactions	***Hydrogen bonds***	***Non-covalent interactions***	**Π Stacking**	**ΔG**
1g	Thr108, Thr132	Gly21, Asn165	Phe182	-	-7.52
1h	Asp45, Ala70	Gly19, Gly21, Asn165	-	-	-7.41
1i	Val229, Thr265, Arg307	Gln194, Asn263	-	-	-7.86
2g	Gln340, Ala355, Val358, Leu 378	Lys 352	Asp 370	-	-7.07
2h	Thr132, Pro134	Ala70, Ala72, Gly106, Gly107, Thr108		Phe 182	-7.45

Table 1. Interactions between berberine analogues and the FtsZ protein. Adapted with permission from Di Somma et al. 2023 International Journal of Molecular Sciences.

These findings strongly suggest a potential increase in binding affinity for these derivatives. Remarkably, compound **2h** accomodated in a different position within the FtsZ active site, diverging from compounds **1g** and **1h**. This compound displayed more interactions with the nucleotide binding site, increasing H-bonds while avoiding contact with Gly19, Gly21, and Asn165. A π-stacking interaction between Phe182 and the naphthalene ring was also predicted.

Conversely, compound **1i** was predicted to interact with the hydrophobic cleft between the H7 and C-terminal β-sheet of the FtsZ protein. Finally, compound **2g** exhibited an affinity for a distinct site on the FtsZ protein, establishing four

hydrophobic interactions, one hydrogen bond with Lys 352 and a non-covalent interaction with Asp 370. The predicted ΔG for all protein-ligand complexes consistently indicated comparable stability

4.3.2 Modulation of FtsZ GTPase activity by berberine derivativess

The ability of berberine derivatives **1c**,**d**,**f**,**i** and **1-2g**,**h** to inhibit FtsZ GTPase activity was further investigated by enzymatic assays. The compounds were chemically synthesized in collaboration with the research group of Prof. Giovanni Lentini (Department of Pharmacy-Pharmaceutical Sciences– University Aldo Moro – Bari). Firstly, FtsZ protein was cloned into the pET28-a plasmid and expressed *in E. coli*. The protein was produced in the soluble fraction and purified by anion exchange chromatography. The protein purity was assessed by SDS-PAGE (Figure 32) and its primary structure was validated by peptide mapping using MALDI-TOF, resulting in a sequence coverage of 91 % (Figure 33).

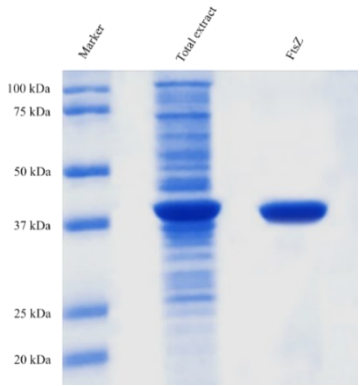

Figure 32. 12.5% SDS-PAGE of the purified FtsZ protein.

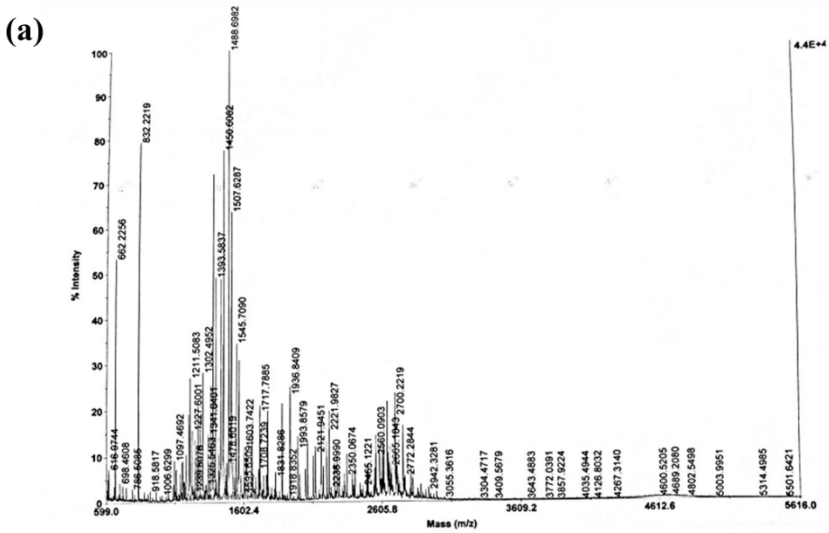

Figure 33. (a) Mass spectrum of FtsZ illustrating the relative abundance of ions plotted against the mass/charge (m/z) ratio. **(b)** The highlighted amino acids depict the peptide map of the FtsZ protein sequence. Sequence coverage was determined by comparing experimental molecular weights with theoretical values obtained through in silico tryptic hydrolysis on the known protein sequence.

The GTPase activity of the purified FtsZ protein was then evaluated both in the presence and absence of 40 μM berberine derivatives, performing GTPase activity assays. The determination of kinetic parameters was accomplished by applying the Michaelis-Menten equation and data elaboration were performed via GraphPad Prism 9 (GraphPad Software, San Diego, CA, USA). This approach

provided a detailed characterization of the enzymatic behavior of FtsZ, shedding light on the impact of berberine derivatives on the enzymatic activity of FtsZ. All examined compounds exhibit the ability to inhibit the GTPase activity of the enzyme, as demonstrated by the kinetic profiles presented in Figure 34. Moreover, distinctive inhibitory mechanisms were observed for the different compounds as indicated by the K_M (μM) and Vmax ($U \cdot min^{-1}$) values (Table 2). The results are in agreement with the structural predictions provided by the docking experiments and allow us to establish that the structure of the berberine analogues is related to specific inhibitory properties.

Compounds **1c**,**d**,**g**,**h**, and **2h** induced a change in the apparent K_M values, while the Vmax values remained unchanged, suggesting a competitive inhibition mechanism. These compounds share a common structural feature, characterized by small groups on the nitrogen atom (H, Me or Et), directing them towards the active site of the enzyme. In contrast, compounds **1f** and **1i** demonstrated a non-competitive inhibition mechanism, characterized by a reduction in the Vmax value while maintaining a constant K_M value. The presence of larger substituents on either the nitrogen atom or the benzyl ring promotes the binding at the C-terminus. Surprisingly, compound **2g** displayed a divergent behavior, exhibiting a simultaneous reduction in both Vmax and K_M. This distinctive pattern is indicative of an acompetitive inhibitory mechanism, revealing a unique mode of interaction between the compound and the enzyme.

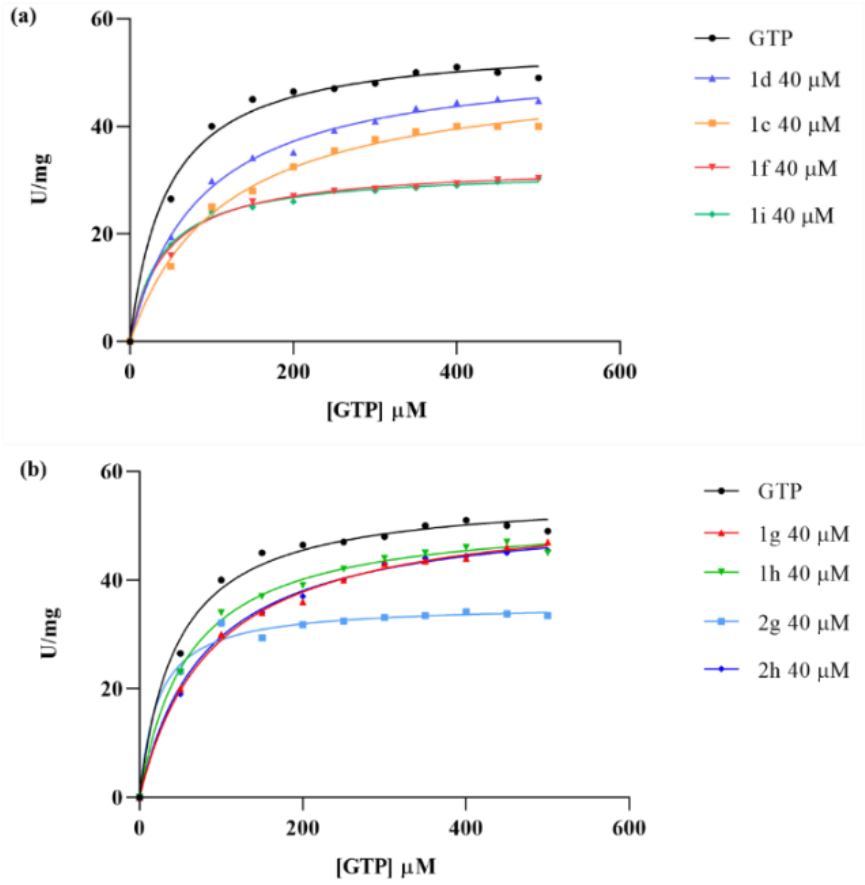

Figure 34. Enzymatic activity assays of FtsZ in the presence of berberine derivatives. The graph depicts enzymatic units per mg of enzyme used as a function of substrate (GTP) concentrations.

Kinetic parameters		
	K_M (μM^{-1})	v_{max} ($U \cdot min^{-1}$)
GTP	45 ± 5	55.86 ± 1.22
1c	114 ± 9	50.80 ± 1.28
1d	85 ± 6	52.96 ± 0.98
1f	43 ± 5	32.88 ± 0.69
1g	88 ± 6	54.51 ± 0.94
1h	60 ± 4	52.26 ± 0.84
1i	40 ± 3	31.97 ± 0.38
2g	23 ± 4	35.58 ± 0.77
2h	80 ± 7	53.34 ± 1.17

Table 2. Kinetic parameters were fitted by nonlinear regression with GraphPad Prism 9. K_M and Vmax values were fitted from the Michaelis-Menten plot. Adapted with permission from Di Somma et al. 2023 International Journal of Molecular Sciences.

The K_i constants were determined to comprehensively describe the competitive inhibition, since it provides crucial information about the affinity and efficacy of the competitive inhibitors. A lower K_i indicates a stronger binding affinity between the inhibitor and the enzyme, suggesting a more effective inhibition. The results presented in the Figure 35 show the kinetic analyses at various concentration of competitive inhibitors. The K_i values were derived by comparing progress curves in the presence of 20 μM, 40 μM, and 60 μM of compounds **1c**,**d**,**g**,**h** and **2h**. The obtained K_i values were 25 μM, 44 μM, 41 μM, 119 μM and 51 μM, respectively. Among the compounds tested, the **1c** analogue

demonstrated the most favorable inhibition profile for FtsZ, as evidenced by its notably low K_i value of 25 μM.

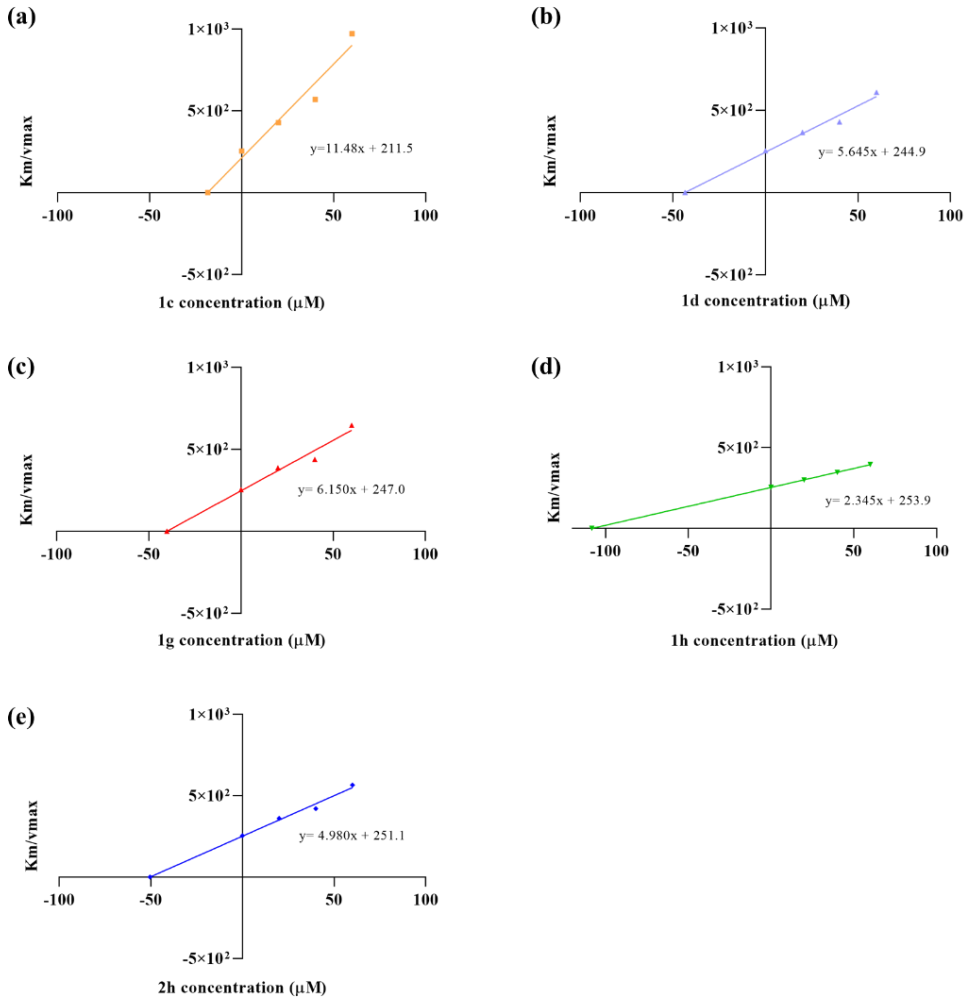

Figure 35. Calibration curves illustrating kinetic profiles for competitive inhibitors, with the y-axis displayng the ratio K_M/vmax calculated from activity assays and the x-axis representing the concentration of compounds used (μM).

Based on these findings, elucidation of the relationship between the structural characteristics of berberine analogues and their binding sites on FtsZ, as well as

their inhibitory properties, is provided. Scaffolds incorporating a benzoyl moiety with two methoxy substituents or a naphthalene ring, and minor substituents on the nitrogen atom (H, Me, or Et), guide the berberine analogues toward the active site of FtsZ (**1c**, **d**, **g**, **h**, and **2h**). Conversely, larger substituents on either the nitrogen atom or the benzyl ring facilitate binding at the C-terminus (**1f**, **i**).

4.3.3 Berberine Analogues Influence on FtsZ Polymerization Dynamics

The impact of berberine derivatives on FtsZ polymerization was assessed through a polymerization assay, aiming to replicate the crucial process orchestrated by FtsZ during *E. coli* cell division *in vitro*. The polymerization assay involved the incubation of FtsZ with 150 μM GTP, both in the absence and the presence of increasing concentrations of berberine-related compounds. FtsZ filaments were isolated via centrifugation, subjected to SDS-PAGE analysis, and the quantification of polymerized protein was measured through densitometric analysis of the corresponding Coomassie-stained gel bands.

As shown in Figure 36, a dose-dependent reduction in the amount of polymerized FtsZ was evident with increasing concentrations of all the inhibitors. Notably, all tested compounds exhibited a negative impact on FtsZ polymerization. Among them, compounds **1c**, **1f**, and **1i** demonstrated a more pronounced inhibitory effect, resulting in a reduction of polymerized FtsZ by 35%, 30%, and 25%, respectively. Significantly, the inhibitory efficacy of the **1i** compound was much higher than that of other compounds, resulting in a substantial decrease in the abundance of FtsZ protofilaments. This reduction reached near-negligible levels at an inhibitor concentration of 60 μM.

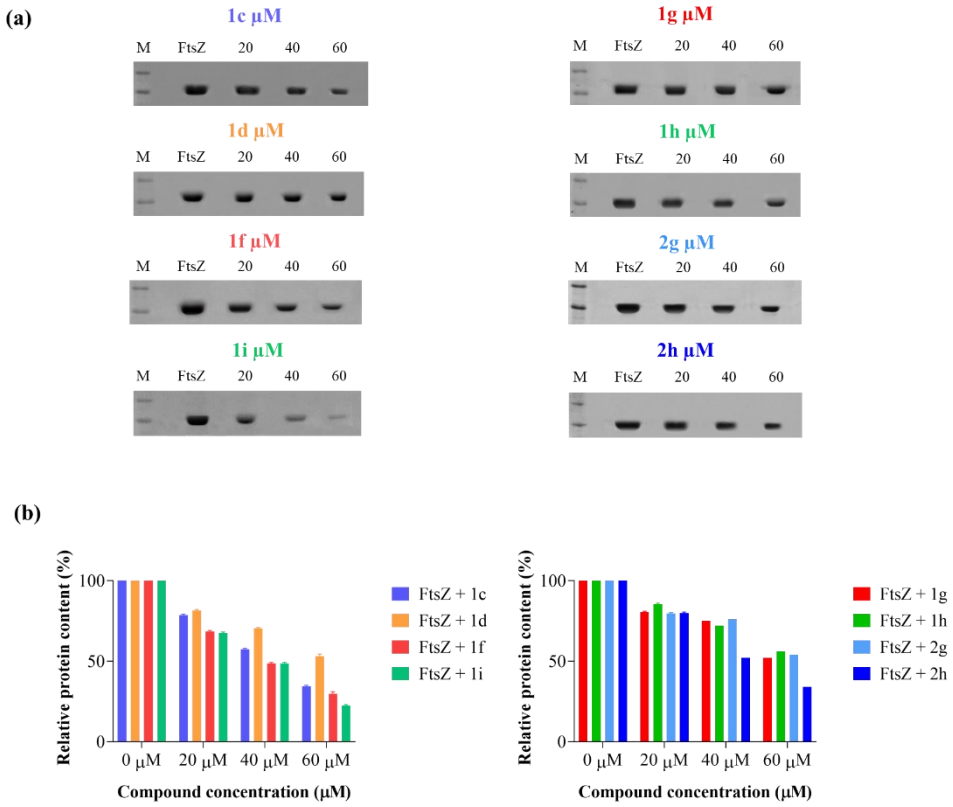

Figure 36. Polymerization assay of recombinant FtsZ (6 µM) carried out with 150µM of GTP in the presence of berberine analogues. **(a)** SDS-PAGE (12.5%) of protein pellet after polymerization reactions. **(b)** Densitometric analysis of SDS-PAGE, showing the percentage of FtsZ polymerization. Adapted with permission from Di Somma et al. 2023 International Journal of Molecular Sciences.

These observations highlighted the potency of berberine analogues, particularly **1i**, in impairing polymerization of FtsZ. This effect was further corroborated by TEM microscopy investigation, enabling direct observation of the filaments in the presence of 60 µM **1i** (Figure 37). When FtsZ is treated with the inhibitor the absence of protofilaments is clear evidence that **1i** compound is able

to prevent FtsZ polymerization (Fig. 37b). As control, FtsZ forms a thick bundle of GTP-induced protofilaments in the absence of the inhibitor (Figure 37a).

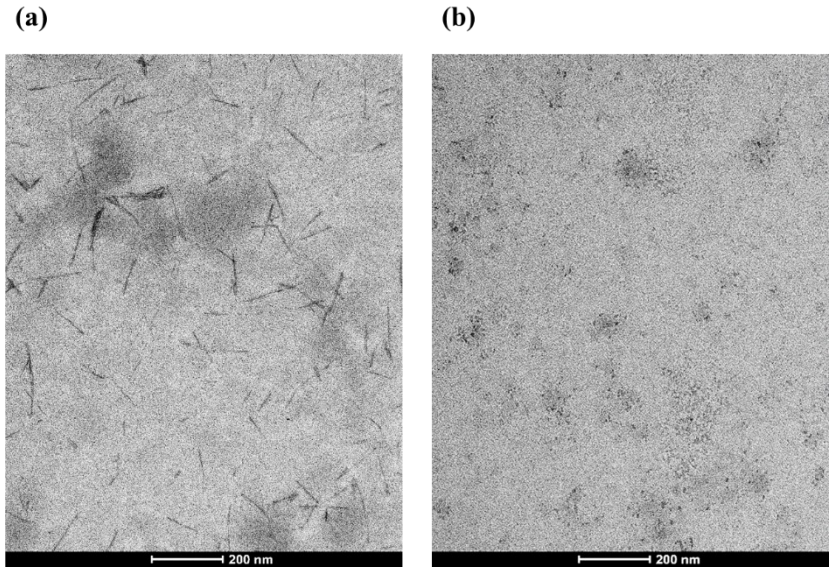

Figure 37. TEM images of FtsZ **(a)** in the absence and **(b)** in the presence **1i** inhibitor.

4.3.4 FtsZ binding studies with derivative 1c

The optimal inhibition of both FtsZ enzymatic activity and polymerization was unequivocally demonstrated in the presence of the **1c** compound. Consequently, fluorescence binding experiments were designed to gain deeper insights into the molecular interactions between **1c** and the target protein FtsZ. Specifically, the **1c** compound was excited at 295 nm, and its intrinsic fluorescence was monitored at increasing concentrations of recombinant FtsZ. The absence of tryptophan residues in the FtsZ protein sequence resulted in minimal emission at 327 nm following excitation at 295 nm, even at the concentrations used. This intrinsic property facilitated the exclusive examination of the fluorescence emitted by the **1c** compound.

Figure 38 showed a significant decrease in the fluorescence intensity of **1c** compound at 327 nm with increasing concentrations of FtsZ. The collected data from fluorescence quenching were used to calculate the K_d value, which resulted 26.64 ± 0.8 nM. These data indicated the formation of a highly stable complex between compound **1c** and the FtsZ protein.

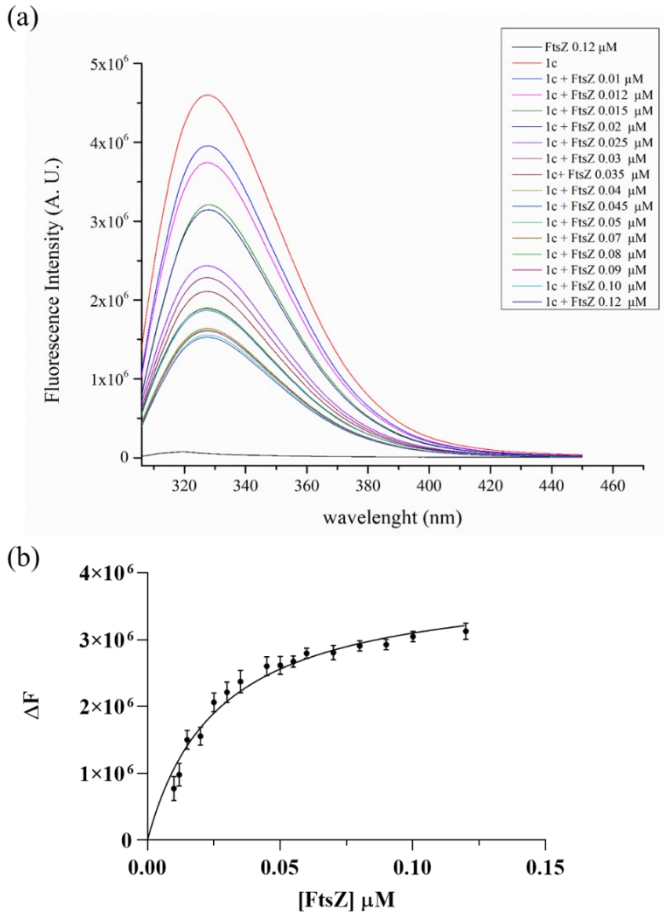

Figure 38. Fluorescence binding assay **(a)** Emission fluorescence spectra of compound **1c** at various concentrations of FtsZ. **(b)** Plot of ΔF at 327 nm against FtsZ concentration. The experimental data were fitted to a non-linear regression model, and the binding constant (K_d) was estimated using GraphPad Prism 9. All experiments were performed in duplicate, and the SD is reported as error bars. Adapted with permission from Di Somma et al. 2023 International Journal of Molecular Sciences.

The specificity of the binding was assessed by recording the absorption spectra of compound **1c**, compared to berberine. Figure 39 showed that compound **1c** did not exhibit any absorbance at 327 nm, in contrast to berberine, which absorbed at

both the excitation and emission wavelengths. This observation underscores the distinct spectral characteristics of compound **1c**, confirming its specific behavior.

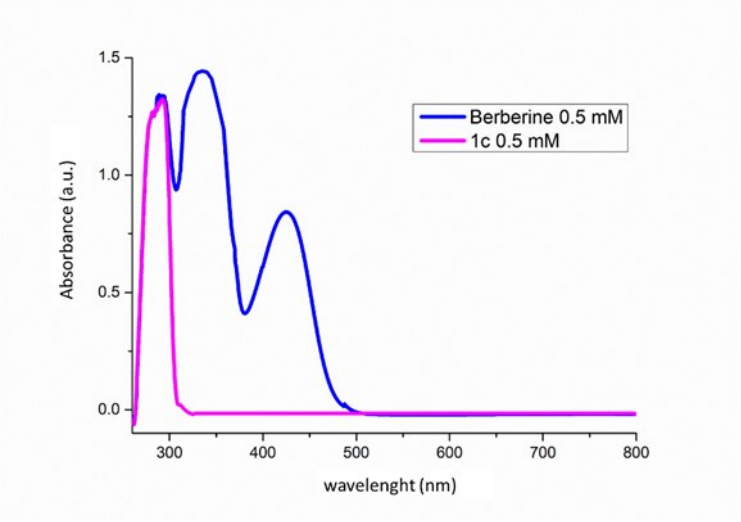

Figure 39. Absorbance spectrum of berberine and **1c** compound 0.5 mM concentration.

4.4 Conclusions

The development of novel berberine derivatives provided new insights in the exploration of compounds capable of maximizing the interactions with the FtsZ target, thereby including the development of potent antibacterial agents. The comparative analysis performed in this study allowed the understanding of the differential impacts of individual compounds on the kinetic behavior of FtsZ, thereby elucidating their peculiar inhibitory mechanisms at a molecular level. Among the tested compounds, the **1c** analogue showed the strongest inhibitory action.

The present study demonstrated that functional inhibition of FtsZ impairs cell division and induces the formation of long multinucleoid cell strands by uncoupling growth and division. Because of its vital role in cell division, its high level of conservation and its absence in eukaryotes, inhibition of FtsZ may affect cellular dynamics and bacterial cell survival, making it a fascinating target for antibacterial drug development.

The results discussed in this chapter were included in the following publication:

Di Somma, A.*, **Cané, C.***, Rotondo, N. P., Cavalluzzi, M.M., Lentini, G. & Duilio, A. (2023). A Comparative Study of the Inhibitory Action of Berberine Derivatives on the Recombinant Protein FtsZ of *E. coli*. *International Journal of Molecular Sciences*, *24 (6), 5674*. doi: 10.3390/ijms24065674

* The authors equally contributed to the work.

Chapter 5 – Mechanism of action of Esc(1-21)-1c in *P. aeruginosa*

5.1 Introduction

P. aeruginosa, a Gram-negative and rod-shaped bacterium, is recognized for its exceptional adaptability and virulence. This ubiquitous opportunistic pathogen is frequently encountered in diverse environments, including soil, water, and hospital settings[131-132]. Its inherent resistance to various antibiotics[133], coupled with its ability to form robust biofilms, often leads to persistent infections that are difficult to eradicate resulting in a significant challenge in clinical settings[134-135].

P. aeruginosa can be isolated from various sources, including several nosocomial and life-threatening infections in patients with CF, burn wounds, UTIs, and pulmonary infections[136]. Infections caused by *P. aeruginosa* are associated with high morbidity and mortality across different patient groups[137]. Notably, it has been categorized as "critical" in the WHO's priority list of bacterial pathogens[138], emphasizing the urgent need for research and development of new antibiotics[139].

P. aeruginosa is recognized as a MDR bacterium due to its inherent high resistance to a broad spectrum of antibiotics, including aminoglycosides, fluoroquinolones, and β-lactams[140-141]. This resistance is primarily attributed to the low permeability of its OM, which hampers the efficient penetration of antibiotic molecules into the cells[142].

Drug resistance in this nosocomial pathogen is additionally linked to efflux pumps consisting of membrane-conserved proteins able to recognize various antibiotics that can be actively expelled from the bacterial cell thus reducing cellular drug accumulation[143-144].

In the perspective of selecting antimicrobial molecules active against *P. aeruginosa*, scientific research has revealed that the peptide Esc (1-21) (GIFSKLAGKKIKNLLISGLKG-NH_2), derived from Esc-1a isolated from the skin of *Rana esculenta*[145], has potent activity against both the planktonic and biofilm forms of *P. aeruginosa* strains. This peptide comprises 21 amino acids, has a net positive charge of +5 and adopts a well-defined amphipathic helical conformation that is crucial for its interaction with microbial membranes. Upon contact, the peptide undergoes a dynamic process of membrane insertion, disrupting the integrity of the lipid bilayer, increasing membrane permeability and compromising its structural integrity[146]. In addition to its potent antimicrobial activity, Esc(1-21) has exhibited low cytotoxicity towards mammalian cells, underscoring its potential as a therapeutic agent with a favorable safety profile. However, the peptide is susceptible to enzymatic cleavage by bacterial proteases present in the microbial environment. This susceptibility poses a significant limitation to the stability of the peptide and efficacy in prolonged antimicrobial activities. Strategies aimed at enhancing the peptide's resistance to proteolytic degradation were developed for overcoming this limitation. The recent identification of the diastereomer Esc(1-21)-1c, bearing two D-amino acids, has revealed lower cytotoxicity against eukaryotic cells and increased resistance to proteolytic degradation in bacteria[147] (Figure 40).

Figure 40. Aminoacidic sequences of Esc-1a, Esc(1-21) and Esc(1-21)-1c.

The diastereomer was designed with a rational basis, considering that D-amino acids are recognized as "α-helix breakers," and a reduction in the α-helix content of the peptide is anticipated to diminish its ability to perturb mammalian membranes. Consequently, a substitution of two L-amino acids with their corresponding D-enantiomers was performed at positions 14 and 17. The stability of the isomer was initially evaluated in the presence of 10% and 30% fresh human serum after 24 hours of incubation at 37°C[148].

The experimental data revealed a reduced degradation of the diastereoisomer (less than 50%) compared to Esc(1–21). The inclusion of two D-amino acids significantly enhanced the resistance of the peptide to proteolytic cleavage caused by both human and bacterial elastases[149].

Given the promising properties of Esc(1-21)-1c, this Chapter specifically focused on investigating the intracellular mechanism of action of Esc(1-21)-1c and its putative specific interactors in *P. aeruginosa*. Proteomic strategies were employed to reveal a previously undescribed role for this AMP, as well as its ability to induce cell death in the bacterium. Firstly, differential proteomic analysis of protein expression in *P. aeruginosa* cells treated with Esc(1-21)-1c and untreated cells were developed to investigate the general impact of the AMP on the bacterial proteome. Then, functional proteomics approaches provided insights into the interactions of the peptide with specific protein targets. This in-depth exploration allowed for the identification of novel molecular mechanisms triggered by Esc(1-21)-1c, contributing to a more nuanced understanding of its effect on the bacterium.

5.2 Experimental methods

5.2.1 Differential Proteomic

Alterations in the proteome of *P. aeruginosa* PAO1 were assessed by cultivating bacterial cells in LB medium (Oxoid) and treating them at 0.5 OD_{600nm}/mL with 60 µg/mL of Esc(1-21)-1c at 37°C for 3 h under stirring. The control for the experiment, carried out in biological duplicate, comprised untreated cells. Cell pellets were recovered by centrifugation for 10 min at 5000 rpm at 4°C, resuspended in PBS, 5% SDS, and 1 mg/mL lysozyme. The cell cultures were sonicated at 200 W power for 20 min on ice, centrifuged at 4°C for 30 min at 15000 rpm to isolate unlysed cells and cellular debris. The recovered supernatant was quantified by BCA assay kit, following the manufacturer's instructions (Thermo Scientific, Rockford, USA). Each sample (50 µg) underwent trypsin digestion on S-trap™ micro spin columns, following the manufacturer's instructions (Protifi, Huntington, NY). Hydrolyzed peptide mixtures were subjected to analysis using LC-MS/MS employing an LTQ Orbitrap XL coupled to a nanoLC system (ThermoFisher Scientific, Waltham, MA).

Specifically, fractionation of all peptide mixtures occurred on a C18 capillary reverse-phase column (200 mm length, 75 µm ID, 5 µm biosphere) using a non-linear gradient (5% to 50%) for eluent B (0.2% formic acid in 95% ACN) in A (0.2% formic acid and 2% ACN in MilliQ water) over 260 minutes. MS/MS analyses were performed in DDA mode, involving the fragmentation of the 10 most intense ions using CID. Each sample was run in duplicate. Raw data obtained from the nano LC-MS/MS procedure were analyzed by MaxQuant[150], using UniProt *P. aeruginosa* as database for Andromeda search[151]. FCs were then computed based on LFQ values.

The selected parameters for protein identification were listed in Table 3:

Parameters	Experimental conditions
Peptides	Minimum 2 (at least 1 unique)
Variable Modifications	Methionine oxidation Pyroglutamate formation (at the N-terminal glutamine)
Accuracy	10 ppm
False Discovery Rate	0.01

Table 3. Selected parameters for LC-MS/MS analysis.

The most interesting proteins were analyzed within bioinformatic tool as STRING program version 12.0 (string-db.org) which predicts PPIs actions networks based both on functional and physical interaction. The interaction's confidence was set as high and the over-representation analysis was done considering statistically significantly enriched categories carrying a p-value <0.05.

5.2.2 Checkerboard assays

The synergistic interactions between Esc (1-21)-1c and antibiotics against *P. aeruginosa* PAO1 were assessed using the checkerboard assay titration method, performed in three independent replicates. Ceftim, Erythromycin, Tetracycline, and Chloramphenicol were the antibiotics employed. The inhibitory effects of drug combinations on bacterial growth were evaluated in MH broth for 16 h at 37°C. Combinations of two compounds were added in serial two-fold dilutions to wells of a 96-well plate containing 1 x 10^6 CFU/mL of *P. aeruginosa* PAO1, reaching a final volume of 100 µL of MH. The plates were then incubated for 24h at 125 rpm at 37°C. The FIC index for the combination of two compounds was determinted using the formula:

$$\text{FIC index} = FIC_A + FIC_B = A / MIC_A + B / MIC_B$$

- A and B are the MICs of the combination of both drug A and drug B;
- MIC_A and MIC_B represent the MIC values of each compound alone.

The FIC Index value was used to categorize the effects of the antibiotics, with the interpretation as follows: FIC ≤0.5, synergy; 0.5<FIC ≤ 1, additivity, 1 < FIC ≤ 2, no interaction, FIC >2, antagonism[152]. The combination of drugs that completely inhibited growth was considered effective, determining the MIC for the combination.

5.2.3 Transcriptional analysis

P. aeruginosa PAO1 cells were grown in 50 mL of LB medium and treated at 0.5 OD_{600nm}/mL with 60 µg/mL of Esc (1-21)-1c at 37°C for 3 h under stirring, using biological triplicates and untreated cells as control. RNA extraction from bacterial cultures was carried out using the RNeasy Minikit (Qiagen), incorporating the on-column DNase I digestion step[153]. 1 mL of each sample was incubated with 2 mL RNA Protect Bacteria Reagent (Qiagen) for 5 min at 25°C. The bacterial suspensions were then centrifuged for 20 min at 4000 rpm at 20°C. The resulting cell pellets were resuspended in 570 µL of TE buffer (10 mM Tris-HCl, 1 mM ethylenediaminetetraacetic acid; pH 8.0) and lysed by the addition of 1 mg/mL lysozyme and 2 cycles of 10 sec pulsed sonication. The purified RNA was treated with 0.2 U/mg of RNA of TURBO DNase for 1 hour at 37°C, in the presence of 0.4 U/ mg *SUPERase-In* (Ambion) to eliminate DNA. The removal of DNase I was performed using the RNeasy Column Purification Kit (Qiagen) following the manufacturer's instructions. The absence of contaminating DNA was confirmed through PCR analysis using the oligonucleotides FW*PpqsB* and RV*PpqsB* (Table 4). RNA samples were quantified using the NanoDrop 2000 spectrophotometer (ThermoFisher Scientific, Waltham, MA). cDNA synthesis was accomplished using 1 µg of purified RNA with the iScript Reverse Transcription Supermix for real time qRT-PCR kit (Bio-Rad Laboratories). The synthesized cDNAs were quantified using the NanoDrop 2000 spectrophotometer (ThermoFisher Scientific, Waltham, MA) and subjected to qRT-PCR analysis using the iTaq Universal SYBR Green Supermix kit (Bio-Rad Laboratories), and the AriaMX thermocycler (Agilent). The oligonucleotides used in qRT-PCR were designed using the Primer-Blast software (www.ncbi.nlm.nih.gov/tools/primer-blast) to avoid the production of aspecific amplicons from cDNAs and are listed in Table 4.

Following 1 min of incubation at 95°C, the amplification process encompassed 40 cycles conducted at 95°C for 10 seconds and 60°C for 45 seconds. Fluorescence readings were captured during the final 15 seconds of the incubation at 60ºC. In each experiment, cDNAs were additionally amplified using FW16S and RV16S oligonucleotides (Table 4) to normalize the data, relying on the expression levels of 16S ribosomal RNA, used as the housekeeping RNA[153]. Expression levels of genes were obtained by calculating the relative FC by the $2^{-\Delta\Delta Ct}$ method. Means and SD were obtained from three biological replicates.

Name	**Sequence (5'-3')**
FW*PpqsB*	CCGCTCGAGCGACCAGGGCTATCGCA
RV*PpqsB*	CCGGAATTCCTTATGCATGAGCTTCTCC
FW*oprM*	TCAACCTGCCGATCTTCACC
RV*oprM*	GAGCTGGTAGTACTCGTCGC
FW*oprD*	AAGACCATGCTGAAGTGGGG
RV*oprD*	CCTGCGTAGGTGGCATAGAG
FW*mexA*	CGAAGGTCTCCCTGAAGCTG
RV*mexA*	AGGATGGCCTTCTGCTTGAC
FW*mexB*	ACCTGAGCAAGTGGTACGTG
RV*mexB*	CTTGACGATCTCCTCGACCG
FW16S	GAGAGTTTGATCCTGGCTCAG
RV16S	CTACGGCTACCTTGTTACGA

Table 4. Oligonucleotides used in this study for gene expression analysis.

5.2.4 LC-MS/MS analysis in MRM scan mode

P. aeruginosa PAO1 cells were grown in 50 mL of LB medium and treated at 0.5 OD_{600nm}/mL with either 64 µg/mL tetracycline or a combination of 64 µg/mL tetracycline and 60 µg/mL Esc(1-21)-1c. The treatments were conducted at 37°C for 3 h under stirring, with biological triplicates, and untreated cells served as the control. Cell pellets were recovered by centrifugation for 10 min at 4°C at 5000 rpm, resuspended in H_2O and subjected to three cycles of freezing and sonication. Protein precipitation was achieved in cold MeOH for 30 minutes at -20°C. After centrifugation, the supernatants were recovered, dried in SpeedVac, and utilized for the metabolomic study, while the pellets were reserved for proteomic analysis.

Metabolomic samples were resuspended in acidified H_2O and desalted using Oasis HLB cartridges. LC-MS/MS analyses were performed by injecting 1 µL of the supernatant into the AB-sciex 5500 QTRAP® system with an Exion LC™ HPLC chromatography system. The mobile phase, generated by mixing eluent A (0.1 % Formic Acid in water) and eluent B (0.1 % Formic Acid in ACN), had a flow rate was 0.200 mL/min. The chromatographic gradient included 5% B for 1 minute, followed by an increase from 5% to 90% B in 4 minutes, holding for 1 minute, returning to 5% B in 2 minutes, and holding for 2 minutes. The analysis was performed using Turbo VTM ion source in positive ion mode, and the multiple reaction monitoring (MRM) mode was employed for the selected analytes. Precursor ion, product ions, collision energy, and declustering potential parameters are detailed in Table 5, and the Skyline software (3.7, 64-bit version MacCoss Lab Software, University of Washington, United States)[76] was employed for data processing, including the integration of extracted mass chromatogram peaks.

Analytes	Rt (min)	Precursor (m/Z)	Product (m/Z)	DP (V)	EP (V)	CE 1/2 (V)	CXP 1/2 (V)	Dwell (msec)
Tetracycline	5.4	445.0	410.0	36	10	27	12	200
Tetracycline	5.4	445.0	427.0	36	10	19	18	200

Table 5. MRM method for tetracycline analysis. **Rt** is the retention time; **DP** is the declustering potential; **CE** is the Collision Energy and **CXP** is the Collision Cell Exit Potential.

The content of tetracycline was quantified using the following calibration curve (Table 6 and Figure 41).

µg/L	1	2	3	Average	St. Dev.	rsd%	LOD	LOQ
7.81	65885	64625	61256	63922	2393.3	3.7	4.1	12.6
15.62	135008	129911	125708	130209	4657.2	3.6		
31.25	369766	374440	346498	363568	14966.6	4.1		
62.5	824587	860854	810975	832139	25782.9	3.1		
125	1835519	1801510	1898211.28	1845080	49054.5	2.7		

Table 6. Calibration curve parameters. **1-2-3** are the response; **rsd%** is the relative SD; **LOD** is the Limit of detection and **LOQ** is the Limit of quantification.

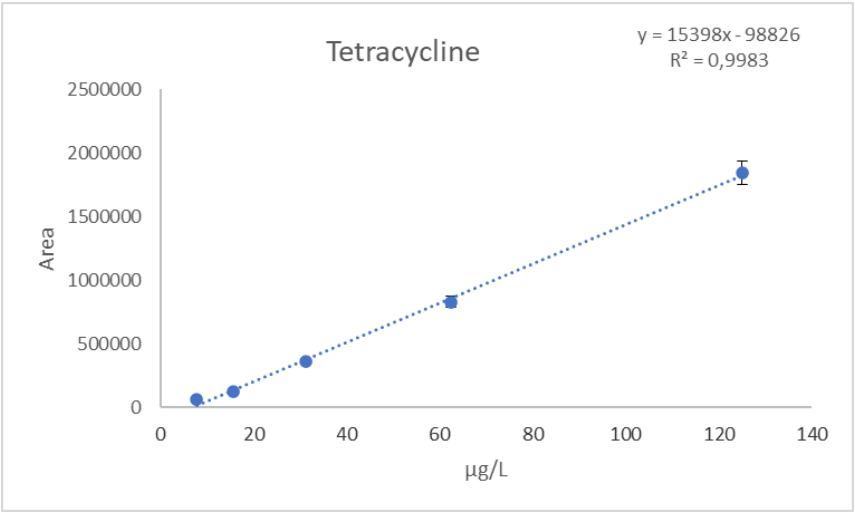

Figure 41. The average of the calibration curves.

For the proteomic analysis, protein pellets were solubilized in 6 M urea and 50 mM AMBIC. Subsequent protein hydrolysis and LC-MRM/MS analysis followed the procedures described in section 2.3.6. The proteotypic peptides were the following:

MexA = IITEGLQFVQPGVEVK

MexB = FLMLAAQNPALQR

OprM = ADQAQLQLTK

5.2.5 Functional Proteomic

200 µL of dry avidin-conjugated agarose beads were incubated with a solution containing 2 mg/mL of biotinylated Esc(1-21)-1c for 30 min at 4 °C under stirring. The supernatant was removed by centrifugation for 10 min at 3000 rpm at 4 °C. Simultaneously, *P. aeruginosa* cells at 0.5 OD_{600nm}/mL were cultured in 1 L of LB medium at 37 °C under stirring for 3 h. The pellet was recovered by centrifugation at 4 °C for 15 min at 5000 rpm and resuspended in 5 mL of Cell Lysis Buffer (20 mM Tris-HCl pH 8.0, 500 mM NaCl, 4 mM DTT, 1 mM PMSF, cOmpleteTM protease inhibitor). Following mechanical lysis, the cell debris was removed, and the supernatant was recovered and subjected to BCA assay kit, following the manufacturer's instructions (Thermo Scientific, Rockford, USA).

2.5 mg of proteins were incubated on free agarose beads for 2h at 4°C under stirring to remove possible non-specific binding, according to the pre-cleaning procedure. The supernatant containing the unbound membrane proteins was recovered by centrifugation for 10 min at 3000 rpm at 4°C and then incubated on agarose beads with the immobilized peptide for 3h at 4°C under stirring. The beads were washed with 5 volumes of PBS and the peptide-interacting proteins were released by competitive elution with 500 µL of PBS supplemented with 2 mM biotin for 1 h at 4°C under stirring. The eluted proteins were quantified by BCA assay. 50 µg of eluted proteins underwent trypsin digestion on S-trap^{TM} micro spin columns, following the manufacturer's instructions (Protifi, Huntington, NY). Hydrolyzed peptide mixtures were analyzed by nano LC-MS/MS, employing an LTQ Orbitrap XL coupled to a nanoLC system (ThermoFisher Scientific, Waltham, MA). Peptide fractionation was performed onto a C18 capillary reverse-phase column (200 mm, 75 µm, 5 µm) operating at a flow rate of 250 nl/min, using a step gradient of eluent B (0.2% formic acid, 95% ACN), and a non-linear 5% to 50% gradient of eluent B (95% ACN, 0.2% formic acid) over 260min. Mass

analyses were performed in DDA mode by fragmenting the 10 most intense ions in the CID modality.

The data obtained were used to search a non-redundant protein database using an in-house version of the Mascot software, leading to the identification of putative Esc(1-21)-1c protein interactors. The parameters used for protein identification were listed in the Table 7.

Parameters	
Fixed Modifications	Carbamidomethyl (C)
Variable Modifications	Oxidation (M) Gln-> pyro-Glu (N-Term Q)
Enzyme	Trypsin
Max Missed Cleavages	3
Minimum Number of Peptides	5
False Discovery Rate (FDR)	0.01

Table 7. Selected parameters for LC-MS/MS analysis.

5.3 Results and Discussion

5.3.1 Investigation on the alteration of *P. aeruginosa* proteome induced by Esc(1-21)-1c via differential proteomic analysis

The investigation into proteomic changes through differential proteomics in *P. aeruginosa* provided insights into the global effects induced in bacterial cells by Esc(1-21)-1c at sub-MIC concentration (60 μg/mL) for 3 hours. Following the peptide treatment, bacterial lysate proteins underwent purification via solid-phase extraction and trypsin digestion. The resulting peptide mixtures were subjected to analysis using LC-MS/MS in DDA mode, according to the label free procedure. Protein lysate from untreated *P. aeruginosa* cells was used as control.

Proteins were identified through MaXQuant software (v.1.5.2.8), with UniProt *P. aeruginosa* PAO1 serving as the reference database. The statistical comparison of expression levels between treated and untreated cells was performed utilizing MaXQuant's LFQ intensity algorithm, yielding the FC for each protein in the sample compared to the control. The statistical analysis provided a quantitative assessment of the alterations in protein expression resulting from the Esc(1-21)-1c treatment. A total of 108 differentially expressed proteins were identified, 57 of which were upregulated while 51 exhibited a decreased expression. The detailed informations for each identified protein, including the protein name, SwissProt code, gene name, and the corresponding FC, are provided in both Table 8 and Table 9.

Swiss-Prot code	Protein name	Gene name	FC
O54439	Acyl carrier protein 1	acpP1	6.81
Q9I3C5	Chaperone protein HtpG	htpG	5.1
Q59638	Dihydrolipoyllysine-residue acetyltransferase	aceF (aceB)	3.3
Q9HV55	Translation initiation factor IF-2	infB	3.24
Q51567	Succinate--CoA ligase [ADP-forming] subunit alpha	sucD	2.88
Q02RW1	Nucleoside diphosphate kinase	ndk	2.73
Q02T68	50S ribosomal protein L5	rplE	2.68
Q9HVL6	50S ribosomal protein L21	rplU	2.64
Q02UU0	Alkyl hydroperoxide reductase C	ahpC	2.63
Q9HVA2	Ketol-acid reductoisomerase (NADP(+))	ilvC	2.6
Q9I3D1	Dihydrolipoyl dehydrogenase	lpdG	2.44
Q9I0A2	50S ribosomal protein L20	rplT	2.28
Q02T73	50S ribosomal protein L16	rplP	2.24
Q59637	Pyruvate dehydrogenase E1 component	aceE	2.21
Q02T88	50S ribosomal protein L7/L12	rplL	2.14
B7UVD3	Succinate--CoA ligase [ADP-forming] subunit beta	sucC	2.09
Q02NB5	Isocitrate dehydrogenase [NADP], IDH	icd	2.05

Q02FR0	Protein GrpE (HSP-70 cofactor)	grpE	2.02
P34750	Fimbrial assembly protein PilQ	pilQ	1.99
P08308	Ornithine carbamoyltransferase, catabolic	arcB	1.95
Q02PG5	Glyceraldehyde-3-phosphate dehydrogenase	gap2	1.94
Q9HWD2	Elongation factor G 1, EF-G 1	fusA	1.92
Q9HT20	ATP synthase subunit beta	atpD	1.87
Q9HWC9	DNA-directed RNA polymerase subunit beta	rpoC	1.86
Q9I2V5	Aconitate hydratase B, ACN, Aconitase	acnB	1.76
Q9HZP6	Electron transfer flavoprotein subunit beta	etfB	1.72
P57668	Thiol peroxidase, Tpx	tpx	1.71
O82851	Elongation factor Ts, EF-Ts	tsf	1.71
Q9HW91	Methyl-accepting chemotaxis protein PctB	pctB	1.71
Q02PH8	Fatty acid oxidation complex subunit alpha	fadB	1.67
Q9HZE0	NAD-specific glutamate dehydrogenase	gdhB	1.68
Q9I5Y1	Fructose-bisphosphate aldolase	fba (fda)	1.67
P26480	RNA polymerase sigma factor RpoD	rpoD	1.66
Q02DF2	ATP synthase subunit alpha	atpA	1.65
P09591	Elongation factor Tu, EF-Tu	tufA; tufB	1.62

Q9HT21	ATP synthase epsilon chain	atpC	1.59
Q9HU15	Beta-ketoacyl-[acyl-carrier-protein] synthase	fabY	1.54
Q02FT1	30S ribosomal protein S15	rpsO	1.53
Q02T87	DNA-directed RNA polymerase subunit beta,	rpoB	1.52
O54438	3-oxoacyl-[acyl-carrier-protein] reductase FabG	fabG	1.47
Q9HVI7	Serine hydroxymethyltransferase 3	glyA2	1.46
P31961	Phosphogluconate dehydratase	edd	1.45
O82850	30S ribosomal protein S2	rpsB	1.45
P32722	Porin D	oprD	1.45
Q9HVC5	Ribose-phosphate pyrophosphokinase, RPPK	prs	1.43
P04739	Type IV major pilin protein PilA (Pilin)	pilA (fimA)	1.35
Q9HT16	ATP synthase subunit b	atpF	1.31
Q02KU3	Trigger factor, TF	tig	1.3
Q02H07	50S ribosomal protein L13	rplM	1.27
Q02RA9	CTP synthase	pyrG	1.25
Q02F86	50S ribosomal protein L9	rplI	1.25
Q9HVN5	Chaperone protein ClpB	clpB	1.25

Q02T90	50S ribosomal protein L1	rplA	1.25
P13981	Arginine deiminase, ADI	arcA	1.24
O52762	Catalase	katA	1.21
P24474	Nitrite reductase	nirS	1.21
Q02FT2	Polyribonucleotide nucleotidyltransferase	pnp	1.21

Table 8. *P. aeruginosa* PAO1 up-regulated proteins.

Swiss-Prot code	Protein name	Gene name	FC
P37798	Biotin carboxylase	accC (fabG)	0.80
Q9I407	Glutaminase-asparaginase	ansB	0.79
Q02RL5	50S ribosomal protein L19	rplS	0.78
P52477	Multidrug resistance protein MexA	mexA	0.78
Q02T91	50S ribosomal protein L11	rplK	0.78
O52759	30S ribosomal protein S4	rpsD	0.77
Q02T66	30S ribosomal protein S8	rpsH	0.77
Q02H08	30S ribosomal protein S9	rpsI	0.76
Q9HVT2	Alpha-2-macroglobulin homolog	PA4489	0.76
Q9HU56	Protein-export protein SecB	secB	0.72

P38100	Carbamoyl-phosphate synthase large chain	carB	0.71
Q02GB4	30S ribosomal protein S20	rpsT	0.71
Q9I6G2	UPF0339 protein PA0329	PA0329	0.71
Q02E46	50S ribosomal protein L28	rpmB	0.71
Q9HZA6	Motility hub protein FimV	fimV	0.70
O52761	50S ribosomal protein L17	rplQ	0.64
Q9HXY5	Skp-like protein	PA3647	0.63
Q02V73	Glycine--tRNA ligase beta subunit	glyS	0.61
Q9I5V8	30S ribosomal protein S21	rpsU	0.60
Q02T67	30S ribosomal protein S14	rpsN	0.60
Q02GB0	50S ribosomal protein L27	rpmA	0.60
Q02T78	50S ribosomal protein L23	rplW	0.58
Q9LCT3	Protein translocase subunit SecA	secA	0.56
Q02RY8	Probable cytosol aminopeptidase	pepA	0.54
Q02T85	30S ribosomal protein S12	rpsL	0.55
Q9HWF8	30S ribosomal protein S11	rpsK	0.53
Q51487	Outer membrane protein OprM	oprM	0.53
Q02T77	50S ribosomal protein L2	rplB	0.52
Q02T70	50S ribosomal protein L14	rplN	0.51
Q9HWF3	50S ribosomal protein L30	rpmD	0.49

Q9HWE4	30S ribosomal protein S17	rpsQ	0.49
Q02EW8	50S ribosomal protein L31	rpmE	0.49
Q02T71	30S ribosomal protein S17	rpsQ	0.49
P47205	UDP-3-O-acyl-N-acetylglucosamine deacetylase	lpxC (envA)	0.47
Q9HZN4	50S ribosomal protein L32	rpmF	0.47
Q9HXP9	30S ribosomal protein S16	rpsP	0.45
Q9HWF2	30S ribosomal protein S5	rpsE	0.45
Q9I0K4	Isocitrate lyase	PA2634	0.45
Q9HTN9	50S ribosomal protein L33	rpmG	0.45
Q02T63	30S ribosomal protein S5	rpsE	0.43
Q9I6Z1	GDP-polyphosphate phosphotransferase	ppk2	0.43
Q9I4Z4	Peptidoglycan-associated lipoprotein, PAL	oprL	0.40
P13794	Outer membrane porin F	oprF	0.40
Q02T72	50S ribosomal protein L29	rpmC	0.38
Q9HXN2	Phosphoribosylformylglycinamidine synthase	purL	0.38
Q9HWF4	50S ribosomal protein L15	rplO	0.34
P57112	Soluble pyridine nucleotide transhydrogenase	sthA	0.30
P52002	Multidrug resistance protein MexB	mexB	0.29

Q9HYT6	RNA polymerase-associated protein RapA	rapA	0.26
P11221	Major outer membrane lipoprotein	oprI	0.22
Q9HUN0	30S ribosomal protein S18	rpsR	0.17

Table 9. *P. aeruginosa* PAO1 down-regulated proteins.

Among the numerous accessory proteins differentially expressed, the proteomic data indicated the down-regulation of MexAB-OprM proteins. These proteins form a well-known complex constituting a tripartite efflux system in *P. aeruginosa*, that plays a pivotal role in MDR by expelling various drug compounds[154].

Since increased expression of efflux pumps is an important mechanism of antibiotic resistance in *P. aeruginosa*, the observed down-regulation of the MexAB-OprM pump suggests that Esc (1-21)-1c might provide a disruption in the antibiotic efflux mechanism, thus contributing to counteract MDR.

Furthermore, the potential reduction in intrinsic resistance is supported by the down-regulation of SecA, SecB, OprF, and OprI proteins, alongside the up-regulation of the porin OprD. SecA, SecB, OprF, and OprI participate in the secretion of proteins, antibiotics, and metabolites, while OprD serves as a major specific porin in *P. aeruginosa*, facilitating antibiotic uptake. Literature data reported that the absence of OprD in *P. aeruginosa* enhances resistance to antibiotics[155].

These proteins, together with MexAB-OprM, were categorized based on their interactions using STRING software, which employs a bioinformatics approach to predict and analyze PPIs. This computational tool integrates diverse sources of evidence, including experimental data, co-expression analysis, and curated

databases, to construct a comprehensive network of protein interactions. By employing STRING software, the relationships and functional associations among these proteins, including their involvement in cellular processes and pathways, can be elucidated with greater precision (Figure 42).

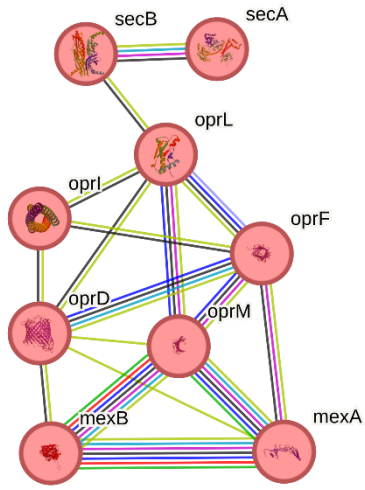

Figure 42. String analysis highlighting robust PPIs within a distinct protein cluster.

In summary, the differential proteomic experiments suggested that Esc(1-21)-1c might affect the tripartite MexAB-OprM efflux pump recognized for its crucial involvement in expelling drug compounds being a pivotal constituent of the intrinsic defense mechanisms of *P. aeruginosa* against antibiotics.

5.3.2 Improving antibiotic efficacy against *P. aeruginosa* with Esc(1-21)-1c

The results of the differential proteomic approach led to the hypothesis of a possible synergistic effects of the peptide with antibiotics that might enhance the overall therapeutic impact of the treatment regimen. The experiments were carried out in collaboration with the research group of Prof. Maria Luisa Mangoni (Department of Biochemical Sciences – University Sapienza – Rome). The concurrent administration of Esc(1-21)-1c and antibiotics might increase the antimicrobial activity and reduce the evolution of resistant strains. This effect has recently been demonstrated with Esc(1-21)-1c when used in combination with aztreonam on *P. aeruginosa*[156], suggesting a strategic approach to develop more effective and sustainable antibacterial interventions.

On this basis, the determination of the FIC index, as described in the section 5.2.2, was instrumental to evaluate the effect of the Esc(1-21)-1c in combination with different antibiotics. Checkerboard titration assays were performed on *P. aeruginosa* PAO1 cells. Different concentrations of both antibiotic(s) and the peptide were added either individually or in combination in a serial two-fold dilution format. FIC values were interpreted as reported in the section 5.2.2 and are summarized in the Table 10.

FIC value	**Effect**
FIC ≤0.5	Synergy
0.5 <FIC ≤ 1	Additivity
1 < FIC ≤ 2	No interaction
FIC >2	Antagonism

Table 10. Interpretation of FIC Indices for the evaluation of the combinatorial effect between Esc(1-21)-1c and different antibiotics.

Results presented in Table 11 report the response to individual components, either the peptide or the antibiotic, as well as their combined effects on *P. aeruginosa*, providing a clear evidence of the potential synergistic or antagonistic interactions between the antibiotic(s) and Esc(1-21)-1c.

Molecules	MIC alone (µg/mL)	MIC in combination (µg/mL)	FIC
Esc(1-21)-1c	6.8	3.4	>0.5
Ceftazidime	8	1	
Esc(1-21)-1c	6.8	1.7	≤0.5
Erythromycin	256	32	
Esc(1-21)-1c	6.8	0.85	≤0.5
Chloramphenicol	32	4	
Esc(1-21)-1c	6.8	1.7	≤0.5
Tetracycline	8	1	

Table 11. Effect of Esc(1-21)-1c and various antibiotics on *P. aeruginosa* cells. Adapted with the permission from Cané et al. 2023. Frontiers in Chemistry.

In addition, the synergistic or additive effects of Esc(1-21)-1c with various antibiotics were illustrated in the corresponding growth curves of *P. aeruginosa* PAO1 (Figure 43) treated with either the peptide or the antibiotic alone or in combination.

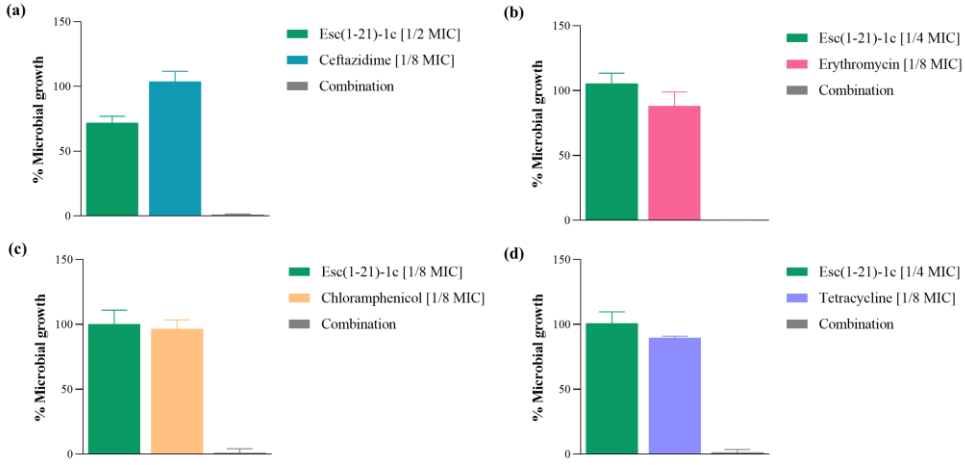

Figure 43. Growth of *P. aeruginosa* PAO1 assessed via spectrophotometry by measuring optical density after a 16-hour treatment with antibiotics or Esc(1-21)-1c, administered individually or in combination. Bacterial growth is presented as a percentage relative to untreated control cells (100%). The results represent the mean ± SD of three independent experiments.

The results demonstrated the remarkable capabilities of the peptide, Esc(1-21)-1c, to elicit diverse responses when combined with different antibiotics. Specifically, the peptide demonstrated a synergistic effect with erythromycin, chloramphenicol, and tetracycline, while exhibiting an additive effect with ceftazidime. In the latter case, it is worth noting that beta-lactams exert their action on cell wall synthesis without requiring entry into the cytoplasm. Considering the mechanism of action of Esc(1-21)-1c as an adjuvant, it is reasonable that it does not have a significant effect on the MIC of this class of compounds.

Furthermore, when *P. aeruginosa* was treated with either the antibiotic or the peptide alone, bacterial cells were able to proliferate. In contrast, when the bacterial cells were submitted to the combined treatment of Esc(1-21)-1c with ceftazidime, erythromycin, chloramphenicol, and tetracycline, no growth was observed, indicating a potentiated antibacterial effect.

5.3.3 Evaluation of MexAB-OprM efflux pump alteration induced by Esc(1-21)-1c

The proteomic analysis revealed alterations in the levels of MexAB-OprM and OprD when exposed to Esc(1-21)-1c. However, the specific mechanisms underlying these alterations remain elusive, with no available information on whether the observed effects occur at the translational or transcriptional level. To explore this aspect, an investigation into the gene expression levels corresponding to both MexAB-OprM efflux pump and OprD was performed. *P. aeruginosa* PAO1 cells were cultured at 0.5 OD/mL and treated with 60 µg/mL Esc(1-21)-1c for 3h. Then, mRNA was extracted from both treated and untreated cells, and subsequent qRT-PCR analysis was performed in collaboration with the research group of Prof. Giordano Rampioni (Department of Science – University Roma III – Rome). Data presented in Figure 44 represents relative levels of mexA, mexB, oprM, and oprD mRNAs in *P. aeruginosa* PAO1 cultures treated with 25 µM Esc(1-21)-1c and provides clear evidence of a substantial reduction in the expression levels of mexA, mexB, and oprM genes, which are constituents of the mexAB-oprM operon, following Esc(1-21)-1c treatment. Furthermore, an increase in the expression of oprD in Esc(1-21)1c-treated cultures was observed in comparison to the control.

.

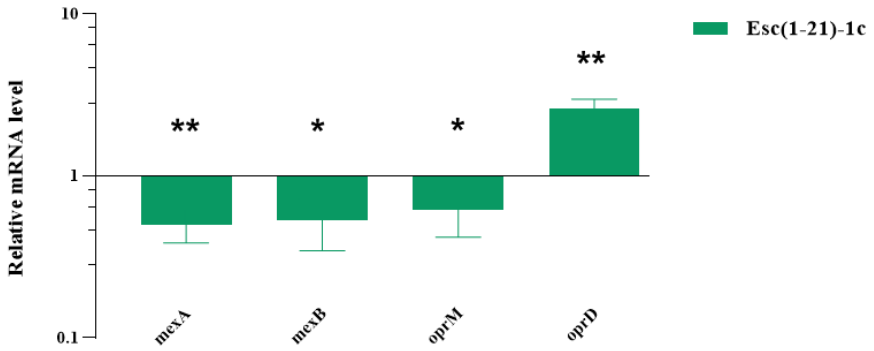

Figure 44. Relative levels of mexA, mexB, oprM, and oprD mRNAs in *P. aeruginosa* PAO1 cultures after treatment with 25 µM Esc(1-21)-1c, compared to untreated cells. Results are presented as the mean ± SD from three independent experiments. Statistical significance was determined through t-test analysis using GraphPad Prism 9 and p-value < 0.001 was indicated as ** in the graph.

These investigations led us to two important considerations. Firstly, these findings are consistent with the data obtained from the proteomic analysis, as the observed effect on the expression of the analyzed genes corresponds to the trend observed in protein expression. More importantly, the results showed that the peptide affects the transcriptional regulation of the efflux pump, suggesting the existence of a unidentified mechanism, modulated by Esc(1-21)-1c.

Differential proteomic data were further validated through a targeted proteomic approach, using LC-MS/MS in MRM scan mode. The experiments were carried out in collaboration with the research group of Prof. Angela Amoresano (Department of Chemical Sciences – University Federico II – Naples). The selection of proteotypic peptides for the specific monitoring of MexA, MexB and OprM were performed using Skyline software, as detailed in the section 5.2.4. Subsequently, *P. aeruginosa* PAO1 cultures were treated with 64 µg/mL tetracycline alone or in combination with 60 µg/mL Esc(1-21)-1c for 3h, with

untreated cultures used as controls. The protein extracts were digested with trypsin and the resulting peptide mixtures analyzed in triplicate by LC-MS/MS in MRM scan mode. The obtained data are presented in the Figure 45 that reports the average peak areas from different replicates for each peptide of MexA, MexB and OprM proteins. A clear reduction in the amount of the monitored proteins could be detected in cultures treated with tetracycline and Esc(1-21)-1c, while tetracycline alone did not affect the protein levels.

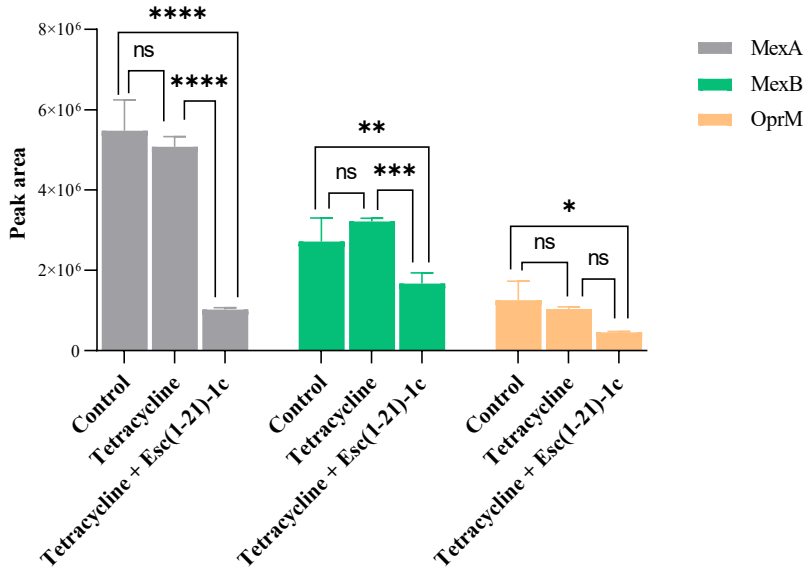

Figure 45. MRM/MS data of MexA, MexB, and OprM proteins in *P. aeruginosa* cells treated with either the antibiotic alone or a combination of antibiotic plus Esc(1-21)-1c. Results are presented as the mean ± SD from two independent experiments. Statistical significance was determined through t-test analysis using GraphPad Prism 9 and p-value < 0.0001 was indicated as **** in the graph.

The comprehensive analysis of all the data collectively supports the conclusion that the treatment with Esc(1-21)-1c has an impact on the intrinsic resistance mechanisms of *P. aeruginosa*. Specifically, the ability of the bacterium to release

antibiotics from its cells and regulate their uptake is significantly impaired under the influence of Esc(1-21)-1c.

5.3.4 Esc(1-21)-1c-mediated reduction in intrinsic tetracycline resistance of *P. aeruginosa*

The downregulation of the MexAB-OprM efflux pump expression induced by Esc(1-21)-1c together with the synergistic effect exerted by the peptide in combination with various antibiotics provided insights into the reduction of intrinsic resistance mechanisms in *P. aeruginosa*. Impairment of the drug release system should led to an accumulation of antibiotics within the bacterial cells with consequential letal effect.

A clear demonstration of this effect was obtained by a quantitative analysis of tetracycline levels in *P. aeruginosa* by LC-MS/MS in MRM scan mode. The choice of tetracycline in these studies is closely linked to the observed synergistic effect when it is combined with Esc(1-21)-1c. In addition, tetracycline has found widespread application in clinical practice for the treatment of various bacterial infections.

The initial step in the quantitative analysis of tetracycline within bacterial cells involved measurements of tetracycline standard solutions at various concentrations. This was undertaken to determine optimal instrument settings and precursor ion-product ion transitions, and to construct a calibration curve for quantitative assessment. Then, *P. aeruginosa* PAO1 cultures were treated with 64 µg/mL tetracycline alone or in combination with 60 µg/mL Esc(1-21)-1c for 3 h, with untreated cultures used as control. Following the extraction and analysis of the metabolites, the quantification of tetracycline was achieved by interpolating the obtained data with the calibration curve constructed using standard solutions of tetracycline (Figure 46).

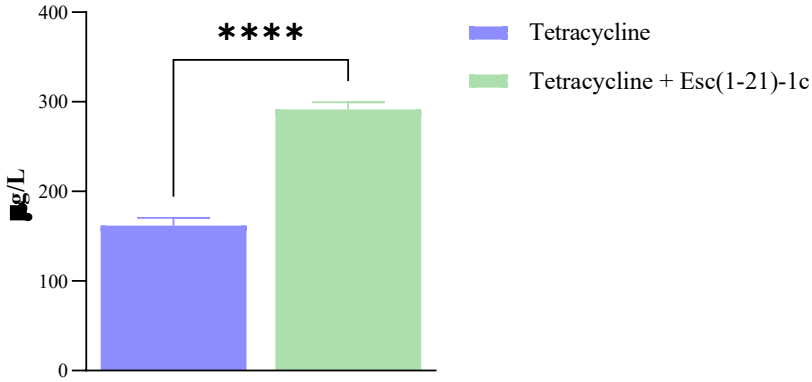

Figure 46. Relative amount of tetracycline in *P. aeruginosa* PAO1 cells treated with either the antibiotic alone or a combination of antibiotic plus Esc(1-21)-1c. Results are presented as the mean ± SD from two independent experiments. Statistical significance was determined through t-test analysis using GraphPad Prism 9 and p-value < 0.0001 was indicated as **** in the graph.

Data revealed a twofold increase in tetracycline concentrations within bacterial cells when *P. aeruginosa* was treated with with Esc(1-21)-1c and tetracycline, compared to those treated with tetracycline alone (~297 vs. ~162 μg/L, respectively). This finding is in agreement with the idea that co-administration of Esc(1-21)-1c together with specific antibiotics can decrease their release thus increasing their intracellular concentration.

5.3.5 Molecular understanding of the mode of action of Esc(1-21)-1c

The down-regulation of MexA-MexB-OprM efflux pump downregulation emerged as a key outcome both in the differential proteomic and transcriptional analyses, prompting further investigations. A functional proteomic experiment was then designed to identify the specific target(s) of Esc (1-21)-1c in *P. aeruginosa*. A biotinylated form of Esc(1-21)-1c was immobilized onto streptavidin-conjugated agarose beads and incubated with a membrane proteins extract from *P. aeruginosa* cultures. The putative interactors of the peptide were eluted by competition and the corresponding pre-cleaning mixture (proteins incubated with the streptavidin-conjugated agarose beads in the absence of Esc(1-21)-1c) was used as control. Proteins from both the sample and pre-cleaning were trypsin-digested on S-trapTM micro spin columns, and the resulting peptide mixtures were analyzed using LC-MS/MS. The acquired data were analyzed by Mascot software, leading to the identification of 245 proteins. Only the proteins identified in the sample were considered as potential interactors of Esc(1-21)-1c, wherease those only occurring in the pre-cleaning were discarded. The putative interactors were then categorized based on the biological processes they belong to, defined by Uniprot database (Figure 47).

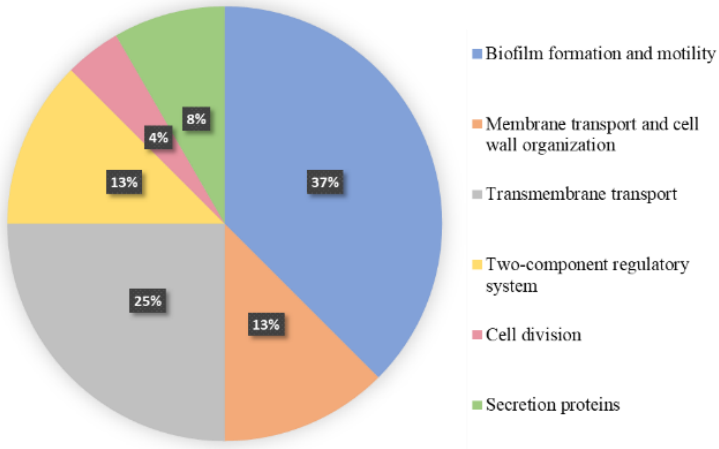

Figure 47. Distribution of Esc(1-21)-1c putative protein partners identified in the pull-down experiment.

Among the identified proteins, several members of TCS, which play a pivotal role in signal transduction pathways in *P. aeruginosa*, were present. TCS are regulatory systems consisting of a RR and a HK, sensitive to environmental changes. The HK undergoes autophosphorylation at a conserved histidine residue, and this phosphoryl group is subsequently transferred to the cognate RR, typically a transcription factor[157]. The RR consists of two distinct structural domains, a RD and an ED. Upon phosphorylation of the RD by the HK domain in response to an external signal, the ED becomes activated and binds to designated promoters, initiating the transcription of target genes[158]. This mechanism is characteristic of proteins within the OmpR/PhoB family, the major class of TCS. The phosphorylation of RR induces an allosteric change, enabling homodimerization and enhancing DNA binding[159-160].

The identified TCS proteins are listed in Table 12. Identification of several RR acting as transcriptional controllers confirmed previous data pointing out to a

mechanism involving the transcriptional inhibition of the MexAB-OprM efflux pump by Esc(1-21)-1c.

Swiss Code	Protein Name	Gene	Peptides	Biological Function
Q9I2U3	Two-component response regulator ParR	parR	3(1)	Two-component regulatory system
Q9HU59	DNA-binding transcriptional regulator NtrC	ntrC	3(1)	Regulation of biofilm formation
Q9HV31	Sensor protein kinase PmrB	pmrB	4(1)	Two-component regulatory system
G3XCT6	Chemotaxis protein CheA	PA1458	1(1)	Chemotaxis
Q9HX42	histidine kinase	ladS	3(1)	Biofilm process
Q9HYE4	histidine kinase	PA3462	2(1)	Sensor kinase activity
Q9I5H3	Probable two-component response regulator	PA0756	5(2)	Two-component regulatory system
Q9HWI4	Histidine kinase	bfiS	4(1)	Biofilm formation
P24908	Putative transcriptional regulator	PA0034	7(1)	Two-component regulatory system
Q9I6K5	EAL domain-containing protein	PA0285	4(1)	Regulation of DNA-templated transcription

Table 12. List of proteins belonging to TCS identified in the Pull-Down experiment.

Literature studies have contributed to defining the functional roles of each protein listed in the Table 12, with particular attention directed towards protein Q9I5H3. In *P. aeruginosa* this protein emerges as a RR belonging to a TCS, with its cognate HK being the sensor protein QseC (Swiss Code Q9I5H2). Despite the acknowledged significance of Q9I5H3, information regarding its specific functions remains limited. Sequence homology studies, using BLASTp database, revealed the highest similarity with *E. coli* K12 QseB protein (Swiss Code P52076). QseB activates the expression of the AcrAB-TolC efflux pump genes of *E. coli*. This pump is integral to the bacterial resistance mechanism, facilitating the expulsion of various antimicrobial compounds from the bacterial cell. QseB responds to external signals, potentially linked to environmental stress or the presence of specific substrates, by modulating the transcriptional activity of the acrAB-tolC operon[161]. Surprisingly, AcrAB-TolC efflux pump of *E. coli* is reported to be the homologous of MexAB-OprM efflux pump of *P. aeruginosa*[162].

This comparative analysis indicated potential conserved roles for the two TCS in *E. coli* and *P. aeruginosa*, suggesting that Q9I5H3 might be a transcriptional activator of the mexAB-oprM operon. According to this hypothesis, the interaction between Esc(1-21)-1c and this transcriptional regulator might then be the cause of the impairment of MexAB-OprM efflux pump. To date, only two activators of MexAB-OprM are known in *P. aeruginosa*. The first one is BrlR protein which binds the promoter region of MexAB-OprM and activates the efflux pump during biofilm formation[163].

A better known activator of the efflux pump is CpxR (RR), firstly identified in *E. coli*, which in *P. aeruginosa* belongs to the TCS together with CpxA (HK). Recent comparative genome analysis showed that CpxR has a consensus binding site (5′-GTAAA-$(N)_{4\text{-}8}$-GTAAA-3′) on the promotor of mexAB-OprM in different Pseudomonas strains, including *P. aeruginosa*[164].

Based on this encouraging information, preliminary protein-DNA docking studies were conducted to evaluate whether Q9I5H3, the putative interactor of Esc(1-21)-1c, could recognize the same consensus binding site of CpxR in the promoter region of mexAB-oprM. The experiments were carried out in collaboration with the research group of Prof. Daniela Montesarchio (Department of Chemical Sciences – University Federico II – Naples). The DNA structure, that includes the consensus sequence, and the dimer of Q9I5H3 were modelled. Docking prediction was carried out using PyDock Server and the result is shown in the Figure 48.

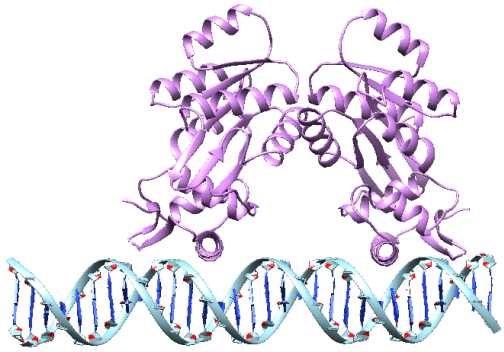

Figure 48. Docking analysis of the DNA consensus sequence with the Q9I5H3 dimer (in purple).

The docking analysis returned a negative score of -68.871, indicative of a favorable interaction between the DNA and the protein. Particularly interesting is the observed binding mode, as the alpha helix of the dimer aligns precisely with the major groove of the consensus sequence in the DNA duplex. Additionally, the amino acids involved in mediating these interactions belong to the ED, particularly the region 123-220, well-recognized for its role in DNA binding.

5.4 Conclusions

The mechanism of action of Esc(1-21)-1c on *P. aeruginosa* was deeply investigated through proteomic approaches to elucidate its molecular features. The possible mechanism exerted by the peptide revealed the inhibition of the MexAB-OprM efflux pump activity at concentrations corresponding to inhibitory sub-MIC values, shedding light on the biological alterations underlying Esc(1-21)-1c treatment.

These results represented a clear evidence of a mechanism responsible for the increased susceptibility of *P. aeruginosa* to various antibiotics following exposure to Esc(1-21)-1c. This effect is attributed to the impairment of the MexAB-OprM efflux pump, possibly occurring through the interaction of the peptide with a putative transcriptional regulator of the pump identified by functional proteomics. Further *in vitro* and *in vivo* studies elucidating the binding of the transcriptional regulator with both Esc(1-21)-1c and the DNA could comprehensively clarify the mechanism of action of Esc(1-219-1) in *P. aeruginosa*.

The results discussed in this chapter were included in the following publication:

Canè, C.*, Casciaro, B.*, Di Somma, A., Loffredo, M. R., Puglisi, E., Battaglia, G., ... & Mangoni, M. L. (2023). The antimicrobial peptide Esc (1-21)-1c increases susceptibility of *Pseudomonas aeruginosa* to conventional antibiotics by decreasing the expression of the MexAB-OprM efflux pump. *Frontiers in Chemistry*, *11*. doi: 10.3389/fchem.2023.1271153

* The authors equally contributed to the work.

Final Discussion

Antibiotic resistance poses an escalating global threat to public health as bacterial infections become progressively difficult to treat with conventional antibiotics. The proliferation of antibiotic-resistant bacterial strains is driven by the excessive and inappropriate use of these drugs in medical and agricultural settings[165]. This, coupled with a limited pipeline for developing new antibiotics, has highlighted the need to develop novel antimicrobial therapies. Identifying new therapeutic targets and implementing innovative strategies are essential to counteract the evolution of antimicrobial resistance. Additionally, supporting the development of new treatment modalities is crucial to effectively combat bacterial infections and preserve the long-term efficacy of antibiotics[166]. The identification of promising protein targets in diverse bacterial systems, as documented in this Ph.D dissertation, establishes a foundation for prospective advancements in antimicrobial therapies. This approach opens avenues for the future design and refinement of novel antibiotics or antimicrobial agents.

The project initially focused on elucidating the mechanism of action of Mag-2 and Temp-L, two well-known AMPs derived from frog skin.

Mag-2 exhibits potent antimicrobial activity against *E. coli*[167]. Since numerous studies indicated the ability of an increasing number of AMPs to cross the bacterial cell membrane and target essential processes necessary for survival[168], an in-depth study into the action of the peptide was performed in order to identify potential protein targets. The investigation stemmed from a previous functional proteomics study that identified a significant number of protein interactors involved in porin activity and protein insertion in the membrane, including OMPs and the BAM complex (ABCD). These findings align with literature reports of Mag-2 interacting with negatively charged membrane phospholipids, leading to the formation of transient pores that disrupt the membrane and facilitate peptide

translocation into the inner membrane[169]. Moreover, molecular docking analyses suggested a direct interaction between the peptide and BamA, a membrane protein responsible for the insertion and folding of OMPs[170], stimulating investigations on this target in *E. coli*.

Within this framework, *in vitro* fluorescence binding assays using recombinant BamA, in the presence of different Mag-2 concentrations, demonstrated the formation of a stable complex with a low K_d value. These results were further corroborated by DLS spectroscopy, establishing a direct interaction between the peptide and BamA.

The Mag-2 interaction with the β-barrel structure of BamA resulted in the potential disruption of OMP folding within the bacterial OM. Functional targeted proteomic experiments revealed a reduced quantity of OMPs in the OM, particularly OmpA and OmpF, supporting the notion that investigating the peptide-BamA complex formation could elucidate key structural determinants leading to impaired OMP folding. A similar phenomenon has been documented in a mutant bamA allele, where there is a moderate reduction (20–30%) in OMP levels[171], indicating an OMP biogenesis defect when BamA function is compromised. These observations suggested the potential for developing novel peptidomimetic drugs tailored to bind BamA, which could be proposed for future pharmaceutical applications, given its involvement in a biologically significant process for *E. coli* survival and absence in humans.

The second peptide, Temp-L, has garnered attention due to its remarkable antimicrobial activity against both Gram-negative and Gram-positive bacteria. Notably, while the mechanism of action of Temp-L has been elucidated in Gram-negative bacteria like *E. coli*[93], a significant gap remains in our understanding regarding its effects on Gram-positive pathogens, particularly *S. aureus*. It is a virulent bacterium known for its extensive array of virulence factors, which

contribute to its pathogenicity and ability to cause a variety of infections, ranging from skin and soft tissue infections to life-threatening conditions such as sepsis and endocarditis. Moreover, the rise of antibiotic-resistant strains of *S. aureus*, including MRSA, presents a formidable challenge in healthcare settings worldwide. With conventional antibiotics losing their efficacy against these resistant strains, alternative therapeutic strategies need to be explored. Consequently, the analysis of the behavior of the Gram-positive bacterium *S. aureus* in the presence of the antimicrobial peptide Temp-L has been investigated.

The effect elucidated by previous morphological and differentially proteomic studies of Temp-L on *S. aureus* presents distinctive characteristics. The peptide induces the formation of vesicle-like structures in *S. aureus*, along with a significant increase in the expression of proteins associated with cell wall organization and fatty acid biosynthesis. This upregulation supports the observed vesicle formation, which is crucial as fatty acids are essential for assembling the lipid bilayer surrounding extracellular vesicles. In this phase of the study, vesicle production was confirmed through DLS and GC-MS analyses. The results revealed alterations in membrane composition post-exposure to Temp-L, while GC-MS analysis demonstrated an increase in total fatty acids extracted from the treated sample compared to the negative control. The phenomenon of membrane vesicle production, as a means to counteract the deleterious effects of antibiotic treatments, has been previously documented in *S. aureus*[172]. Moreover, genes implicated in fatty acid biosynthesis were found to be upregulated in a *S. aureus* mutant with a reduced telavancin susceptibility[173], and increased amounts of longer-chain, unsaturated fatty acids were identified in *S. aureus* strains resistant to thrombin-induced platelet microbicidal protein[174]. Under antibiotic stress conditions, *S. aureus* greatly increased the secretion of extracellular vesicles compared to bacterial cells grown without stress[175].

In addition to the enhancement of cell wall and fatty acid biosynthesis pathways, proteomic analysis revealed a reduction in the abundance of various proteins implicated in modulating virulence factors. The expression of virulence proteins in *S. aureus* is governed by a complex regulatory network involving loci associated with the expression of adhesins, known as MSCRAMMs[176]. These proteins exhibit specific interactions with key plasma or extracellular matrix components in normal tissues or those adhering to biomedical devices[177].

Adhesion and invasion assays on eukaryotic A549 cells (human type 2 pneumocytes) infected with Temp-L treated *S. aureus* confirmed the impact of the peptide on the adhesion and invasion characteristics of *S. aureus*, leading to a reduction in its infectivity.

These results suggested that targeting virulence could be a novel alternative strategy, weakening the bacterium by compromising its ability to cause disease[178]. This approach focuses on attenuating the harmful effects of the bacterium on the host, providing a potential avenue for developing antimicrobial therapies that are less prone to eliciting resistance.

The direct use of AMPs as pharmaceuticals is hindered by several challenges, prompting the need for the development of synthetic molecules or modified peptides. One primary issue is the susceptibility of AMPs to degradation by proteases in the body, which can diminish their efficacy and therapeutic potential[179]. Additionally, the emergence of antimicrobial resistance against AMPs poses a significant threat to their long-term effectiveness in combating infectious diseases. To address these challenges, researchers are exploring the design and synthesis of molecules or modified peptides with improved stability, specificity, and reduced risk of resistance development, aiming to enhance their therapeutic utility while minimizing adverse effects on the host microbiota.

For these reasons, and to further the pursuit of identifying protein targets in combating antibiotic resistance, endeavors have been focused on designing novel compounds derived from berberine and a newly modified antimicrobial peptide named Esc(1-21)-1c.

The study on berberine derivatives was conducted to evaluate whether appropriate modifications of berberine can specifically interfere with the enzymatic activity of FtsZ. This choice was motivated by two main considerations: firstly, berberine, a well-known alkaloid with documented antimicrobial activity against *E. coli*, has a broad and recognized therapeutic potential and is known to target the FtsZ protein in *E. coli*, an essential component for bacterial cell division; secondly, there is a need for the development of new derivatives that overcome the undesired pharmacokinetic properties and poor water solubility of berberine.

Recently, molecular docking studies and structure-activity relationship analyses have been employed to identify molecules with enhanced affinity for the active site of the target protein, yielding promising results[94]. On these grounds, new derivatives of berberine have been chemically synthesized and investigated. Surprisingly, these novel derivatives demonstrated structural advantages associated with enhanced solubility and antimicrobial activity, showing greater inhibitory action against FtsZ.

This has been evidenced through enzymatic assays conducted with a recombinant form of FtsZ, confirming different inhibition mechanisms, as suggested by docking predictions. Analogues **1c, d,g,h** and **2h** led to the development of a competitive inhibitory mechanism, with analogue **1c** demonstrating the most potent inhibitory effect, as evidenced by a twofold increase in the K_M value and remarkably low K_i values. These results are encouraging, as recent literature studies have demonstrated that the antimicrobial

peptide Temp-L in *E. coli* inhibits the enzymatic activity of FtsZ[93] with K_M values comparable to those obtained for compound **1c**. However, compound **1c** presents the advantage of potential direct use as an antibacterial agent compared to the disadvantages that an antimicrobial peptide may exhibit.

Moreover, compounds **1f** and **1i** demonstrated a non-competitive inhibitory mechanism, as evidenced by the reduction in the V_{max} value. Additionally, compound **2g** showed decreased K_M and V_{max} values, indicating an acompetitive mechanism. This mechanism induces a conformational change in the enzyme, resulting in reduced substrate affinity at the active site and a decrease in both kinetic parameters.

The impact of berberine analogues inhibition on FtsZ GTPase activity also influenced FtsZ polymerization in a dose-dependent manner, with compounds **1c**, **1f**, and **1i** exhibiting the greatest inhibitory effects. Particularly noteworthy was the performance of analogue **1c** among the tested compounds, displaying significant efficacy in both inhibiting FtsZ GTPase activity and preventing protein polymerization. Consequently, a more extensive investigation was conducted to explore the interaction between compound **1c** and the target protein FtsZ, using fluorescence binding assays. The binding of **1c** to FtsZ resulted in the formation of a stable complex, characterized by a K_d in the low nanomolar range.

FtsZ, like BamA, exhibits a high level of conservation and is absent in eukaryotes. Serving as the main protein in the divisome complex, these characteristics make it a compelling target for antibacterial drug development with the goal of inhibiting cell division[180].

The project ended with the employment of proteomic strategies to elucidate the mechanism of action of a previously unexplored antimicrobial peptide, Esc(1-21)-1c, against *P. aeruginosa*, a prominent etiological agent of respiratory

infections, notably in individuals with CF[181]. By employing a combined approach of differential proteomics and gene expression analysis, it was discovered that the peptide induces transcriptional downregulation of an efflux pump closely linked to the development of intrinsic resistance in *P. aeruginosa*. Specifically, a reduction in MexAB-Oprm efflux pump expression, concomitant with an increase in OprD protein associated with OM permeability[182], was observed.

These findings were corroborated through direct quantification of the specific proteins using LC-MS/MS procedures in MRM scan mode. The MexAB-OprM system is pivotal in the MDR mechanism of *P. aeruginosa*, actively extruding a diverse array of antimicrobials[183], and it has already been observed that overproduction of the MexAB-OprM efflux system resulting from mutations in the nalB repressor gene confers increased resistance to several antibacterial agents in *P. aeruginosa*[184]. The decreased function of the MexAB-OprM pump in expelling drugs, along with the increased intake activity facilitated by the OprD porin, results in higher drug concentrations within the bacterial cells. This heightened drug content renders the bacteria more prone to antibiotic susceptibility. This outcome was validated through direct quantification of tetracycline levels in *P. aeruginosa* cells treated with Esc(1-21)-1c, employing MRM analyses. The findings revealed a notably elevated tetracycline concentration in the peptide-treated samples compared to the controls.

Interestingly, Esc(1-21)-1c demonstrates a synergistic effect when combined with tetracycline. It cannot be excluded that this effect might arise from membrane permeabilization induced by the presence of the peptide. Nevertheless, the enhancement of intracellular drug uptake represents a significant demand, and the effect of Esc(1-21)-1c could contribute to achieving this goal. The present findings are consistent with existing literature, highlighting the suppression of oprM and mexA gene expression in *P. aeruginosa* cells, alongside the upregulation of oprD

gene transcription and intracellular antibiotic concentration (specifically ceftazidime), induced by Trp-containing peptides L11W and L12W[185].

In addition, the mechanism of Esc(1-21)-1c was fully elucidated through functional proteomic studies aimed at identifying one or more protein targets. Surprisingly, a transcriptional regulator belonging to a TCS was identified. The decreased pump expression might result from a direct interaction of the peptide with this regulator engaged in activating the MexAB-OprM efflux system[186]. These studies are preliminary and require future *in vitro* and *in vivo* validations to comprehensively understand the specific functions of the regulator and its putative interaction with the peptide.

Collectively, the outcomes of this project lay the groundwork for the potential development of new antimicrobial therapies-based identification of protein targets. The achievement of these objectives has been made possible by studying the mechanism of action of various antimicrobial agents that specifically affected both Gram-negative and Gram-positive bacteria.

Appendix A- Identification of protein targets in skeletal muscle-extracellular matrix: proteomic investigation in Duchenne Muscular Dystrophy

A.1 Introduction

During the third year of the Ph.D., six months were spent at the Institute NeuroMyoGène, University Claude Bernard - Lyon 1, supervisor Dr. Bénédicte Chazaud. Based on the importance to discover protein targets, differential proteomic approaches have been developed to understand the involvement of skeletal muscle-extracellular matrix (sk-ECM) proteins in the pathogenesis of Duchenne Muscular Dystrophy (DMD).

DMD is a chronic inherited disease caused by mutations in the dmd gene, resulting in recurring myofiber lesions and muscle wasting[187]. Muscle degeneration in DMD is associated with an inflammatory response that can make the muscle damage more severe and cause additional tissue damage. DMD patient muscles exhibit variable degrees of atrophy, hypertrophy, necrosis, regeneration, and fibrosis. Primarly affecting boys, symptoms typically manifest in early childhood[188].

DMD arises from mutation in the dystrophin gene, leading to the absence or insufficient production of dystrophin, a protein crucial for maintaining muscle cell integrity. The lack of dystrophin at the sarcolemma is responsible for myonecrosis triggered by mechanical stretch and chronic inflammation[189].

Specifically, dystrophin belongs to the Dystrophin-Glycoprotein Complex (DGC) that connects the cytoskeletal F-actin inside the cells with the extracellular matrix (ECM) outside the cell[190] (Figure A1).

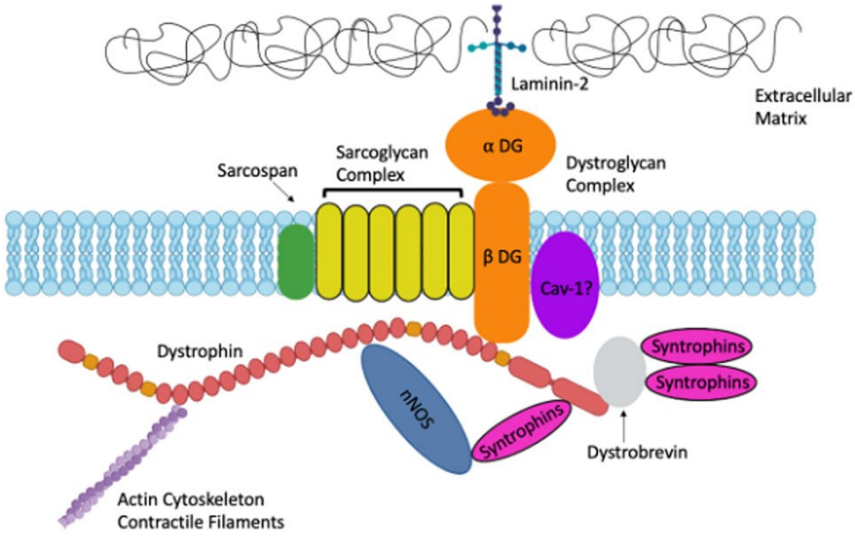

Figure A1. Structure of the dystrophin-glycoprotein complex (DGC)[189].

Dystrophin deficiency renders myofibers susceptible to contraction-induced injury, disrupting the DGC, affecting the calcium homeostasis, and subsequently affecting the contraction-relaxation process[191] . At early stages, myofiber damages are compensated by myogenesis mediated by muscle stem cells (MuSCs). In healthy regenerating muscle, blood monocyte-derived macrophages clear debris and activate MuSCs, transforming into restorative macrophages that support myogenesis and angiogenesis[192-193].

Fibro-Adipogenic Progenitors (FAPs) stimulate MuSC differentiation and regulate ECM remodeling. In muscular dystrophies, recurrent myofiber damage overwhelms MuSC capacities, resulting in the persistence of inflammatory macrophages and activated FAPs, which overproduce ECM, leading to fibrosis[194-195].

Over the years, a cure for DMD has not been found, and treatment options have primarily focused on managing symptoms and improving the quality of life[196].

Ongoing research aims to develop innovative therapies and interventions to address the underlying genetic and molecular aspects of the condition, offering hope for improved outcomes in the future.

Therapeutic targeting in DMD represents a multifaceted endeavor that encompasses a spectrum of investigational approaches aimed at ameliorating the progressive muscle degeneration characteristic of the disease[197]. Emerging strategies primarily focus on restoring or compensating for the deficiency of dystrophin, the protein crucial for maintaining muscle cell integrity. As an example, gene editing techniques, including CRISPR/Cas9, are under exploration for their potential to correct the underlying genetic mutations responsible for DMD[197].

To date, sk-ECM alterations in DMD have been considered only as the result of myofiber damages of the inflammatory response, or of an unbalanced ECM degradation/synthesis by fibroblasts[198]. However, the direct influence on muscle cells due to the sk-ECM alterations remains an unexplored topic that needs to be investigated. Since DMD is due to mutations in dystrophin-glycoprotein complex (DGC) that links ECM, it is reasonable to hypothesize that ECM is not a passive object of the effects of muscle damage, but plays a direct role in DMD[199].

Over the past decade, mass-spectrometry-based proteomics had a major impact on the global characterization of skeletal muscles[200]. Proteomic analyses enable the comprehensive profiling of the muscle proteome, aiding in the identification of dysregulated pathways and potential therapeutic targets. Moreover, proteomics allows the elucidation of the precise roles of many genes as components of protein complexes[201], and there is a growing consensus that defects in different protein complexes are the cause of overlapping clinical manifestations. Thus, the identification of such complexes can elucidate the cellular mechanisms

contributing to different diseases and enable the determination of specific protein candidates for attenuating the disease phenotype under study[202].

Recent proteomic investigations have been suggested that CA_3 protein levels are elevated in dystrophic chicken muscle compared to normal muscle[203]. CA_3 is selectively expressed in a few tissues, rendering it a more specific and sensitive marker for muscular dystrophies. Interestingly, carbonic anhydrase inhibitors have have demonstrated favorable effects in animal models of dystrophinopathies, suggesting that they could potentially be explored for human therapy[204]. Another instance of the utility of proteomics in identifying protein alterations in certain muscular dystrophies is exemplified by *De Palma* et al. where a differential proteomic analysis of muscle tissue from patients with dysferlin deficiency revealed a remodeling of fiber type. This sheds light on how the absence of dysferlin can compromise muscle fibers in muscular dystrophy patients[205].

As research advances, the convergence of proteomic insights with therapeutic strategies exemplifies a synergistic approach toward comprehensively addressing the pathophysiology of DMD. Particularly, differential proteomic analyses coupled to advanced extraction strategies are able to overcome the huge problem of cellular heterogeneity allowing the analysis of proteomic changes[206].

In this Appendix, a differential proteomics approach was employed to identify molecular alterations in DMD. To enhance specificity in identification, the proteome obtained from dystrophic mice was compared to wild-type (WT) mice and mice subjected to cardiotoxin (CTX) injection. CTX belongs to the family of snake venom toxins induces inflammation after 4-days post injury and can trigger the regeneration events after 8 days post injury.

A.2 Experimental methods

A.2.1 Decellularization

Wild type (WT) and dystrophic (Mdx) 10-weeks-old male mice were anesthetized with isoflurane inhalation (Forene) and sacrificed. Gastrocnemius muscles were dissected and 45 mg were cut into small pieces, incubated for 2 h 30 min at 600 rpm at 23°C in 500 mM NaCl and 180 mM HEPES pH 7.4. Samples were centrifuged for 10 min at 13000 rpm at 23°C. The muscles were treated with 0.75 % (w/v) SD and 0.3% (w/v) SDS for 16 h at 600 rpm at 23 °C and with 1% (v/v) Triton X-100 for 1 h at 600 rpm at 23 °C to remove all remaining cell fragments. The resulting tissues were washed twice in ddH_2O for 1 h 30 min at 23 °C at 600 rpm and centrifuged for 10 min at 13000 rpm at 23 °C. The muscles were finally incubated in 4 M GuHCl and 50 mM Ch_3COONa for 72 h at 600 rpm at 23 °C. All incubation buffers, including H_2O, were supplemented with cOmpleteTM protease inhibitors and 25 mM EDTA. The extracted fractions were used for proteomics and LC-MS/MS analysis[207]. The decellularization was performed on biological triplicates.

A.2.2 Cardiotoxin injection in the gastrocnemius

Intramuscular injection of cardiotoxin (CTX - 12 µM, Latoxan) was performed in the gastrocnemius muscle of adult 9-week-old WT male mice. Mice were sacrificed after 4 and 8 days, corresponding to early and late ECM remodeling, and the gastrocnemius muscles were decellularized and the extracted proteins were subjected to proteomic and LC-MS/MS analysis.

A.2.3 DNA extraction and quantification

DNA was isolated with a commercially available DNeasy Blood & Tissue Kit (Qiagen, Germantown-Maryland). The total DNA content was measured by absorption at 260 nm on a UV–VIS spectrophotometer (Nanodrop 2000,

ThermoFisher) and normalized to the initial wet weight of the sample. The measurements were done in triplicates and statistical analysis was performed with Two-way ANOVA ($p<0.05$).

A.2.4 Quantitative and qualitative analysis

The protein content of the decellularized muscle was quantified by the BCA Protein Assay Kit (Pierce, Bonn, Germany) according to the manufacturer's instructions. The concentration of all obtained fractions was calculated interpolating the data in the calibration curve. 25 µg of extracted proteins for all conditions were separated using 10% SDS-PAGE and stained with Coomassie Brilliant Blue solution (Bio-Rad, USA).

A.2.5 Proteomic experiment

25 µg of extracted proteins were subjected to reduction with 10 mM DTT for 45 min at 65°C and alkylation with 25 mM IAM for 40 min at 25°C. The detergent was removed onto SP_3 Magnetic Beads before enzymatic treatments. Peptide mixtures were obtained performing in solution hydrolyses with 10 U/µL PNGase for 3h at 37°C, followed by lysC (1:150) for 2 h at 37°C, and trypsin (1:50) for 16h at 37°C. The resulting peptide mixtures were desalified onto Pierce C18 columns, dried in speedvac and analyzed by LC-MS/MS using a Q-Orbitrap (Q Exactive HF; Thermo Fisher Scientific) mass spectrometer in a Top 20 HCD (Higher Collision Dissociation) data-dependent acquisition. Raw data obtained from nano LC-MS/MS were analyzed with MaxQuant software[150] using the UniProt mouse database for Andromeda search[151]. The FCs were calculated according to LFQ values.

A.3 Results

A.3.1 Decellularization of the gastrocnemius for differential proteomic investigation

An efficient decellularization method was applied on four muscles (resting WT, Mdx and regenerating WT 4 and 8 days post-Ctx injury) in the aim to get a high ECM protein content recovery with a high reproducibility. The decellularization of the ECM for each condition was verified by measuring the DNA content of the decellularized muscle, using the appropriate controls (Figure A2). The DNA content of decellularized ECM was significantly decreased, confirming that the ECMs were decellularized (Figure A2).

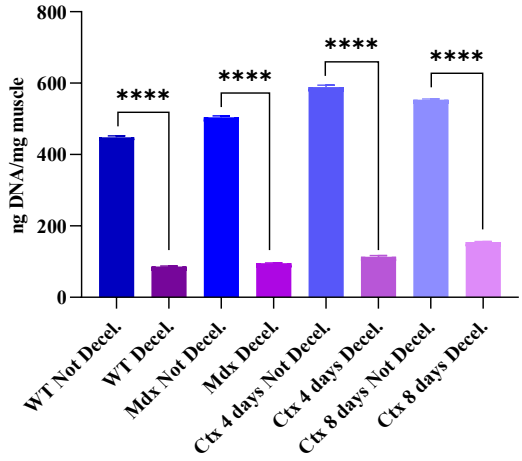

Figure A2. DNA content of decellularized (Decel.) compared to not decelullarized muscle (Not Decel.) was expressed as ng of DNA per mg of muscle for each sample. Results are presented as the mean ± SD from three independent experiments. Statistical significance was determined through t-test analysis using GraphPad Prism 9 and p-value < 0.0001 was indicated as **** in the graph.

A.3.2 Quantitative and qualitative analyses of the ECM extracted protein

The decellularization of the gastrocnemius allowed to extract the ECM proteins, obtaining different protein fractions depending on the buffer in which they were extracted. All the fractions for the WT, Mdx, Ctx-induced injury after 4- and 8-days conditions (Ctx-4 days and Ctx-8 days, respectively) were quantified by BCA assay and separated according to their molecular weight by SDS-PAGE (Figure A3).

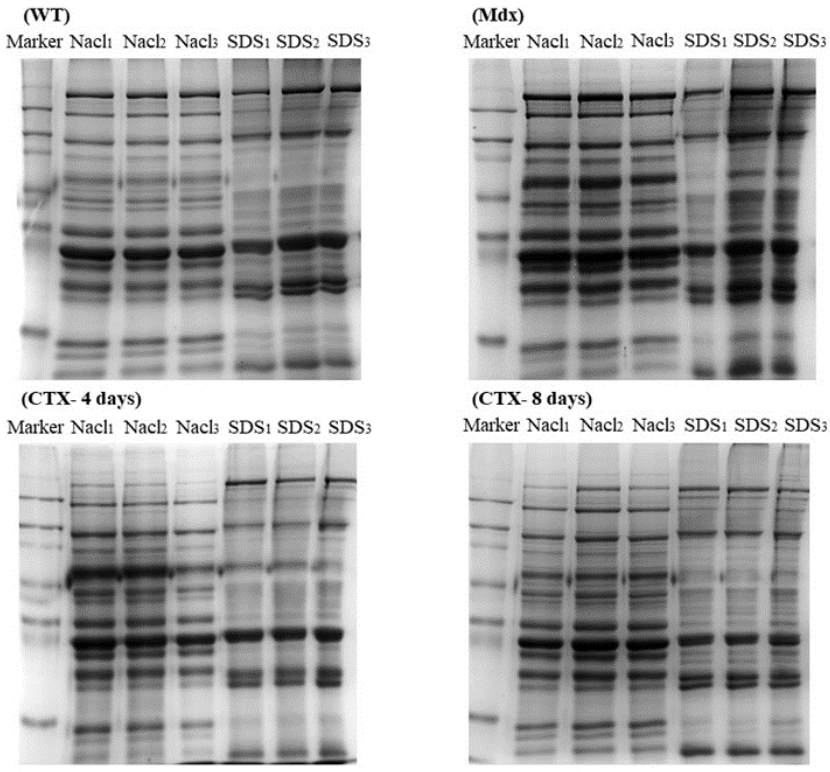

Figure A3. 25 µg for each NaCl and SDS fractions with biological triplicates were analyzed by SDS-PAGE.

An increase in protein expression was observed both in Mdx and in CTX-induced injury WT after 4 days. In addition, SDS-PAGE showed a similarity between the protein pattern of the CTX-induced injury WT after 8 days and WT protein profile. This is in accordance with the return to homeostasis of the regenerating muscle 8 days after injury, en route to restore basal conditions[208]. Protein expression appears to be perturbed both quantitatively and qualitatively in Mdx mice and mice injured with CTX. This may be due to differences in muscle structure or compensation mechanisms that counteract pathophysiological processes. The reasons for these variations in protein expression were investigated in detail by differential proteomic investigations, in order to select only the ECM proteins and discard the ones coming from the inside of cells (i.e. mitochondrial, cytoplasmatic proteins).

A.3.3 Differential proteomic

Proteins were identified and their expression levels quantified by comparing the proteins identified in Mdx condition with those of WT, regenerating WT 4 and 8 days post-CTX injury, using the MaXQuant software for statistical significance. The main differentially expressed proteins belonging to ECM were selected and are listed in the Table A1.

Swiss-Prot code	Protein name	Gene	Mdx vs WT	Mdx vs Ctx-4	Mdx vs Ctx-8
P97352	Protein S100-A13	S100a13			
P31725	Protein S100-A9	S100a9			
O88947	Coagulation factor X	F10			
P28665	Murinoglobulin-1	Mug1			
Q9CZI7	Annexin	Anxa2			
Q7TMN7	Annexin	Anxa4			
Q922A2	Annexin GN=Anxa7	Anxa7			
P97384	Annexin A11	Anxa11			
E9PV24	Fibrinogen alpha chain	Fga			
A0A0G2JGD2	Protein S100-A4	S100a4			
Q53X15	Protein S100	S100a8			
Q3V1T9	Plasminogen	Plg			
Q6XLQ8	Calumenin	Calu			
P10605	Cathepsin B	Ctsb			
B1B0C7	Basement membrane-specific heparan sulfate proteoglycan	Hspg2			

Q8CBE6	Dystroglycan 1	Dag1			
Q3UYK7	SPARC-like protein 1	Sparcl1			
Q549A5	Clusterin	Clu			
Q3TCF1	Fibronectin	Fn1			
P07758	Alpha-1-antitrypsin 1-1	Serpina1a			
Q00898	Alpha-1-antitrypsin 1-5	Serpina1e			
Q9QZF2	Glypican-1	Gpc1			
P28653	Biglycan	Bgn			
A0A0A6YWH7	Antithrombin-III	Serpinc1			
Q8BT06	Tetraspanin	Cd63			
Q3UCW4	Cathepsin D	Ctsd			
P01592	Immunoglobulin J chain	Jchain			
O08677	Kininogen-1	Kng1			
B1AWB9	Collagen, type V, alpha 1	Col5a1			
Q3UIW3	Lysosome-associated membrane glycoprotein 2	Lamp2			
Q61646	Haptoglobin	Hp			
P09813	Apolipoprotein A-II	Apoa2			
Q60994	Adiponectin	Adipoq			
Q3UEM7	Fibrinogen C-terminal domain-containing protein	Fgg			
Q3U8W3	Granulins domain-containing protein	Grn			
Q62009	Periostin	Postn			

P11531	Dystrophin Dp71d(Delta71,73-74)	Dmd			
Q3UKR1	Decorin	Dcn			
Q9D2N4	Dystrobrevin	Dtna			
Q5GQ64	Gamma-synuclein	Sngc			
P04441	H-2 class II histocompatibility antigen gamma chain	Cd74			
P82349	Beta-sarcoglycan	Sgcb			
Q91WQ0	SERPIN domain-containing protein	Serpina6			
Q543D2	Fibromodulin	Fmod			
Q80ZP8	Armet protein	Manf			
Q00897	Alpha-1-antitrypsin 1-4	Serpina1d			
Q9QZF2	Glypican-1	Gpc1			
Q80YX1	Tenascin	Tnc			
P19324	Serpin H1	Serpinh1			
Q9Z1T2	Thrombospondin-4	Thbs4			
Q3TGL4	FBLN2	Fbln2			
P09055	Integrin beta-1	Itgb1			
Q62009	Periostin	Postn			
P48036	Annexin A5	Anxa5			
P10107	Annexin	Anxa1			

	Not found
	Up-regulated
	Down-regulated

Table A1. Differentially expressed Mdx proteins compared to WT, regenerating WT 4 and 8 days post-CTX injury. Up-regulated proteins are in blue, down-regulated proteins are in green, and proteins showing no variations are in orange.

The results highlighted the up-regulation of numerous proteins involved in the inflammatory response when comparing Mdx to WT conditions. Specifically, biglycan and SPARC were found to be up-regulated, consistent with literature data. The increased expression of biglycan may compensate for the absence of dystrophin by stabilizing the interaction between the dystrophin-associated protein complex (DAPC) and the ECM[209].

Surprisingly, down-regulation of Anxa1 and Anxa5 were observed in the Mdx condition compared to regenerating WT muscle at 4 and 8 days post-CTX injury. These proteins are involved in membrane repair at sarcolemma. According to the "lipid patch" model, following the rupture of the plasma membrane, the influx of extracellular Ca^{2+} into the cell triggers the activation of a repair mechanism, wherein intracellular vesicles fuse to form a lipid patch near the damaged membrane, blocking the entry of Ca^{2+}. The Ca^{2+} concentration gradient activates membrane repair proteins, primarily Anxa1 and 2, which then translocate to the rupture site. Anxa5 is mainly involved in the membrane sealing and forms a 2D matrix that strengthens the membrane and prevents wound expansion (Figure A4)[210].

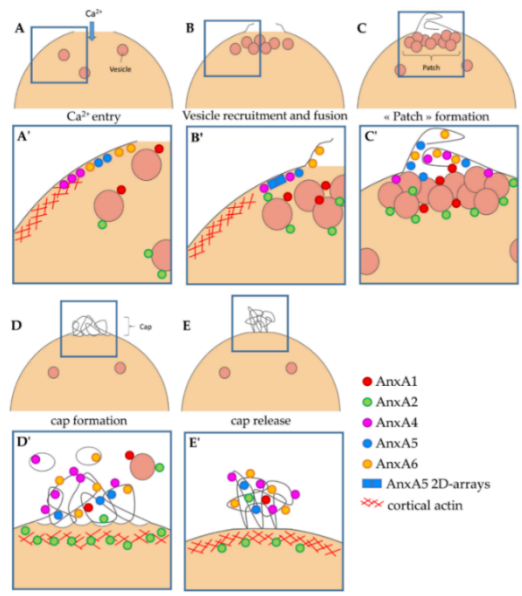

Figure A4. Lipid patch model.

If Anxa5 is down-expressed in Mdx mice, the failure to repair the membrane results in the death of damaged cells and may contribute to tissue degeneration and the development of degenerative disease. In certain forms of muscular dystrophy, such as DMD, the frequency of sarcolemma rupture is significantly higher than in normal muscle, potentially leading to the impairment of the membrane repair mechanism[211]. In this regard, scientific research is specifically directed towards discovering therapeutic targets capable of addressing calcium overload, and current therapies aim to develop membrane stabilizers such as copolymers[212].

In conclusion, our differential proteomics results have contributed to a biochemical understanding of the possible causes related to the ongoing muscle degeneration in DMD, highlighting possible dysfunctions of Anxa5.

A.4 Conclusions

In DMD there is an aberrant accumulation of ECM, which stands as the primary contributor to the progressive loss of muscle function[213]. This prompted an exploration into the ECM involvement in DMD pathology, with a particular focus on understanding the differential expression of sk-ECM proteins in both regenerative and dystrophic states through differential proteomics. The objective was to unravel the role of skeletal muscle in the context of DMD, shedding light on the molecular processes that underlie the disease progression.

The outcomes of this analysis revealed insights into the potential disruption of the membrane repair system at sarcolemma. This disruption results in a continuous cycle of repair attempts that remain perpetually incomplete, primarily attributed to the likely malfunctioning of Anxa5. The findings suggest a critical role for ECM dysregulation, particularly in the context of the sarcolemmal membrane repair system, as a contributing factor to the pathogenesis of this muscular disorder. The results of this study have demonstrated that MS-based proteomics can identify promising targets for a genetic disease like DMD.

The project presented in this appendix was funded by the European Federation of Immunological Societies (Short-Term Fellowship) and the European Molecular Biology Organization (Scientific Exchange Grant) during the research period conducted in Lyon.

Bibliography

(1) Banin, E.; Hughes, D.; Kuipers, O. P. Editorial: Bacterial Pathogens, Antibiotics and Antibiotic Resistance. *FEMS Microbiology Reviews* **2017**, *41* (3), 450–452. https://doi.org/10.1093/femsre/fux016.

(2) Dadgostar, P. Antimicrobial Resistance: Implications and Costs. *IDR* **2019**, *Volume 12*, 3903–3910. https://doi.org/10.2147/IDR.S234610.

(3) Urban-Chmiel, R.; Marek, A.; Stępień-Pyśniak, D.; Wieczorek, K.; Dec, M.; Nowaczek, A.; Osek, J. Antibiotic Resistance in Bacteria—A Review. *Antibiotics* **2022**, *11* (8), 1079. https://doi.org/10.3390/antibiotics11081079.

(4) Friedman, N. D.; Temkin, E.; Carmeli, Y. The Negative Impact of Antibiotic Resistance. *Clinical Microbiology and Infection* **2016**, *22* (5), 416–422. https://doi.org/10.1016/j.cmi.2015.12.002.

(5) Anand, U.; Jacobo-Herrera, N.; Altemimi, A.; Lakhssassi, N. A Comprehensive Review on Medicinal Plants as Antimicrobial Therapeutics: Potential Avenues of Biocompatible Drug Discovery. *Metabolites* **2019**, *9* (11), 258. https://doi.org/10.3390/metabo9110258.

(6) Goossens, H. The Chennai Declaration on Antimicrobial Resistance in India. *The Lancet Infectious Diseases* **2013**, *13* (2), 105–106. https://doi.org/10.1016/S1473-3099(12)70346-8.

(7) Christaki, E.; Marcou, M.; Tofarides, A. Antimicrobial Resistance in Bacteria: Mechanisms, Evolution, and Persistence. *J Mol Evol* **2020**, *88* (1), 26–40. https://doi.org/10.1007/s00239-019-09914-3.

(8) Zhang, G.; Feng, J. The Intrinsic Resistance of Bacteria. *Yi Chuan* **2016**, *38* (10), 872–880. https://doi.org/10.16288/j.yczz.16-159.

(9) Jian, Z.; Zeng, L.; Xu, T.; Sun, S.; Yan, S.; Yang, L.; Huang, Y.; Jia, J.; Dou, T. Antibiotic Resistance Genes in Bacteria: Occurrence, Spread, and Control. *J Basic Microbiol* **2021**, *61* (12), 1049–1070. https://doi.org/10.1002/jobm.202100201.

(10) Uddin, T. M.; Chakraborty, A. J.; Khusro, A.; Zidan, B. R. M.; Mitra, S.; Emran, T. B.; Dhama, K.; Ripon, Md. K. H.; Gajdács, M.; Sahibzada, M. U. K.; Hossain, Md. J.; Koirala, N. Antibiotic Resistance in Microbes: History, Mechanisms, Therapeutic Strategies and Future Prospects. *Journal of Infection and Public Health* **2021**, *14* (12), 1750–1766. https://doi.org/10.1016/j.jiph.2021.10.020.

(11) C Reygaert, W.; Department of Biomedical Sciences, Oakland University William Beaumont School of Medicine, Rochester, MI, USA. An Overview of the Antimicrobial Resistance Mechanisms of Bacteria. *AIMS Microbiology* **2018**, *4* (3), 482–501. https://doi.org/10.3934/microbiol.2018.3.482.

(12) Kumar, A.; Schweizer, H. Bacterial Resistance to Antibiotics: Active Efflux and Reduced Uptake. *Advanced Drug Delivery Reviews* **2005**, *57* (10), 1486–1513. https://doi.org/10.1016/j.addr.2005.04.004.

(13) Peraman, R.; Sure, S. K.; Dusthackeer, V. N. A.; Chilamakuru, N. B.; Yiragamreddy, P. R.; Pokuri, C.; Kutagulla, V. K.; Chinni, S. Insights on Recent Approaches in Drug Discovery Strategies and Untapped Drug Targets against Drug Resistance. *Futur J Pharm Sci* **2021**, *7* (1), 56. https://doi.org/10.1186/s43094-021-00196-5.

(14) Glen, K. A.; Lamont, I. L. β-Lactam Resistance in Pseudomonas Aeruginosa: Current Status, Future Prospects. *Pathogens* **2021**, *10* (12), 1638. https://doi.org/10.3390/pathogens10121638.

(15) Li, X.-Z.; Nikaido, H. Efflux-Mediated Drug Resistance in Bacteria: *Drugs* **2004**, *64* (2), 159–204. https://doi.org/10.2165/00003495-200464020-00004.

(16) Xuan, J.; Feng, W.; Wang, J.; Wang, R.; Zhang, B.; Bo, L.; Chen, Z.-S.; Yang, H.; Sun, L. Antimicrobial Peptides for Combating Drug-Resistant Bacterial Infections. *Drug Resistance Updates* **2023**, *68*, 100954. https://doi.org/10.1016/j.drup.2023.100954.

(17) Álvarez-Martínez, F. J.; Barrajón-Catalán, E.; Micol, V. Tackling Antibiotic Resistance with Compounds of Natural Origin: A Comprehensive Review. *Biomedicines* **2020**, *8* (10), 405. https://doi.org/10.3390/biomedicines8100405.

(18) Erdem Büyükkiraz, M.; Kesmen, Z. Antimicrobial Peptides (AMPs): A Promising Class of Antimicrobial Compounds. *Journal of Applied Microbiology* **2022**, *132* (3), 1573–1596. https://doi.org/10.1111/jam.15314.

(19) Lazzaro, B. P.; Zasloff, M.; Rolff, J. Antimicrobial Peptides: Application Informed by Evolution. *Science* **2020**, *368* (6490), eaau5480. https://doi.org/10.1126/science.aau5480.

(20) Di Somma, A.; Moretta, A.; Canè, C.; Cirillo, A.; Duilio, A. Antimicrobial and Antibiofilm Peptides. *Biomolecules* **2020**, *10* (4), 652. https://doi.org/10.3390/biom10040652.

(21) Ladram, A. Antimicrobial Peptides from Frog Skin Biodiversity and Therapeutic Promises. *Front Biosci* **2016**, *21* (7), 1341–1371. https://doi.org/10.2741/4461.

(22) Rinaldi, A. C. Antimicrobial Peptides from Amphibian Skin: An Expanding Scenario: Commentary. *Current Opinion in Chemical Biology* **2002**, *6* (6), 799–804. https://doi.org/10.1016/S1367-5931(02)00401-5.

(23) Ciumac, D.; Gong, H.; Hu, X.; Lu, J. R. Membrane Targeting Cationic Antimicrobial Peptides. *Journal of Colloid and Interface Science* **2019**, *537*, 163–185. https://doi.org/10.1016/j.jcis.2018.10.103.

(24) Pirtskhalava, M.; Vishnepolsky, B.; Grigolava, M.; Managadze, G. Physicochemical Features and Peculiarities of Interaction of AMP with the Membrane. *Pharmaceuticals* **2021**, *14* (5), 471. https://doi.org/10.3390/ph14050471.

(25) Savitskaya, A.; Masso-Silva, J.; Haddaoui, I.; Enany, S. Exploring the Arsenal of Antimicrobial Peptides: Mechanisms, Diversity, and Applications. *Biochimie* **2023**, *214*, 216–227. https://doi.org/10.1016/j.biochi.2023.07.016.

(26) Bahar, A.; Ren, D. Antimicrobial Peptides. *Pharmaceuticals* **2013**, *6* (12), 1543–1575. https://doi.org/10.3390/ph6121543.

(27) Benfield, A. H.; Henriques, S. T. Mode-of-Action of Antimicrobial Peptides: Membrane Disruption vs. Intracellular Mechanisms. *Front. Med. Technol.* **2020**, *2*, 610997. https://doi.org/10.3389/fmedt.2020.610997.

(28) Atanasov, A. G.; Waltenberger, B.; Pferschy-Wenzig, E.-M.; Linder, T.; Wawrosch, C.; Uhrin, P.; Temml, V.; Wang, L.; Schwaiger, S.; Heiss, E. H.; Rollinger, J. M.; Schuster, D.; Breuss, J. M.; Bochkov, V.; Mihovilovic, M. D.; Kopp, B.; Bauer, R.; Dirsch, V. M.; Stuppner, H. Discovery and Resupply of Pharmacologically Active Plant-Derived Natural Products: A Review. *Biotechnology Advances* **2015**, *33* (8), 1582–1614. https://doi.org/10.1016/j.biotechadv.2015.08.001.

(29) Isah, T. Stress and Defense Responses in Plant Secondary Metabolites Production. *Biol Res* **2019**, *52* (1), 39. https://doi.org/10.1186/s40659-019-0246-3.

(30) Balunas, M. J.; Kinghorn, A. D. Drug Discovery from Medicinal Plants. *Life Sciences* **2005**, *78* (5), 431–441. https://doi.org/10.1016/j.lfs.2005.09.012.

(31) Manandhar, S.; Luitel, S.; Dahal, R. K. In Vitro Antimicrobial Activity of Some Medicinal Plants against Human Pathogenic Bacteria. *Journal of Tropical Medicine* **2019**, *2019*, 1–5. https://doi.org/10.1155/2019/1895340.

(32) the International Natural Product Sciences Taskforce; Atanasov, A. G.; Zotchev, S. B.; Dirsch, V. M.; Supuran, C. T. Natural Products in Drug Discovery: Advances and Opportunities. *Nat Rev Drug Discov* **2021**, *20* (3), 200–216. https://doi.org/10.1038/s41573-020-00114-z.

(33) Thomford, N.; Senthebane, D.; Rowe, A.; Munro, D.; Seele, P.; Maroyi, A.; Dzobo, K. Natural Products for Drug Discovery in the 21st Century: Innovations for Novel Drug Discovery. *IJMS* **2018**, *19* (6), 1578. https://doi.org/10.3390/ijms19061578.

(34) Mantravadi, P.; Kalesh, K.; Dobson, R.; Hudson, A.; Parthasarathy, A. The Quest for Novel Antimicrobial Compounds: Emerging Trends in Research, Development, and Technologies. *Antibiotics* **2019**, *8* (1), 8. https://doi.org/10.3390/antibiotics8010008.

(35) May, K. L.; Grabowicz, M. The Bacterial Outer Membrane Is an Evolving Antibiotic Barrier. *Proc. Natl. Acad. Sci. U.S.A.* **2018**, *115* (36), 8852–8854. https://doi.org/10.1073/pnas.1812779115.

(36) Rosas, N. C.; Lithgow, T. Targeting Bacterial Outer-Membrane Remodelling to Impact Antimicrobial Drug Resistance. *Trends in Microbiology* **2022**, *30* (6), 544–552. https://doi.org/10.1016/j.tim.2021.11.002.

(37) Spencer, J. J.; Pitts, R. E.; Pearson, R. A.; King, L. B. The Effects of Antimicrobial Peptides WAM-1 and LL-37 on Multidrug-Resistant Acinetobacter Baumannii. *Pathogens and Disease* **2018**, *76* (2). https://doi.org/10.1093/femspd/fty007.

(38) Vetterli, S. U.; Zerbe, K.; Müller, M.; Urfer, M.; Mondal, M.; Wang, S.-Y.; Moehle, K.; Zerbe, O.; Vitale, A.; Pessi, G.; Eberl, L.; Wollscheid, B.; Robinson, J. A. Thanatin Targets the Intermembrane Protein Complex Required for Lipopolysaccharide Transport in *Escherichia Coli*. *Sci. Adv.* **2018**, *4* (11), eaau2634. https://doi.org/10.1126/sciadv.aau2634.

(39) Smith, E. C. J.; Kaatz, G. W.; Seo, S. M.; Wareham, N.; Williamson, E. M.; Gibbons, S. The Phenolic Diterpene Totarol Inhibits Multidrug Efflux Pump Activity in *Staphylococcus Aureus*. *Antimicrob Agents Chemother* **2007**, *51* (12), 4480–4483. https://doi.org/10.1128/AAC.00216-07.

(40) Garcia, Í. R.; De Oliveira Garcia, F. A.; Pereira, P. S.; Coutinho, H. D. M.; Siyadatpanah, A.; Norouzi, R.; Wilairatana, P.; De Lourdes Pereira, M.; Nissapatorn, V.; Tintino, S. R.; Rodrigues, F. F. G. Microbial Resistance: The Role of Efflux Pump Superfamilies and Their Respective Substrates. *Life Sciences* **2022**, *295*, 120391. https://doi.org/10.1016/j.lfs.2022.120391.

(41) AlMatar, M.; Albarri, O.; Makky, E. A.; Köksal, F. Efflux Pump Inhibitors: New Updates. *Pharmacol. Rep* **2021**, *73* (1), 1–16. https://doi.org/10.1007/s43440-020-00160-9.

(42) Thakur, V.; Uniyal, A.; Tiwari, V. A Comprehensive Review on Pharmacology of Efflux Pumps and Their Inhibitors in Antibiotic Resistance.

European Journal of Pharmacology **2021**, *903*, 174151. https://doi.org/10.1016/j.ejphar.2021.174151.

(43) Tambat, R.; Jangra, M.; Mahey, N.; Chandal, N.; Kaur, M.; Chaudhary, S.; Verma, D. K.; Thakur, K. G.; Raje, M.; Jachak, S.; Khatri, N.; Nandanwar, H. Microbe-Derived Indole Metabolite Demonstrates Potent Multidrug Efflux Pump Inhibition in Staphylococcus Aureus. *Front. Microbiol.* **2019**, *10*, 2153. https://doi.org/10.3389/fmicb.2019.02153.

(44) Laws, M.; Jin, P.; Rahman, K. M. Efflux Pumps in Mycobacterium Tuberculosis and Their Inhibition to Tackle Antimicrobial Resistance. *Trends in Microbiology* **2022**, *30* (1), 57–68. https://doi.org/10.1016/j.tim.2021.05.001.

(45) Ruer, S.; Pinotsis, N.; Steadman, D.; Waksman, G.; Remaut, H. Virulence-targeted Antibacterials: Concept, Promise, and Susceptibility to Resistance Mechanisms. *Chem Biol Drug Des* **2015**, *86* (4), 379–399. https://doi.org/10.1111/cbdd.12517.

(46) Quinn, R. J.; Barraza, I.; García-Diéguez, L.; Pajon, C.; Krausfeldt, L. E.; Ibrahim, K.; Enzinna, L. A.; Thorn, M. E.; Eldakar, O. T.; Craddock, T. J. A.; Smith, R. P. Periodically Disturbing the Spatial Structure of Biofilms Can Affect the Production of an Essential Virulence Factor in *Pseudomonas Aeruginosa*. *mSystems* **2021**, *6* (5), e00961-21. https://doi.org/10.1128/mSystems.00961-21.

(47) Cianciotto, N. P.; White, R. C. Expanding Role of Type II Secretion in Bacterial Pathogenesis and Beyond. *Infect Immun* **2017**, *85* (5), e00014-17. https://doi.org/10.1128/IAI.00014-17.

(48) Cusumano, C. K.; Pinkner, J. S.; Han, Z.; Greene, S. E.; Ford, B. A.; Crowley, J. R.; Henderson, J. P.; Janetka, J. W.; Hultgren, S. J. Treatment and Prevention of Urinary Tract Infection with Orally Active FimH Inhibitors. *Sci. Transl. Med.* **2011**, *3* (109). https://doi.org/10.1126/scitranslmed.3003021.

(49) Eswara, P. J.; Ramamurthi, K. S. Bacterial Cell Division: Nonmodels Poised to Take the Spotlight. *Annu. Rev. Microbiol.* **2017**, *71* (1), 393–411. https://doi.org/10.1146/annurev-micro-102215-095657.

(50) Den Blaauwen, T.; Andreu, J. M.; Monasterio, O. Bacterial Cell Division Proteins as Antibiotic Targets. *Bioorganic Chemistry* **2014**, *55*, 27–38. https://doi.org/10.1016/j.bioorg.2014.03.007.

(51) Meissner, F.; Geddes-McAlister, J.; Mann, M.; Bantscheff, M. The Emerging Role of Mass Spectrometry-Based Proteomics in Drug Discovery. *Nat Rev Drug Discov* **2022**, *21* (9), 637–654. https://doi.org/10.1038/s41573-022-00409-3.

(52) Monteoliva, L. Differential Proteomics: An Overview of Gel and Non-Gel Based Approaches. *Briefings in Functional Genomics and Proteomics* **2004**, *3* (3), 220–239. https://doi.org/10.1093/bfgp/3.3.220.

(53) Iacobucci, I.; Monaco, V.; Cozzolino, F.; Monti, M. From Classical to New Generation Approaches: An Excursus of -Omics Methods for Investigation of TIVEaction Networks. *Journal of Proteomics* **2021**, *230*, 103990. https://doi.org/10.1016/j.jprot.2020.103990.

(54) Elbehiry, A.; Marzouk, E.; Abalkhail, A.; El-Garawany, Y.; Anagreyyah, S.; Alnafea, Y.; Almuzaini, A. M.; Alwarhi, W.; Rawway, M.; Draz, A. The Development of Technology to Prevent, Diagnose, and Manage Antimicrobial Resistance in Healthcare-Associated Infections. *Vaccines* **2022**, *10* (12), 2100. https://doi.org/10.3390/vaccines10122100.

(55) Bandow, J. E.; Brötz, H.; Leichert, L. I. O.; Labischinski, H.; Hecker, M. Proteomic Approach to Understanding Antibiotic Action. *Antimicrob Agents Chemother* **2003**, *47* (3), 948–955. https://doi.org/10.1128/AAC.47.3.948-955.2003.

(56) Batoni, G.; Maisetta, G.; Lisa Brancatisano, F.; Esin, S.; Campa, M. Use of Antimicrobial Peptides Against Microbial Biofilms: Advantages and Limits. *CMC* **2011**, *18* (2), 256–279. https://doi.org/10.2174/092986711794088399.

(57) Zasloff, M. Magainins, a Class of Antimicrobial Peptides from Xenopus Skin: Isolation, Characterization of Two Active Forms, and Partial cDNA Sequence of a Precursor. *Proc. Natl. Acad. Sci. U.S.A.* **1987**, *84* (15), 5449–5453. https://doi.org/10.1073/pnas.84.15.5449.

(58) Pettersen, E. F.; Goddard, T. D.; Huang, C. C.; Couch, G. S.; Greenblatt, D. M.; Meng, E. C.; Ferrin, T. E. UCSF Chimera—A Visualization System for Exploratory Research and Analysis. *J Comput Chem* **2004**, *25* (13), 1605–1612. https://doi.org/10.1002/jcc.20084.

(59) Billah, Md. M.; Saha, S. K.; Or Rashid, Md. M.; Hossain, F.; Yamazaki, M. Effect of Osmotic Pressure on Pore Formation in Lipid Bilayers by the Antimicrobial Peptide Magainin 2. *Phys. Chem. Chem. Phys.* **2022**, *24* (11), 6716–6731. https://doi.org/10.1039/D1CP05764B.

(60) Matsuzaki, K.; Sugishita, K.; Ishibe, N.; Ueha, M.; Nakata, S.; Miyajima, K.; Epand, R. M. Relationship of Membrane Curvature to the Formation of Pores by Magainin 2. *Biochemistry* **1998**, *37* (34), 11856–11863. https://doi.org/10.1021/bi980539y.

(61) Bechinger, B.; Zasloff, M.; Opella, S. J. Structure and Orientation of the Antibiotic Peptide Magainin in Membranes by Solid-state Nuclear Magnetic Resonance Spectroscopy. *Protein Science* **1993**, *2* (12), 2077–2084. https://doi.org/10.1002/pro.5560021208.

(62) Tamba, Y.; Yamazaki, M. Single Giant Unilamellar Vesicle Method Reveals Effect of Antimicrobial Peptide Magainin 2 on Membrane Permeability. *Biochemistry* **2005**, *44* (48), 15823–15833. https://doi.org/10.1021/bi051684w.

(63) Wenk, M. R.; Seelig, J. Magainin 2 Amide Interaction with Lipid Membranes: Calorimetric Detection of Peptide Binding and Pore Formation. *Biochemistry* **1998**, *37* (11), 3909–3916. https://doi.org/10.1021/bi972615n.

(64) Doyle, M. T.; Bernstein, H. D. Bacterial Outer Membrane Proteins Assemble via Asymmetric Interactions with the BamA β-Barrel. *Nat Commun* **2019**, *10* (1), 3358. https://doi.org/10.1038/s41467-019-11230-9.

(65) Wang, X.; Peterson, J. H.; Bernstein, H. D. Bacterial Outer Membrane Proteins Are Targeted to the Bam Complex by Two Parallel Mechanisms. *mBio* **2021**, *12* (3), e00597-21. https://doi.org/10.1128/mBio.00597-21.

(66) Rollauer, S. E.; Sooreshjani, M. A.; Noinaj, N.; Buchanan, S. K. Outer Membrane Protein Biogenesis in Gram-Negative Bacteria. *Phil. Trans. R. Soc. B* **2015**, *370* (1679), 20150023. https://doi.org/10.1098/rstb.2015.0023.

(67) Han, L.; Zheng, J.; Wang, Y.; Yang, X.; Liu, Y.; Sun, C.; Cao, B.; Zhou, H.; Ni, D.; Lou, J.; Zhao, Y.; Huang, Y. Structure of the BAM Complex and Its Implications for Biogenesis of Outer-Membrane Proteins. *Nat Struct Mol Biol* **2016**, *23* (3), 192–196. https://doi.org/10.1038/nsmb.3181.

(68) Anwari, K.; Webb, C. T.; Poggio, S.; Perry, A. J.; Belousoff, M.; Celik, N.; Ramm, G.; Lovering, A.; Sockett, R. E.; Smit, J.; Jacobs-Wagner, C.; Lithgow, T. The Evolution of New Lipoprotein Subunits of the Bacterial Outer Membrane BAM Complex. *Molecular Microbiology* **2012**, *84* (5), 832–844. https://doi.org/10.1111/j.1365-2958.2012.08059.x.

(69) Warner, L. R.; Gatzeva-Topalova, P. Z.; Doerner, P. A.; Pardi, A.; Sousa, M. C. Flexibility in the Periplasmic Domain of BamA Is Important for Function. *Structure* **2017**, *25* (1), 94–106. https://doi.org/10.1016/j.str.2016.11.013.

(70) Browning, D. F.; Bavro, V. N.; Mason, J. L.; Sevastsyanovich, Y. R.; Rossiter, A. E.; Jeeves, M.; Wells, T. J.; Knowles, T. J.; Cunningham, A. F.; Donald, J. W.; Palmer, T.; Overduin, M.; Henderson, I. R. Cross-species Chimeras Reveal BAMA POTRA and B -barrel Domains Must Be Fine-tuned for Efficient OMP Insertion. *Molecular Microbiology* **2015**, *97* (4), 646–659. https://doi.org/10.1111/mmi.13052.

(71) Malinverni, J. C.; Silhavy, T. J. Assembly of Outer Membrane β-Barrel Proteins: The Bam Complex. *EcoSal Plus* **2011**, *4* (2), ecosalplus.4.3.8. https://doi.org/10.1128/ecosalplus.4.3.8.

(72) Braginskaya, T. G.; Dobitchin, P. D.; Ivanova, M. A.; Klyubin, V. V.; Lomakin, A. V.; Noskin, V. A.; Shmelev, G. E.; Tolpina, S. P. Analysis of the Polydispersity by Photon Correlation Spectroscopy. Regularization Procedure. *Phys. Scr.* **1983**, *28* (1), 73–79. https://doi.org/10.1088/0031-8949/28/1/009.

(73) Gallucci, N.; Vitiello, G.; Di Girolamo, R.; Imbimbo, P.; Monti, D. M.; Tarallo, O.; Vergara, A.; Russo Krauss, I.; Paduano, L. Towards the Development of Antioxidant Cerium Oxide Nanoparticles for Biomedical Applications: Controlling the Properties by Tuning Synthesis Conditions. *Nanomaterials* **2021**, *11* (2), 542. https://doi.org/10.3390/nano11020542.

(74) Newby, Z. E. R.; O'Connell, J. D.; Gruswitz, F.; Hays, F. A.; Harries, W. E. C.; Harwood, I. M.; Ho, J. D.; Lee, J. K.; Savage, D. F.; Miercke, L. J. W.; Stroud, R. M. A General Protocol for the Crystallization of Membrane Proteins for X-Ray Structural Investigation. *Nat Protoc* **2009**, *4* (5), 619–637. https://doi.org/10.1038/nprot.2009.27.

(75) Illiano, A.; Pinto, G.; Gaglione, R.; Arciello, A.; Amoresano, A. Inflammation Protein Quantification by Multiple Reaction Monitoring Mass

Spectrometry in Lipopolysaccharide-stimulated THP-1 Cells. *Rapid Comm Mass Spectrometry* **2021**, *35* (20), e9166. https://doi.org/10.1002/rcm.9166.

(76) Abbatiello, S. E.; Mani, D. R.; Schilling, B.; MacLean, B.; Zimmerman, L. J.; Feng, X.; Cusack, M. P.; Sedransk, N.; Hall, S. C.; Addona, T.; Allen, S.; Dodder, N. G.; Ghosh, M.; Held, J. M.; Hedrick, V.; Inerowicz, H. D.; Jackson, A.; Keshishian, H.; Kim, J. W.; Lyssand, J. S.; Riley, C. P.; Rudnick, P.; Sadowski, P.; Shaddox, K.; Smith, D.; Tomazela, D.; Wahlander, A.; Waldemarson, S.; Whitwell, C. A.; You, J.; Zhang, S.; Kinsinger, C. R.; Mesri, M.; Rodriguez, H.; Borchers, C. H.; Buck, C.; Fisher, S. J.; Gibson, B. W.; Liebler, D.; MacCoss, M.; Neubert, T. A.; Paulovich, A.; Regnier, F.; Skates, S. J.; Tempst, P.; Wang, M.; Carr, S. A. Design, Implementation and Multisite Evaluation of a System Suitability Protocol for the Quantitative Assessment of Instrument Performance in Liquid Chromatography-Multiple Reaction Monitoring-MS (LC-MRM-MS). *Molecular & Cellular Proteomics* **2013**, *12* (9), 2623–2639. https://doi.org/10.1074/mcp.M112.027078.

(77) Overly Cottom, C.; Stephenson, R.; Wilson, L.; Noinaj, N. Targeting BAM for Novel Therapeutics against Pathogenic Gram-Negative Bacteria. *Antibiotics* **2023**, *12* (4), 679. https://doi.org/10.3390/antibiotics12040679.

(78) Gu, Y.; Li, H.; Dong, H.; Zeng, Y.; Zhang, Z.; Paterson, N. G.; Stansfeld, P. J.; Wang, Z.; Zhang, Y.; Wang, W.; Dong, C. Structural Basis of Outer Membrane Protein Insertion by the BAM Complex. *Nature* **2016**, *531* (7592), 64–69. https://doi.org/10.1038/nature17199.

(79) Zhou, G.; Wang, Q.; Wang, Y.; Wen, X.; Peng, H.; Peng, R.; Shi, Q.; Xie, X.; Li, L. Outer Membrane Porins Contribute to Antimicrobial Resistance in Gram-Negative Bacteria. *Microorganisms* **2023**, *11* (7), 1690. https://doi.org/10.3390/microorganisms11071690.

(80) Barber, M. Methicillin-Resistant Staphylococci. *Journal of Clinical Pathology* **1961**, *14* (4), 385–393. https://doi.org/10.1136/jcp.14.4.385.

(81) Cheung, G. Y. C.; Bae, J. S.; Otto, M. Pathogenicity and Virulence of *Staphylococcus Aureus*. *Virulence* **2021**, *12* (1), 547–569. https://doi.org/10.1080/21505594.2021.1878688.

(82) S. Butler, M.; A. Cooper, M. Screening Strategies to Identify New Antibiotics. *CDT* **2012**, *13* (3), 373–387. https://doi.org/10.2174/138945012799424624.

(83) Kane, T. L.; Carothers, K. E.; Lee, S. W. Virulence Factor Targeting of the Bacterial Pathogen Staphylococcus Aureus for Vaccine and Therapeutics. *CDT* **2018**, *19* (2), 111–127. https://doi.org/10.2174/1389450117666161128123536.

(84) Hamdan-Partida, A.; González-García, S.; De La Rosa García, E.; Bustos-Martínez, J. Community-Acquired Methicillin-Resistant Staphylococcus Aureus Can Persist in the Throat. *International Journal of Medical Microbiology* **2018**, *308* (4), 469–475. https://doi.org/10.1016/j.ijmm.2018.04.002.

(85) González-García, S.; Hamdan-Partida, A.; José Valdez-Alarcón, J.; Bustos-Hamdan, A.; Bustos-Martínez, J. Main Factors of *Staphylococcus Aureus* Associated with the Interaction to the Cells for Their Colonization and Persistence. In *Infectious Diseases*; Bustos-Martínez, J., José Valdez-Alarcón, J., Eds.; IntechOpen, 2023; Vol. 17. https://doi.org/10.5772/intechopen.107974.

(86) Howden, B. P.; Giulieri, S. G.; Wong Fok Lung, T.; Baines, S. L.; Sharkey, L. K.; Lee, J. Y. H.; Hachani, A.; Monk, I. R.; Stinear, T. P. Staphylococcus Aureus Host Interactions and Adaptation. *Nat Rev Microbiol* **2023**, *21* (6), 380–395. https://doi.org/10.1038/s41579-023-00852-y.

(87) Foster, T. J. Surface Proteins of *Staphylococcus Aureus*. *Microbiol Spectr* **2019**, *7* (4), 7.4.2. https://doi.org/10.1128/microbiolspec.GPP3-0046-2018.

(88) D'Andrea, L. D.; Romanelli, A. Temporins: Multifunctional Peptides from Frog Skin. *IJMS* **2023**, *24* (6), 5426. https://doi.org/10.3390/ijms24065426.

(89) Casciaro, B.; Loffredo, M. R.; Cappiello, F.; Fabiano, G.; Torrini, L.; Mangoni, M. L. The Antimicrobial Peptide Temporin G: Anti-Biofilm, Anti-Persister Activities, and Potentiator Effect of Tobramycin Efficacy Against Staphylococcus Aureus. *IJMS* **2020**, *21* (24), 9410. https://doi.org/10.3390/ijms21249410.

(90) Simmaco, M.; Mignogna, G.; Canofeni, S.; Miele, R.; Mangoni, M. L.; Barra, D. Temporins, Antimicrobial Peptides from the European Red Frog *Rana Temporaria*. *European Journal of Biochemistry* **1996**, *242* (3), 788–792. https://doi.org/10.1111/j.1432-1033.1996.0788r.x.

(91) Zhang, S.; Ma, M.; Shao, Z.; Zhang, J.; Fu, L.; Li, X.; Fang, W.; Gao, L. Structure and Formation Mechanism of Antimicrobial Peptides Temporin B- and L-Induced Tubular Membrane Protrusion. *IJMS* **2021**, *22* (20), 11015. https://doi.org/10.3390/ijms222011015.

(92) Manzo, G.; Ferguson, P. M.; Hind, C. K.; Clifford, M.; Gustilo, V. B.; Ali, H.; Bansal, S. S.; Bui, T. T.; Drake, A. F.; Atkinson, R. A.; Sutton, J. M.; Lorenz, C. D.; Phoenix, D. A.; Mason, A. J. Temporin L and Aurein 2.5 Have Identical Conformations but Subtly Distinct Membrane and Antibacterial Activities. *Sci Rep* **2019**, *9* (1), 10934. https://doi.org/10.1038/s41598-019-47327-w.

(93) Di Somma, A.; Avitabile, C.; Cirillo, A.; Moretta, A.; Merlino, A.; Paduano, L.; Duilio, A.; Romanelli, A. The Antimicrobial Peptide Temporin L Impairs E. Coli Cell Division by Interacting with FtsZ and the Divisome Complex.

Biochimica et Biophysica Acta (BBA) - General Subjects **2020**, *1864* (7), 129606. https://doi.org/10.1016/j.bbagen.2020.129606.

(94) Di Somma, A.; Canè, C.; Moretta, A.; Duilio, A. Interaction of Temporin-L Analogues with the E. Coli FtsZ Protein. *Antibiotics* **2021**, *10* (6), 704. https://doi.org/10.3390/antibiotics10060704.

(95) De Gregorio, E.; Esposito, E. P.; Zarrilli, R.; Di Nocera, P. P. Contact-Dependent Growth Inhibition Proteins in Acinetobacter Baylyi ADP1. *Curr Microbiol* **2018**, *75* (11), 1434–1440. https://doi.org/10.1007/s00284-018-1540-y.

(96) Uhlmann, J.; Rohde, M.; Siemens, N.; Kreikemeyer, B.; Bergman, P.; Johansson, L.; Norrby-Teglund, A. LL-37 Triggers Formation of ***Streptococcus Pyogenes*** Extracellular Vesicle-Like Structures with Immune Stimulatory Properties. *J Innate Immun* **2016**, *8* (3), 243–257. https://doi.org/10.1159/000441896.

(97) Parsons, J. B.; Rock, C. O. Is Bacterial Fatty Acid Synthesis a Valid Target for Antibacterial Drug Discovery? *Current Opinion in Microbiology* **2011**, *14* (5), 544–549. https://doi.org/10.1016/j.mib.2011.07.029.

(98) Bessa, L. J.; Ferreira, M.; Gameiro, P. Evaluation of Membrane Fluidity of Multidrug-Resistant Isolates of Escherichia Coli and Staphylococcus Aureus in Presence and Absence of Antibiotics. *Journal of Photochemistry and Photobiology B: Biology* **2018**, *181*, 150–156. https://doi.org/10.1016/j.jphotobiol.2018.03.002.

(99) Kuhn, S.; Slavetinsky, C. J.; Peschel, A. Synthesis and Function of Phospholipids in Staphylococcus Aureus. *International Journal of Medical Microbiology* **2015**, *305* (2), 196–202. https://doi.org/10.1016/j.ijmm.2014.12.016.

(100) Mishra, N. N.; McKinnell, J.; Yeaman, M. R.; Rubio, A.; Nast, C. C.; Chen, L.; Kreiswirth, B. N.; Bayer, A. S. *In Vitro* Cross-Resistance to Daptomycin and Host Defense Cationic Antimicrobial Peptides in Clinical Methicillin-Resistant Staphylococcus Aureus Isolates. *Antimicrob Agents Chemother* **2011**, *55* (9), 4012–4018. https://doi.org/10.1128/AAC.00223-11.

(101) Kumaraswamy, M.; Wiull, K.; Joshi, B.; Sakoulas, G.; Kousha, A.; Vaaje-Kolstad, G.; Johannessen, M.; Hegstad, K.; Nizet, V.; Askarian, F. Bacterial Membrane-Derived Vesicles Attenuate Vancomycin Activity against Methicillin-Resistant Staphylococcus Aureus. *Microorganisms* **2021**, *9* (10), 2055. https://doi.org/10.3390/microorganisms9102055.

(102) Liu, Z.-H.; Wu, Q.-Y.; Xu, F.; Zhang, X.; Liao, X.-B. Biofunction and Clinical Potential of Extracellular Vesicles from Methicillin-Resistant Staphylococcus Aureus. *Microbiological Research* **2023**, *266*, 127238. https://doi.org/10.1016/j.micres.2022.127238.

(103) Korem, M.; Gov, Y.; Kiran, M. D.; Balaban, N. Transcriptional Profiling of Target of RNAIII-Activating Protein, a Master Regulator of Staphylococcal Virulence. *Infect Immun* **2005**, *73* (10), 6220–6228. https://doi.org/10.1128/IAI.73.10.6220-6228.2005.

(104) Schmidt, K. A.; Manna, A. C.; Cheung, A. L. SarT Influences *sarS* Expression in *Staphylococcus Aureus*. *Infect Immun* **2003**, *71* (9), 5139–5148. https://doi.org/10.1128/IAI.71.9.5139-5148.2003.

(105) Poyart, C.; Pellegrini, E.; Marceau, M.; Baptista, M.; Jaubert, F.; Lamy, M.; Trieu-Cuot, P. Attenuated Virulence of *Streptococcus Agalactiae* Deficient in D -alanyl-lipoteichoic Acid Is Due to an Increased Susceptibility to Defensins and Phagocytic Cells. *Molecular Microbiology* **2003**, *49* (6), 1615–1625. https://doi.org/10.1046/j.1365-2958.2003.03655.x.

(106) Sobhani, Z.; Akaberi, M.; Amiri, M. S.; Ramezani, M.; Emami, S. A.; Sahebkar, A. Medicinal Species of the Genus Berberis: A Review of Their Traditional and Ethnomedicinal Uses, Phytochemistry and Pharmacology. In *Pharmacological Properties of Plant-Derived Natural Products and Implications for Human Health*; Barreto, G. E., Sahebkar, A., Eds.; Advances in Experimental Medicine and Biology; Springer International Publishing: Cham, 2021; Vol. 1308, pp 547–577. https://doi.org/10.1007/978-3-030-64872-5_27.

(107) Rahimi-Madiseh, M.; Lorigoini, Z.; Zamani-gharaghoshi, H.; Rafieian-kopaei, M. Berberis Vulgaris: Specifications and Traditional Uses. *Iranian Journal of Basic Medical Sciences* **2017**, *20* (5). https://doi.org/10.22038/ijbms.2017.8690.

(108) Gaba, S.; Saini, A.; Singh, G.; Monga, V. An Insight into the Medicinal Attributes of Berberine Derivatives: A Review. *Bioorganic & Medicinal Chemistry* **2021**, *38*, 116143. https://doi.org/10.1016/j.bmc.2021.116143.

(109) Wang, K.; Feng, X.; Chai, L.; Cao, S.; Qiu, F. The Metabolism of Berberine and Its Contribution to the Pharmacological Effects. *Drug Metabolism Reviews* **2017**, *49* (2), 139–157. https://doi.org/10.1080/03602532.2017.1306544.

(110) Kong, Y.; Li, L.; Zhao, L.-G.; Yu, P.; Li, D.-D. A Patent Review of Berberine and Its Derivatives with Various Pharmacological Activities (2016–2020). *Expert Opinion on Therapeutic Patents* **2022**, *32* (2), 211–223. https://doi.org/10.1080/13543776.2021.1974001.

(111) Wu, S.; Yang, K.; Hong, Y.; Gong, Y.; Ni, J.; Yang, N.; Ding, W. A New Perspective on the Antimicrobial Mechanism of Berberine Hydrochloride Against Staphylococcus Aureus Revealed by Untargeted Metabolomic Studies. *Front. Microbiol.* **2022**, *13*, 917414. https://doi.org/10.3389/fmicb.2022.917414.

(112) Domadia, P. N.; Bhunia, A.; Sivaraman, J.; Swarup, S.; Dasgupta, D. Berberine Targets Assembly of Escherichia Coli Cell Division Protein FtsZ. *Biochemistry* **2008**, *47* (10), 3225–3234. https://doi.org/10.1021/bi7018546.

(113) Battaje, R. R.; Panda, D. Lessons from Bacterial Homolog of Tubulin, FtsZ for Microtubule Dynamics. *Endocrine-Related Cancer* **2017**, *24* (9), T1–T21. https://doi.org/10.1530/ERC-17-0118.

(114) McQuillen, R.; Xiao, J. Insights into the Structure, Function, and Dynamics of the Bacterial Cytokinetic FtsZ-Ring. *Annu. Rev. Biophys.* **2020**, *49* (1), 309–341. https://doi.org/10.1146/annurev-biophys-121219-081703.

(115) Xiao, J.; Goley, E. D. Redefining the Roles of the FtsZ-Ring in Bacterial Cytokinesis. *Current Opinion in Microbiology* **2016**, *34*, 90–96. https://doi.org/10.1016/j.mib.2016.08.008.

(116) Barrows, J. M.; Goley, E. D. FtsZ Dynamics in Bacterial Division: What, How, and Why? *Current Opinion in Cell Biology* **2021**, *68*, 163–172. https://doi.org/10.1016/j.ceb.2020.10.013.

(117) Morrison, J. J.; Conti, J.; Camberg, J. L. Assembly and Architecture of Escherichia Coli Divisome Proteins FtsA and FtsZ. *Journal of Biological Chemistry* **2022**, *298* (3), 101663. https://doi.org/10.1016/j.jbc.2022.101663.

(118) Hale, C. A.; De Boer, P. A. J. Direct Binding of FtsZ to ZipA, an Essential Component of the Septal Ring Structure That Mediates Cell Division in E. Coli. *Cell* **1997**, *88* (2), 175–185. https://doi.org/10.1016/S0092-8674(00)81838-3.

(119) Attaibi, M.; Den Blaauwen, T. An Updated Model of the Divisome: Regulation of the Septal Peptidoglycan Synthesis Machinery by the Divisome. *IJMS* **2022**, *23* (7), 3537. https://doi.org/10.3390/ijms23073537.

(120) Cameron, T. A.; Margolin, W. Insights into the Assembly and Regulation of the Bacterial Divisome. *Nat Rev Microbiol* **2024**, *22* (1), 33–45. https://doi.org/10.1038/s41579-023-00942-x.

(121) Milani, G.; Cavalluzzi, M. M.; Solidoro, R.; Salvagno, L.; Quintieri, L.; Di Somma, A.; Rosato, A.; Corbo, F.; Franchini, C.; Duilio, A.; Caputo, L.; Habtemariam, S.; Lentini, G. Molecular Simplification of Natural Products: Synthesis, Antibacterial Activity, and Molecular Docking Studies of Berberine Open Models. *Biomedicines* **2021**, *9* (5), 452. https://doi.org/10.3390/biomedicines9050452.

(122) Yang, J.; Zhang, Y. I-TASSER Server: New Development for Protein Structure and Function Predictions. *Nucleic Acids Res* **2015**, *43* (W1), W174–W181. https://doi.org/10.1093/nar/gkv342.

(123) Dodda, L. S.; Cabeza de Vaca, I.; Tirado-Rives, J.; Jorgensen, W. L. LigParGen Web Server: An Automatic OPLS-AA Parameter Generator for Organic Ligands. *Nucleic Acids Research* **2017**, *45* (W1), W331–W336. https://doi.org/10.1093/nar/gkx312.

(124) Schneidman-Duhovny, D.; Inbar, Y.; Nussinov, R.; Wolfson, H. J. PatchDock and SymmDock: Servers for Rigid and Symmetric Docking. *Nucleic Acids Research* **2005**, *33* (Web Server), W363–W367. https://doi.org/10.1093/nar/gki481.

(125) Mashiach, E.; Schneidman-Duhovny, D.; Andrusier, N.; Nussinov, R.; Wolfson, H. J. FireDock: A Web Server for Fast Interaction Refinement in Molecular Docking. *Nucleic Acids Research* **2008**, *36* (Web Server), W229–W232. https://doi.org/10.1093/nar/gkn186.

(126) Salentin, S.; Schreiber, S.; Haupt, V. J.; Adasme, M. F.; Schroeder, M. PLIP: Fully Automated Protein–Ligand Interaction Profiler. *Nucleic Acids Res* **2015**, *43* (W1), W443–W447. https://doi.org/10.1093/nar/gkv315.

(127) Xue, L. C.; Rodrigues, J. P.; Kastritis, P. L.; Bonvin, A. M.; Vangone, A. PRODIGY: A Web Server for Predicting the Binding Affinity of Protein–Protein Complexes. *Bioinformatics* **2016**, *32* (23), 3676–3678. https://doi.org/10.1093/bioinformatics/btw514.

(128) Rivas, G.; López, A.; Mingorance, J.; Ferrándiz, M. J.; Zorrilla, S.; Minton, A. P.; Vicente, M.; Andreu, J. M. Magnesium-Induced Linear Self-Association of the FtsZ Bacterial Cell Division Protein Monomer. *Journal of Biological Chemistry* **2000**, *275* (16), 11740–11749. https://doi.org/10.1074/jbc.275.16.11740.

(129) Zheng, Y.-Y.; Du, R.-L.; Cai, S.-Y.; Liu, Z.-H.; Fang, Z.-Y.; Liu, T.; So, L.-Y.; Lu, Y.-J.; Sun, N.; Wong, K.-Y. Study of Benzofuroquinolinium Derivatives as a New Class of Potent Antibacterial Agent and the Mode of Inhibition Targeting FtsZ. *Front. Microbiol.* **2018**, *9*, 1937. https://doi.org/10.3389/fmicb.2018.01937.

(130) Kaul, M.; Parhi, A. K.; Zhang, Y.; LaVoie, E. J.; Tuske, S.; Arnold, E.; Kerrigan, J. E.; Pilch, D. S. A Bactericidal Guanidinomethyl Biaryl That Alters the Dynamics of Bacterial FtsZ Polymerization. *J. Med. Chem.* **2012**, *55* (22), 10160–10176. https://doi.org/10.1021/jm3012728.

(131) Crone, S.; Vives-Flórez, M.; Kvich, L.; Saunders, A. M.; Malone, M.; Nicolaisen, M. H.; Martínez-García, E.; Rojas-Acosta, C.; Catalina Gomez-Puerto, M.; Calum, H.; Whiteley, M.; Kolter, R.; Bjarnsholt, T. The Environmental Occurrence of *Pseudomonas Aeruginosa*. *APMIS* **2020**, *128* (3), 220–231. https://doi.org/10.1111/apm.13010.

(132) Deredjian, A.; Colinon, C.; Brothier, E.; Favre-Bonté, S.; Cournoyer, B.; Nazaret, S. Antibiotic and Metal Resistance among Hospital and Outdoor Strains of Pseudomonas Aeruginosa. *Research in Microbiology* **2011**, *162* (7), 689–700. https://doi.org/10.1016/j.resmic.2011.06.007.

(133) Laborda, P.; Hernando-Amado, S.; Martínez, J. L.; Sanz-García, F. Antibiotic Resistance in Pseudomonas. In *Pseudomonas aeruginosa*; Filloux, A., Ramos, J.-L., Eds.; Advances in Experimental Medicine and Biology; Springer International Publishing: Cham, 2022; Vol. 1386, pp 117–143. https://doi.org/10.1007/978-3-031-08491-1_5.

(134) Pang, Z.; Raudonis, R.; Glick, B. R.; Lin, T.-J.; Cheng, Z. Antibiotic Resistance in Pseudomonas Aeruginosa: Mechanisms and Alternative Therapeutic Strategies. *Biotechnology Advances* **2019**, *37* (1), 177–192. https://doi.org/10.1016/j.biotechadv.2018.11.013.

(135) Ben Haj Khalifa, A.; Moissenet, D.; Vu Thien, H.; Khedher, M. Virulence Factors in Pseudomonas Aeruginosa: Mechanisms and Modes of Regulation. *Annales de biologie clinique* **2011**, *69* (4), 393–403. https://doi.org/10.1684/abc.2011.0589.

(136) Azam, M. W.; Khan, A. U. Updates on the Pathogenicity Status of Pseudomonas Aeruginosa. *Drug Discovery Today* **2019**, *24* (1), 350–359. https://doi.org/10.1016/j.drudis.2018.07.003.

(137) Wood, S. J.; Kuzel, T. M.; Shafikhani, S. H. Pseudomonas Aeruginosa: Infections, Animal Modeling, and Therapeutics. *Cells* **2023**, *12* (1), 199. https://doi.org/10.3390/cells12010199.

(138) Mancuso, G.; Midiri, A.; Gerace, E.; Biondo, C. Bacterial Antibiotic Resistance: The Most Critical Pathogens. *Pathogens* **2021**, *10* (10), 1310. https://doi.org/10.3390/pathogens10101310.

(139) Jurado-Martín, I.; Sainz-Mejías, M.; McClean, S. Pseudomonas Aeruginosa: An Audacious Pathogen with an Adaptable Arsenal of Virulence Factors. *IJMS* **2021**, *22* (6), 3128. https://doi.org/10.3390/ijms22063128.

(140) Michalska, A. D.; Sacha, P. T.; Ojdana, D.; Wieczorek, A.; Tryniszewska, E. Prevalence of Resistance to Aminoglycosides and Fluoroquinolones among Pseudomonas Aeruginosa Strains in a University Hospital in Northeastern Poland. *Braz. J. Microbiol.* **2014**, *45* (4), 1455–1458. https://doi.org/10.1590/S1517-83822014000400041.

(141) Alvarez-Ortega, C.; Wiegand, I.; Olivares, J.; Hancock, R. E. W.; Martínez, J. L. The Intrinsic Resistome of *Pseudomonas Aeruginosa* to β-Lactams. *Virulence* **2011**, *2* (2), 144–146. https://doi.org/10.4161/viru.2.2.15014.

(142) Ude, J.; Tripathi, V.; Buyck, J. M.; Söderholm, S.; Cunrath, O.; Fanous, J.; Claudi, B.; Egli, A.; Schleberger, C.; Hiller, S.; Bumann, D. Outer Membrane Permeability: Antimicrobials and Diverse Nutrients Bypass Porins in *Pseudomonas Aeruginosa*. *Proc. Natl. Acad. Sci. U.S.A.* **2021**, *118* (31), e2107644118. https://doi.org/10.1073/pnas.2107644118.

(143) Ivanov, M. E.; Fursova, N. K.; Potapov, V. D. Pseudomonas Aeruginosa Efflux Pump Superfamily (Review of Literature). *Klin. lab. diagn.* **2022**, *67* (1), 53–58. https://doi.org/10.51620/0869-2084-2022-67-1-53-58.

(144) Lorusso, A. B.; Carrara, J. A.; Barroso, C. D. N.; Tuon, F. F.; Faoro, H. Role of Efflux Pumps on Antimicrobial Resistance in Pseudomonas Aeruginosa. *IJMS* **2022**, *23* (24), 15779. https://doi.org/10.3390/ijms232415779.

(145) Islas-Rodrìguez, A. E.; Marcellini, L.; Orioni, B.; Barra, D.; Stella, L.; Mangoni, M. L. Esculentin 1–21: A Linear Antimicrobial Peptide from Frog Skin with Inhibitory Effect on Bovine Mastitis-causing Bacteria. *Journal of Peptide Science* **2009**, *15* (9), 607–614. https://doi.org/10.1002/psc.1148.

(146) Loffredo, M. R.; Ghosh, A.; Harmouche, N.; Casciaro, B.; Luca, V.; Bortolotti, A.; Cappiello, F.; Stella, L.; Bhunia, A.; Bechinger, B.; Mangoni, M. L. Membrane Perturbing Activities and Structural Properties of the Frog-Skin Derived Peptide Esculentin-1a(1-21)NH2 and Its Diastereomer Esc(1-21)-1c: Correlation with Their Antipseudomonal and Cytotoxic Activity. *Biochimica et Biophysica Acta (BBA) - Biomembranes* **2017**, *1859* (12), 2327–2339. https://doi.org/10.1016/j.bbamem.2017.09.009.

(147) Casciaro, B.; Cappiello, F.; Cacciafesta, M.; Mangoni, M. L. Promising Approaches to Optimize the Biological Properties of the Antimicrobial Peptide Esculentin-1a(1–21)NH2: Amino Acids Substitution and Conjugation to Nanoparticles. *Front. Chem.* **2017**, *5*, 26. https://doi.org/10.3389/fchem.2017.00026.

(148) Grieco, P.; Carotenuto, A.; Auriemma, L.; Saviello, M. R.; Campiglia, P.; Gomez-Monterrey, I. M.; Marcellini, L.; Luca, V.; Barra, D.; Novellino, E.; Mangoni, M. L. The Effect of D-Amino Acid Substitution on the Selectivity of Temporin L towards Target Cells: Identification of a Potent Anti-Candida Peptide. *Biochimica et Biophysica Acta (BBA) - Biomembranes* **2013**, *1828* (2), 652–660. https://doi.org/10.1016/j.bbamem.2012.08.027.

(149) Cappiello, F.; Di Grazia, A.; Segev-Zarko, L.; Scali, S.; Ferrera, L.; Galietta, L.; Pini, A.; Shai, Y.; Di, Y. P.; Mangoni, M. L. Esculentin-1a-Derived Peptides Promote Clearance of Pseudomonas Aeruginosa Internalized in Bronchial Cells of Cystic Fibrosis Patients and Lung Cell Migration: Biochemical Properties and a Plausible Mode of Action. *Antimicrob Agents Chemother* **2016**, *60* (12), 7252–7262. https://doi.org/10.1128/AAC.00904-16.

(150) Tyanova, S.; Temu, T.; Cox, J. The MaxQuant Computational Platform for Mass Spectrometry-Based Shotgun Proteomics. *Nat Protoc* **2016**, *11* (12), 2301–2319. https://doi.org/10.1038/nprot.2016.136.

(151) Cox, J.; Neuhauser, N.; Michalski, A.; Scheltema, R. A.; Olsen, J. V.; Mann, M. Andromeda: A Peptide Search Engine Integrated into the MaxQuant Environment. *J. Proteome Res.* **2011**, *10* (4), 1794–1805. https://doi.org/10.1021/pr101065j.

(152) Pollini, S.; Brunetti, J.; Sennati, S.; Rossolini, G. M.; Bracci, L.; Pini, A.; Falciani, C. Synergistic Activity Profile of an Antimicrobial Peptide against Multidrug-resistant and Extensively Drug-resistant Strains of Gram-negative Bacterial Pathogens. *Journal of Peptide Science* **2017**, *23* (4), 329–333. https://doi.org/10.1002/psc.2978.

(153) Letizia, M.; Mellini, M.; Fortuna, A.; Visca, P.; Imperi, F.; Leoni, L.; Rampioni, G. PqsE Expands and Differentially Modulates the RhlR Quorum Sensing Regulon in Pseudomonas Aeruginosa. *Microbiol Spectr* **2022**, *10* (3), e00961-22. https://doi.org/10.1128/spectrum.00961-22.

(154) Pan, Y.; Xu, Y.; Wang, Z.; Fang, Y.; Shen, J. Overexpression of MexAB-OprM Efflux Pump in Carbapenem-Resistant Pseudomonas Aeruginosa. *Arch Microbiol* **2016**, *198* (6), 565–571. https://doi.org/10.1007/s00203-016-1215-7.

(155) Li, H.; Luo, Y.-F.; Williams, B. J.; Blackwell, T. S.; Xie, C.-M. Structure and Function of OprD Protein in Pseudomonas Aeruginosa: From Antibiotic Resistance to Novel Therapies. *International Journal of Medical Microbiology* **2012**, *302* (2), 63–68. https://doi.org/10.1016/j.ijmm.2011.10.001.

(156) Casciaro, B.; Loffredo, M. R.; Luca, V.; Verrusio, W.; Cacciafesta, M.; Mangoni, M. L. Esculentin-1a Derived Antipseudomonal Peptides: Limited

Induction of Resistance and Synergy with Aztreonam. *PPL* **2019**, *25* (12), 1155–1162. https://doi.org/10.2174/0929866525666181101104649.

(157) Bhagirath, A. Y.; Li, Y.; Patidar, R.; Yerex, K.; Ma, X.; Kumar, A.; Duan, K. Two Component Regulatory Systems and Antibiotic Resistance in Gram-Negative Pathogens. *IJMS* **2019**, *20* (7), 1781. https://doi.org/10.3390/ijms20071781.

(158) Sultan, M.; Arya, R.; Kim, K. K. Roles of Two-Component Systems in Pseudomonas Aeruginosa Virulence. *IJMS* **2021**, *22* (22), 12152. https://doi.org/10.3390/ijms222212152.

(159) Bielecki, P.; Jensen, V.; Schulze, W.; Gödeke, J.; Strehmel, J.; Eckweiler, D.; Nicolai, T.; Bielecka, A.; Wille, T.; Gerlach, R. G.; Häussler, S. Cross Talk between the Response Regulators PhoB and TctD Allows for the Integration of Diverse Environmental Signals in *Pseudomonas Aeruginosa*. *Nucleic Acids Res* **2015**, *43* (13), 6413–6425. https://doi.org/10.1093/nar/gkv599.

(160) Barbieri, C. M.; Wu, T.; Stock, A. M. Comprehensive Analysis of OmpR Phosphorylation, Dimerization, and DNA Binding Supports a Canonical Model for Activation. *Journal of Molecular Biology* **2013**, *425* (10), 1612–1626. https://doi.org/10.1016/j.jmb.2013.02.003.

(161) Li, W.; Xue, M.; Yu, L.; Qi, K.; Ni, J.; Chen, X.; Deng, R.; Shang, F.; Xue, T. QseBC Is Involved in the Biofilm Formation and Antibiotic Resistance in *Escherichia Coli* Isolated from Bovine Mastitis. *PeerJ* **2020**, *8*, e8833. https://doi.org/10.7717/peerj.8833.

(162) Auda, I. G.; Ali Salman, I. M.; Odah, J. Gh. Efflux Pumps of Gram-Negative Bacteria in Brief. *Gene Reports* **2020**, *20*, 100666. https://doi.org/10.1016/j.genrep.2020.100666.

(163) Liao, J.; Schurr, M. J.; Sauer, K. The MerR-Like Regulator BrlR Confers Biofilm Tolerance by Activating Multidrug Efflux Pumps in Pseudomonas Aeruginosa Biofilms. *J Bacteriol* **2013**, *195* (15), 3352–3363. https://doi.org/10.1128/JB.00318-13.

(164) Tian, Z.-X.; Yi, X.-X.; Cho, A.; O'Gara, F.; Wang, Y.-P. CpxR Activates MexAB-OprM Efflux Pump Expression and Enhances Antibiotic Resistance in Both Laboratory and Clinical nalB-Type Isolates of Pseudomonas Aeruginosa. *PLoS Pathog* **2016**, *12* (10), e1005932. https://doi.org/10.1371/journal.ppat.1005932.

(165) Salam, Md. A.; Al-Amin, Md. Y.; Salam, M. T.; Pawar, J. S.; Akhter, N.; Rabaan, A. A.; Alqumber, M. A. A. Antimicrobial Resistance: A Growing Serious Threat for Global Public Health. *Healthcare* **2023**, *11* (13), 1946. https://doi.org/10.3390/healthcare11131946.

(166) Mulani, M. S.; Kamble, E. E.; Kumkar, S. N.; Tawre, M. S.; Pardesi, K. R. Emerging Strategies to Combat ESKAPE Pathogens in the Era of Antimicrobial Resistance: A Review. *Front. Microbiol.* **2019**, *10*, 539. https://doi.org/10.3389/fmicb.2019.00539.

(167) Haukland, H. H.; Ulvatne, H.; Sandvik, K.; Vorland, L. H. The Antimicrobial Peptides Lactoferricin B and Magainin 2 Cross over the Bacterial Cytoplasmic Membrane and Reside in the Cytoplasm. *FEBS Letters* **2001**, *508* (3), 389–393. https://doi.org/10.1016/S0014-5793(01)03100-3.

(168) Le, C.-F.; Fang, C.-M.; Sekaran, S. D. Intracellular Targeting Mechanisms by Antimicrobial Peptides. *Antimicrob Agents Chemother* **2017**, *61* (4), e02340-16. https://doi.org/10.1128/AAC.02340-16.

(169) Murzyn, K.; Pasenkiewicz-Gierula, M. Construction of a Toroidal Model for the Magainin Pore. *Journal of Molecular Modeling* **2003**, *9* (4), 217–224. https://doi.org/10.1007/s00894-003-0127-z.

(170) Xu, Q.; Guo, M.; Yu, F. β-Barrel Assembly Machinery (BAM) Complex as Novel Antibacterial Drug Target. *Molecules* **2023**, *28* (9), 3758. https://doi.org/10.3390/molecules28093758.

(171) Bennion, D.; Charlson, E. S.; Coon, E.; Misra, R. Dissection of β-Barrel Outer Membrane Protein Assembly Pathways through Characterizing BamA POTRA 1 Mutants of Escherichia Coli: BamA POTRA 1 Mutants. *Molecular Microbiology* **2010**, *77* (5), 1153–1171. https://doi.org/10.1111/j.1365-2958.2010.07280.x.

(172) Andreoni, F.; Toyofuku, M.; Menzi, C.; Kalawong, R.; Mairpady Shambat, S.; François, P.; Zinkernagel, A. S.; Eberl, L. Antibiotics Stimulate Formation of Vesicles in *Staphylococcus Aureus* in Both Phage-Dependent and -Independent Fashions and via Different Routes. *Antimicrob Agents Chemother* **2019**, *63* (2), e01439-18. https://doi.org/10.1128/AAC.01439-18.

(173) Song, Y.; Lunde, C. S.; Benton, B. M.; Wilkinson, B. J. Studies on the Mechanism of Telavancin Decreased Susceptibility in a Laboratory-Derived Mutant. *Microbial Drug Resistance* **2013**, *19* (4), 247–255. https://doi.org/10.1089/mdr.2012.0195.

(174) Bayer, A. S.; Prasad, R.; Chandra, J.; Koul, A.; Smriti, M.; Varma, A.; Skurray, R. A.; Firth, N.; Brown, M. H.; Koo, S.-P.; Yeaman, M. R. In Vitro Resistance of *Staphylococcus Aureus* to Thrombin-Induced Platelet Microbicidal Protein Is Associated with Alterations in Cytoplasmic Membrane Fluidity. *Infect Immun* **2000**, *68* (6), 3548–3553. https://doi.org/10.1128/IAI.68.6.3548-3553.2000.

(175) Kim, S. W.; Seo, J.-S.; Park, S. B.; Lee, A. R.; Lee, J. S.; Jung, J. W.; Chun, J. H.; Lazarte, J. M. S.; Kim, J.; Kim, J.-H.; Song, J.-W.; Franco, C.; Zhang, W.; Ha, M. W.; Paek, S.-M.; Jung, M.; Jung, T. S. Significant Increase in the Secretion of Extracellular Vesicles and Antibiotics Resistance from Methicillin-Resistant Staphylococcus Aureus Induced by Ampicillin Stress. *Sci Rep* **2020**, *10* (1), 21066. https://doi.org/10.1038/s41598-020-78121-8.

(176) Ghasemian, A.; Najar Peerayeh, S.; Bakhshi, B.; Mirzaee, M. The Microbial Surface Components Recognizing Adhesive Matrix Molecules (MSCRAMMs) Genes among Clinical Isolates of Staphylococcus Aureus from Hospitalized Children. *Iran J Pathol* **2015**, *10* (4), 258–264.

(177) Vaudaux, P.; Francois, P.; Bisognano, C.; Kelley, W. L.; Lew, D. P.; Schrenzel, J.; Proctor, R. A.; McNamara, P. J.; Peters, G.; Von Eiff, C. Increased Expression of Clumping Factor and Fibronectin-Binding Proteins by *hemB* Mutants of *Staphylococcus Aureus* Expressing Small Colony Variant Phenotypes. *Infect Immun* **2002**, *70* (10), 5428–5437. https://doi.org/10.1128/IAI.70.10.5428-5437.2002.

(178) Duperthuy, M. Antimicrobial Peptides: Virulence and Resistance Modulation in Gram-Negative Bacteria. *Microorganisms* **2020**, *8* (2), 280. https://doi.org/10.3390/microorganisms8020280.

(179) Aoki, W.; Ueda, M. Characterization of Antimicrobial Peptides toward the Development of Novel Antibiotics. *Pharmaceuticals* **2013**, *6* (8), 1055–1081. https://doi.org/10.3390/ph6081055.

(180) Silber, N.; Matos De Opitz, C. L.; Mayer, C.; Sass, P. Cell Division Protein FtsZ: From Structure and Mechanism to Antibiotic Target. *Future Microbiology* **2020**, *15* (9), 801–831. https://doi.org/10.2217/fmb-2019-0348.

(181) Malhotra, S.; Hayes, D.; Wozniak, D. J. Cystic Fibrosis and Pseudomonas Aeruginosa: The Host-Microbe Interface. *Clin Microbiol Rev* **2019**, *32* (3), e00138-18. https://doi.org/10.1128/CMR.00138-18.

(182) Xu, Y.; Zheng, X.; Zeng, W.; Chen, T.; Liao, W.; Qian, J.; Lin, J.; Zhou, C.; Tian, X.; Cao, J.; Zhou, T. Mechanisms of Heteroresistance and Resistance to Imipenem in Pseudomonas Aeruginosa. *IDR* **2020**, *Volume 13*, 1419–1428. https://doi.org/10.2147/IDR.S249475.

(183) Avakh, A.; Grant, G. D.; Cheesman, M. J.; Kalkundri, T.; Hall, S. The Art of War with Pseudomonas Aeruginosa: Targeting Mex Efflux Pumps Directly to Strategically Enhance Antipseudomonal Drug Efficacy. *Antibiotics* **2023**, *12* (8), 1304. https://doi.org/10.3390/antibiotics12081304.

(184) Jo, J. T. H.; Brinkman, F. S. L.; Hancock, R. E. W. Aminoglycoside Efflux in *Pseudomonas Aeruginosa* : Involvement of Novel Outer Membrane Proteins. *Antimicrob Agents Chemother* **2003**, *47* (3), 1101–1111. https://doi.org/10.1128/AAC.47.3.1101-1111.2003.

(185) Shang, D.; Han, X.; Du, W.; Kou, Z.; Jiang, F. Trp-Containing Antibacterial Peptides Impair Quorum Sensing and Biofilm Development in Multidrug-Resistant Pseudomonas Aeruginosa and Exhibit Synergistic Effects With Antibiotics. *Front. Microbiol.* **2021**, *12*, 611009. https://doi.org/10.3389/fmicb.2021.611009.

(186) Aguilar-Rodea, P.; Zúñiga, G.; Cerritos, R.; Rodríguez-Espino, B. A.; Gomez-Ramirez, U.; Nolasco-Romero, C. G.; López-Marceliano, B.; Rodea, G. E.; Mendoza-Elizalde, S.; Reyes-López, A.; Olivares Clavijo, H.; Vigueras Galindo, J. C.; Velázquez-Guadarrama, N.; Rosas-Pérez, I. Nucleotide Substitutions in the mexR, nalC and nalD Regulator Genes of the MexAB-OprM Efflux Pump Are Maintained in Pseudomonas Aeruginosa Genetic Lineages.

PLoS ONE **2022**, *17* (5), e0266742. https://doi.org/10.1371/journal.pone.0266742.

(187) Duan, D.; Goemans, N.; Takeda, S.; Mercuri, E.; Aartsma-Rus, A. Duchenne Muscular Dystrophy. *Nat Rev Dis Primers* **2021**, *7* (1), 13. https://doi.org/10.1038/s41572-021-00248-3.

(188) Yiu, E. M.; Kornberg, A. J. Duchenne Muscular Dystrophy. *J Paediatrics Child Health* **2015**, *51* (8), 759–764. https://doi.org/10.1111/jpc.12868.

(189) Kaplan, K. M.; Morgan, K. G. The Importance of Dystrophin and the Dystrophin Associated Proteins in Vascular Smooth Muscle. *Front. Physiol.* **2022**, *13*, 1059021. https://doi.org/10.3389/fphys.2022.1059021.

(190) Dowling, P.; Gargan, S.; Murphy, S.; Zweyer, M.; Sabir, H.; Swandulla, D.; Ohlendieck, K. The Dystrophin Node as Integrator of Cytoskeletal Organization, Lateral Force Transmission, Fiber Stability and Cellular Signaling in Skeletal Muscle. *Proteomes* **2021**, *9* (1), 9. https://doi.org/10.3390/proteomes9010009.

(191) Lovering, R. M.; Iyer, S. R.; Edwards, B.; Davies, K. E. Alterations of Neuromuscular Junctions in Duchenne Muscular Dystrophy. *Neuroscience Letters* **2020**, *737*, 135304. https://doi.org/10.1016/j.neulet.2020.135304.

(192) Chazaud, B. Inflammation and Skeletal Muscle Regeneration: Leave It to the Macrophages! *Trends in Immunology* **2020**, *41* (6), 481–492. https://doi.org/10.1016/j.it.2020.04.006.

(193) Arnold, L.; Henry, A.; Poron, F.; Baba-Amer, Y.; Van Rooijen, N.; Plonquet, A.; Gherardi, R. K.; Chazaud, B. Inflammatory Monocytes Recruited after Skeletal Muscle Injury Switch into Antiinflammatory Macrophages to

Support Myogenesis. *The Journal of Experimental Medicine* **2007**, *204* (5), 1057–1069. https://doi.org/10.1084/jem.20070075.

(194) Yin, H.; Price, F.; Rudnicki, M. A. Satellite Cells and the Muscle Stem Cell Niche. *Physiological Reviews* **2013**, *93* (1), 23–67. https://doi.org/10.1152/physrev.00043.2011.

(195) Juban, G.; Saclier, M.; Yacoub-Youssef, H.; Kernou, A.; Arnold, L.; Boisson, C.; Ben Larbi, S.; Magnan, M.; Cuvellier, S.; Théret, M.; Petrof, B. J.; Desguerre, I.; Gondin, J.; Mounier, R.; Chazaud, B. AMPK Activation Regulates LTBP4-Dependent TGF-B1 Secretion by Pro-Inflammatory Macrophages and Controls Fibrosis in Duchenne Muscular Dystrophy. *Cell Reports* **2018**, *25* (8), 2163-2176.e6. https://doi.org/10.1016/j.celrep.2018.10.077.

(196) Messina, S.; Vita, G. L. Clinical Management of Duchenne Muscular Dystrophy: The State of the Art. *Neurol Sci* **2018**, *39* (11), 1837–1845. https://doi.org/10.1007/s10072-018-3555-3.

(197) Verhaart, I. E. C.; Aartsma-Rus, A. Therapeutic Developments for Duchenne Muscular Dystrophy. *Nat Rev Neurol* **2019**, *15* (7), 373–386. https://doi.org/10.1038/s41582-019-0203-3.

(198) Starosta, A.; Konieczny, P. Therapeutic Aspects of Cell Signaling and Communication in Duchenne Muscular Dystrophy. *Cell. Mol. Life Sci.* **2021**, *78* (11), 4867–4891. https://doi.org/10.1007/s00018-021-03821-x.

(199) Karsdal, M. A.; Nielsen, M. J.; Sand, J. M.; Henriksen, K.; Genovese, F.; Bay-Jensen, A.-C.; Smith, V.; Adamkewicz, J. I.; Christiansen, C.; Leeming, D. J. Extracellular Matrix Remodeling: The Common Denominator in Connective Tissue Diseases *Possibilities for Evaluation and Current Understanding of the Matrix as More Than a Passive Architecture, but a Key Player in Tissue Failure*.

ASSAY and Drug Development Technologies **2013**, *11* (2), 70–92. https://doi.org/10.1089/adt.2012.474.

(200) Carr, S. J.; Zahedi, R. P.; Lochmüller, H.; Roos, A. Mass Spectrometry-based Protein Analysis to Unravel the Tissue Pathophysiology in Duchenne Muscular Dystrophy. *Proteomics Clinical Apps* **2018**, *12* (2), 1700071. https://doi.org/10.1002/prca.201700071.

(201) Barabási, A.-L.; Oltvai, Z. N. Network Biology: Understanding the Cell's Functional Organization. *Nat Rev Genet* **2004**, *5* (2), 101–113. https://doi.org/10.1038/nrg1272.

(202) Lage, K.; Karlberg, E. O.; Størling, Z. M.; Ólason, P. Í.; Pedersen, A. G.; Rigina, O.; Hinsby, A. M.; Tümer, Z.; Pociot, F.; Tommerup, N.; Moreau, Y.; Brunak, S. A Human Phenome-Interactome Network of Protein Complexes Implicated in Genetic Disorders. *Nat Biotechnol* **2007**, *25* (3), 309–316. https://doi.org/10.1038/nbt1295.

(203) Ayoglu, B.; Chaouch, A.; Lochmüller, H.; Politano, L.; Bertini, E.; Spitali, P.; Hiller, M.; Niks, E. H.; Gualandi, F.; Pontén, F.; Bushby, K.; Aartsma-Rus, A.; Schwartz, E.; Le Priol, Y.; Straub, V.; Uhlén, M.; Cirak, S.; 'T Hoen, P. A. C.; Muntoni, F.; Ferlini, A.; Schwenk, J. M.; Nilsson, P.; Al-Khalili Szigyarto, C. Affinity Proteomics within Rare Diseases: A BIO - NMD Study for Blood Biomarkers of Muscular Dystrophies. *EMBO Mol Med* **2014**, *6* (7), 918–936. https://doi.org/10.15252/emmm.201303724.

(204) Dowling, P.; Gargan, S.; Zweyer, M.; Sabir, H.; Swandulla, D.; Ohlendieck, K. Proteomic Profiling of Carbonic Anhydrase CA3 in Skeletal Muscle. *Expert Review of Proteomics* **2021**, *18* (12), 1073–1086. https://doi.org/10.1080/14789450.2021.2017776.

(205) De Palma, S.; Morandi, L.; Mariani, E.; Begum, S.; Cerretelli, P.; Wait, R.; Gelfi, C. Proteomic Investigation of the Molecular Pathophysiology of Dysferlinopathy. *Proteomics* **2006**, *6* (1), 379–385. https://doi.org/10.1002/pmic.200500098.

(206) Wilm, M. Quantitative Proteomics in Biological Research. *Proteomics* **2009**, *9* (20), 4590–4605. https://doi.org/10.1002/pmic.200900299.

(207) Dussoyer, M.; Page, A.; Delolme, F.; Rousselle, P.; Nyström, A.; Moali, C. Comparison of Extracellular Matrix Enrichment Protocols for the Improved Characterization of the Skin Matrisome by Mass Spectrometry. *Journal of Proteomics* **2022**, *251*, 104397. https://doi.org/10.1016/j.jprot.2021.104397.

(208) Hardy, D.; Besnard, A.; Latil, M.; Jouvion, G.; Briand, D.; Thépenier, C.; Pascal, Q.; Guguin, A.; Gayraud-Morel, B.; Cavaillon, J.-M.; Tajbakhsh, S.; Rocheteau, P.; Chrétien, F. Comparative Study of Injury Models for Studying Muscle Regeneration in Mice. *PLoS ONE* **2016**, *11* (1), e0147198. https://doi.org/10.1371/journal.pone.0147198.

(209) Ito, M.; Ehara, Y.; Li, J.; Inada, K.; Ohno, K. Protein-Anchoring Therapy of Biglycan for *Mdx* Mouse Model of Duchenne Muscular Dystrophy. *Human Gene Therapy* **2017**, *28* (5), 428–436. https://doi.org/10.1089/hum.2015.088.

(210) Croissant, C.; Carmeille, R.; Brévart, C.; Bouter, A. Annexins and Membrane Repair Dysfunctions in Muscular Dystrophies. *IJMS* **2021**, *22* (10), 5276. https://doi.org/10.3390/ijms22105276.

(211) Cooper, S. T.; Head, S. I. Membrane Injury and Repair in the Muscular Dystrophies. *Neuroscientist* **2015**, *21* (6), 653–668. https://doi.org/10.1177/1073858414558336.

(212) Law, M. L.; Cohen, H.; Martin, A. A.; Angulski, A. B. B.; Metzger, J. M. Dysregulation of Calcium Handling in Duchenne Muscular Dystrophy-Associated Dilated Cardiomyopathy: Mechanisms and Experimental Therapeutic Strategies. *JCM* **2020**, *9* (2), 520. https://doi.org/10.3390/jcm9020520.

(213) Zhang, W.; Liu, Y.; Zhang, H. Extracellular Matrix: An Important Regulator of Cell Functions and Skeletal Muscle Development. *Cell Biosci* **2021**, *11* (1), 65. https://doi.org/10.1186/s13578-021-00579-4.